

Anti-neuroinflammatory effects of *Auricularia polytricha* extracts on bisphenol A (BPA)-induced microglial cell activation and reduction of hippocampal cell damage



Mr. Chanin Sillapachaiyaporn

จุฬาลงกรณ์มหาวิทยาลัย  
CHULALONGKORN UNIVERSITY

A Dissertation Submitted in Partial Fulfillment of the Requirements  
for the Degree of Doctor of Philosophy in Clinical Biochemistry and  
Molecular Medicine

Department of Clinical Chemistry  
FACULTY OF ALLIED HEALTH SCIENCES

Chulalongkorn University

Academic Year 2022

Copyright of Chulalongkorn University

ฤทธิ์ยับยั้งการอักเสบของสารสกัดเห็ดหูหนูช้าง (*Auricularia polytricha*) ต่อการ  
กระตุ้นเซลล์ไมโครเกลียที่เหนียวนำด้วยสารบิสฟีนอลเอ และการลดความเสียหายของเซลล์สมอง  
ส่วนฮิปโปแคมปัส



วิทยานิพนธ์นี้เป็นส่วนหนึ่งของการศึกษาตามหลักสูตรปริญญาวิทยาศาสตรดุษฎีบัณฑิต  
สาขาวิชาชีวเคมีคลินิกและอณูทางการแพทย์ ภาควิชาเคมีคลินิก  
คณะสหเวชศาสตร์ จุฬาลงกรณ์มหาวิทยาลัย  
ปีการศึกษา 2565  
ลิขสิทธิ์ของจุฬาลงกรณ์มหาวิทยาลัย

Thesis Title	Anti-neuroinflammatory effects of <i>Auricularia polytricha</i> extracts on bisphenol A (BPA)-induced microglial cell activation and reduction of hippocampal cell damage
By	Mr. Chanin Sillapachaiyaporn
Field of Study	Clinical Biochemistry and Molecular Medicine
Thesis Advisor	Assistant Professor TEWIN TENCOMNAO, Ph.D.
Thesis Co Advisor	Professor SEUNG JOON BAEK, Ph.D. Assistant Professor TEWARIT SARACHANA, Ph.D.

---

Accepted by the FACULTY OF ALLIED HEALTH SCIENCES, Chulalongkorn University in Partial Fulfillment of the Requirement for the Doctor of Philosophy

.....  
Dean of the FACULTY OF ALLIED  
HEALTH SCIENCES  
(Associate Professor PALANEE AMMARANOND, Ph.D.)

DISSERTATION COMMITTEE

..... Chairman  
(Associate Professor Krai Meemon, Ph.D.)  
..... Thesis Advisor  
(Assistant Professor TEWIN TENCOMNAO, Ph.D.)  
..... Thesis Co-Advisor  
(Professor SEUNG JOON BAEK, Ph.D.)  
..... Thesis Co-Advisor  
(Assistant Professor TEWARIT SARACHANA, Ph.D.)  
..... Examiner  
(Assistant Professor VIROJ BOONYARATANAKORNKIT,  
Ph.D.)  
..... Examiner  
(Assistant Professor SIRIPORN CHUCHAWANKUL, Ph.D.)  
..... Examiner  
(SIRIPORN SANGSUTHUM, Ph.D.)

CHULALONGKORN UNIVERSITY

ชรินทร์ ศิลปชัยพร : ฤทธิ์ยับยั้งการอักเสบของสารสกัดเห็ดหูหนูช้าง (*Auricularia polytricha*) ต่อการกระตุ้นเซลล์ไมโครเกลียที่เหนี่ยวนำด้วยสารบิสฟีนอลเอ และการลดความเสียหายของเซลล์สมองส่วนฮิปโปแคมปัส. ( *Anti-neuroinflammatory effects of *Auricularia polytricha* extracts on bisphenol A (BPA)-induced microglial cell activation and reduction of hippocampal cell damage*) อ.ที่ปรึกษาหลัก : ผศ. ดร.เทวิน เทนคำเนา, อ.ที่ปรึกษาร่วม : ศ. ดร. ชิ่ง จุน แบล, ผศ. ดร.เทวฤทธิ์ สระระชนะ

บิสฟีนอลเอเป็นสารที่นิยมใช้ในการผลิตพลาสติกประเภทโพลีคาร์บอเนต และมีรายงานพบว่าสารบิสฟีนอลเอก่อให้เกิดการอักเสบของระบบประสาท ซึ่งเป็นพยาธิสภาพของสมองที่มีการหลั่งสารกระตุ้นการอักเสบปริมาณมาก เช่น tumor necrosis factor-alpha (TNF- $\alpha$ ) โดยสาร TNF- $\alpha$  ที่มากเกินไปสามารถเหนี่ยวนำให้เกิดการตายของเซลล์ประสาทและนำไปสู่การเกิดโรคความเสื่อมของระบบประสาทได้ จากบทความวิจัยพบว่าเห็ดหูหนูช้างเป็นเห็ดที่สามารถรับประทานได้และอุดมไปด้วยฤทธิ์ทางแพทย์ งานวิจัยนี้จึงได้ทำการทดสอบฤทธิ์ยับยั้งการอักเสบของสารสกัดเห็ดหูหนูช้างต่อการกระตุ้นเซลล์ไมโครเกลียที่เหนี่ยวนำด้วยสารบิสฟีนอลเอ พบว่าสารสกัดเห็ดหูหนูช้างสามารถยับยั้งการอักเสบของเซลล์ไมโครเกลียที่เหนี่ยวนำด้วยสารบิสฟีนอลเอ โดยลดการแสดงออกของสารกระตุ้นการอักเสบผ่านกระบวนการถ่ายทอดสัญญาณ NF- $\kappa$ B และมีฤทธิ์ต้านอนุมูลอิสระโดยการเพิ่มการแสดงออกของเอนไซม์ต้านอนุมูลอิสระ superoxide dismutase-1 (SOD-1) และลดการสะสมของสารอนุมูลอิสระในเซลล์ไมโครเกลียที่เหนี่ยวนำด้วยสารบิสฟีนอลเอจากนั้นผู้วิจัยได้ทำการแยกสารบริสุทธิ์เออร์โกสเตอรอลจากสารสกัดเห็ดหูหนูช้างและทำการทดสอบฤทธิ์ของสารบริสุทธิ์ พบว่าสารเออร์โกสเตอรอลมีฤทธิ์ยับยั้งการอักเสบและต้านอนุมูลอิสระในเซลล์ไมโครเกลียที่เหนี่ยวนำด้วยสารบิสฟีนอลเอ นอกจากนี้ผู้วิจัยได้ทำการทดสอบฤทธิ์ปกป้องเซลล์ประสาทของสารเออร์โกสเตอรอลต่อเซลล์สมองส่วนฮิปโปแคมปัสที่ถูกเหนี่ยวนำด้วยสาร TNF- $\alpha$  พบว่าเออร์โกสเตอรอลสามารถลดความเสียหายของเซลล์สมองส่วนฮิปโปแคมปัสที่ถูกเหนี่ยวนำด้วยสาร TNF- $\alpha$  โดยเพิ่มการแสดงออกของเอนไซม์ต้านอนุมูลอิสระ SOD-1 และการกำจัดสารอนุมูลอิสระผ่านกระบวนการถ่ายทอดสัญญาณต้านอนุมูลอิสระในเซลล์สมองส่วนฮิปโปแคมปัส และจากผลการทดสอบด้วยอาร์เรย์แอนติบอดี (Antibody array) พบว่าสารเออร์โกสเตอรอลมีฤทธิ์เพิ่มการแสดงออกของโปรตีน phospho-Akt อีกทั้งสารเออร์โกสเตอรอลมีฤทธิ์ยับยั้งการแสดงออกของยีน glutamate ionotropic receptor N-methyl-D-aspartate type subunit 2B gene (*Grin2b*) ผ่านกระบวนการถ่ายทอดสัญญาณของ early growth response-1 (EGR-1) ในเซลล์สมองส่วนฮิปโปแคมปัสที่ถูกเหนี่ยวนำด้วยสาร TNF- $\alpha$  งานวิจัยนี้เป็นการค้นพบคุณสมบัติทางเภสัชวิทยาใหม่ของสารสกัดเห็ดหูหนูช้าง และสารเออร์โกสเตอรอลต่อการต้านการอักเสบของระบบประสาทและการปกป้องเซลล์ประสาท ซึ่งจะเป็นประโยชน์ต่อผู้ป่วยโรคความเสื่อมของระบบประสาท

สาขาวิชา ชีวเคมีคลินิกและอนุทางการแพทย์  
ปีการศึกษา 2565

ลายมือชื่อนิสิต .....  
ลายมือชื่อ อ.ที่ปรึกษาหลัก .....  
ลายมือชื่อ อ.ที่ปรึกษาร่วม .....  
ลายมือชื่อ อ.ที่ปรึกษาร่วม .....

# # 6271002637 : MAJOR CLINICAL BIOCHEMISTRY AND MOLECULAR MEDICINE

KEYWORD Bisphenol A, *Auricularia polytricha*, Ergosterol, Neuroinflammation, D: Neuroprotection

Chanin Sillapachaiyaporn : Anti-neuroinflammatory effects of *Auricularia polytricha* extracts on bisphenol A (BPA)-induced microglial cell activation and reduction of hippocampal cell damage. Advisor: Asst. Prof. TEWIN TENCOMNAO, Ph.D. Co-advisor: Prof. SEUNG JOON BAEK, Ph.D., Asst. Prof. TEWARIT SARACHANA, Ph.D.

Bisphenol A (BPA) is widely used in the production of polycarbonate plastics, it has been reported that BPA can activate neuroinflammation. Neuroinflammation is a brain pathology that involves the high levels of pro-inflammatory mediators, including tumor necrosis factor-alpha (TNF- $\alpha$ ). An excessive TNF- $\alpha$  expression could result in neuronal cell death and subsequently lead to neurodegeneration. *Auricularia polytricha* (AP) is an edible mushroom with several medicinal properties. Herein, the anti-neuroinflammatory effects of AP extracts against BPA-induced BV2 microglial inflammation were investigated. Hexane (APH) and ethanol (APE) extracts of AP inhibited BPA-induced neuroinflammation in BV2 cells by reducing the expression of pro-inflammatory cytokines. These anti-inflammatory effects were regulated by the NF- $\kappa$ B signaling pathway. In addition, APH and APE exhibited antioxidative effects by increasing a superoxide dismutase-1 (SOD-1), an antioxidant enzyme, and restoring an accumulation of reactive oxygen species (ROS) in BPA-induced BV2 cells. Further, ergosterol was isolated from APE and also showed anti-inflammatory and antioxidative activities in BPA-induced BV2 cells. Besides, the neuroprotective effects of ergosterol against the TNF- $\alpha$ -induced HT-22 hippocampal cell injury were investigated. Ergosterol attenuated the toxicity of TNF- $\alpha$  on HT-22 cells, by increasing the expression of SOD-1 and by facilitating the scavenging of ROS through antioxidant signaling. Based on the antibody array, the phospho-Akt was activated in the presence of ergosterol, and this finding was also supported by Western blotting analysis. Furthermore, ergosterol inhibited the transcriptional expressions of the glutamate ionotropic receptor *N*-methyl-D-aspartate type subunit 2B gene (*Grin2b*) through an early growth response-1 (EGR-1) signaling in TNF- $\alpha$ -treated HT-22 cells. These findings demonstrate novel therapeutic activities of AP extracts and ergosterol in anti-neuroinflammation and neuroprotection that might be of benefit for patients with neurodegenerative diseases.

Field of Study:	Clinical Biochemistry and Molecular Medicine	Student's Signature .....
Academic Year:	2022	Advisor's Signature .....
		Co-advisor's Signature .....
		Co-advisor's Signature .....

## ACKNOWLEDGEMENTS

The Royal Golden Jubilee (RGJ) Ph.D. Program scholarship from the National Research Council of Thailand (NRCT) and the Second Century Fund (C2F) scholarship from Chulalongkorn University, are gratefully acknowledged. Moreover, this research project was supported by the 90th Anniversary Chulalongkorn University Fund (Ratchadaphiseksomphot Endowment Fund, GCUGR1125643032D) and the National Research Foundation of Korea (NRF) grant (NRF-2021R1A2B2002923).

I would like to express my very great appreciation to Asst. Prof. Dr. Tewin Tencomnao, my advisor; Prof. Dr. Baek Seung Joon, Asst. Prof. Dr. Siriporn Chuchawankul, Assoc. Prof. Dr. Alison Ung, and Asst. Prof. Dr. Tewarit Sarachana, my co-advisors. This work would not have been completed without their support, encouragement, and guidance.

I would like to acknowledge Asst. Prof. Dr. Monruedee Sukprasansap and Prof. Dr. David Schube for providing BV2 mouse microglial and HT-22 hippocampal cell lines, respectively.

I particularly grateful for assistance given by the Clinical Biochemistry and Molecular Medicine lab members, especially Sunita Nilkhet, Dr. Panthakarn Rangsinth, Sakawrat Janpajit, Atsadang Theerasri, and Kuljira Mongkolpobsin. Besides, I also thank my colleagues in the Signal Transduction Laboratory, College of Veterinary Medicine, Seoul National University, Pattawika Lertpatipanpong, Kanokkarn Boonruang, Hong Yukyung, Lee Jaehak, and Kim Ilju for their kind assistance.

My special thanks are extended to my important friends, Surangrat Thongkorn, Nutpakal Ketprasit, and Dr. Naricha Pupinyo for their being great friends and cheering up. It would be difficult to pass through any obstacles without their support.

Last but most importantly, I must express my deepest gratitude to my family for taking care of me and always supporting my dreams. This accomplishment would not have been possible without them. Thank you.

Chanin Sillapachaiyaporn

## TABLE OF CONTENTS

	<b>Page</b>
ABSTRACT (THAI) .....	iii
ABSTRACT (ENGLISH).....	iv
ACKNOWLEDGEMENTS.....	v
TABLE OF CONTENTS.....	vi
LIST OF TABLES.....	xi
LIST OF FIGURES .....	xii
CHAPTER I INTRODUCTION.....	1
1. Background and significant.....	1
2. Research questions.....	4
3. Research hypothesis.....	5
4. Research objectives .....	5
5. Conceptual framework.....	6
CHAPTER II LITERATURE REVIEW .....	7
1. Alzheimer’s disease .....	7
2. Neuroinflammation in Alzheimer’s disease .....	8
3. Bisphenol A .....	11
3.1. Effect of bisphenol A on amyloidosis .....	12
3.2. Effect of bisphenol A on neuroinflammation.....	12
4. Roles of TNF- $\alpha$ in neurodegenerative disorders .....	13
5. The effects of TNF- $\alpha$ on ionotropic glutamate receptors in neurodegenerative disorders .....	15
6. Medicinal properties of <i>Auricularia polytricha</i> (AP).....	17
7. Ergosterol.....	20
7.1. Anti-inflammatory effect of ergosterol .....	21
7.2. Antioxidative effect of ergosterol.....	22
7.3. Drug-likeness and pharmacokinetic properties of ergosterol.....	22

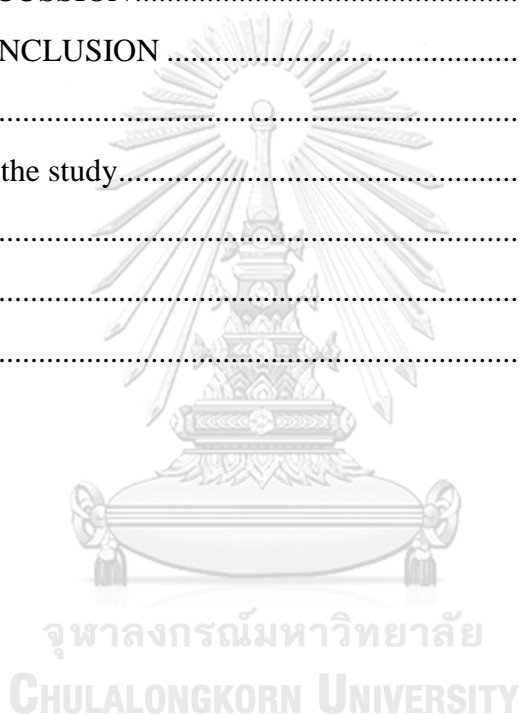
8. Cell models .....	25
8.1. Mouse microglial cell line (BV2 cell line).....	25
8.2. Mouse hippocampal cell line (HT-22 cell line).....	25
CHAPTER III MATERIALS AND METHODS .....	27
1. Laboratory instrument and equipment.....	27
2. Chemicals and reagents .....	31
3. Experimental workflow .....	38
4. Mushroom extract preparation.....	39
5. <i>In vitro</i> non-cell-based antioxidant assays.....	40
5.1. Total phenolic content analysis .....	40
5.2. Total flavonoid content analysis.....	41
5.3. Free radical scavenging assays.....	41
5.3.1. ABTS assay .....	41
5.3.1. DPPH assay .....	41
6. Cytotoxicity of BPA against BV2 microglial cells.....	42
7. Neuroinflammatory effects of BPA on BV2 microglial cells .....	43
7.1. BV2 microglial cell morphological changes against BPA induction.....	43
7.2. Pro-inflammatory cytokine mRNA expression of BPA-induced BV2 microglial cells .....	43
7.3. Pro-inflammatory cytokine secretion of BPA-induced BV2 microglial cells .....	44
8. Cytotoxicity of AP extracts against BV2 microglial cells.....	45
9. Anti-neuroinflammatory effects of AP extracts on BPA-induced BV2 microglial cells.....	45
9.1. The effect of AP extracts on BPA-induced BV2 microglial cell morphological changes .....	45
9.2. The effect of AP extracts on pro-inflammatory cytokine mRNA expression in BPA-induced BV2 microglial cells.....	46
9.3. The effect of AP extracts on pro-inflammatory cytokine secretion in BPA- induced BV2 microglial cells .....	46



10. Molecular mechanisms of AP extracts on BPA-induced BV2 microglial activation .....	47
10.1. The expression of NF- $\kappa$ B signaling-associated proteins.....	47
10.2. Dual luciferase assay of NF- $\kappa$ B activity.....	48
10.3. Nuclear translocation of NF- $\kappa$ B p65 .....	48
11. Antioxidative effects of AP crude extracts on BV2 microglial cells.....	49
11.1. Protein expression of SOD-1, antioxidant enzyme .....	49
11.2. Intracellular reactive oxygen species (ROS) in BV2 cells.....	49
12. Neuroprotective effects of AP extracts on HT-22 hippocampal cell damage ...	50
12.1. Conditioned medium preparation.....	50
12.2. HT-22 hippocampal cell viability.....	51
12.3. Co-culture of BV2 microglial and HT-22 hippocampal cells .....	51
12.4. Intracellular ROS in HT-22 hippocampal cells.....	52
13. Chemical compound isolation .....	53
13.1. Thin-layer chromatography (TLC).....	53
13.2. Column chromatography (CC).....	53
13.3. Crystallization .....	54
14. Chemical compound identification.....	54
14.1. Thin-layer chromatography (TLC) of APH and APE-1.....	54
14.2. Nuclear magnetic resonance (NMR).....	54
15. Anti-neuroinflammatory effects of ergosterol against BPA-induced BV2 cells	54
15.1. Cytotoxicity of ergosterol against BV2 microglial cells .....	54
15.2. The expression of NF- $\kappa$ B signaling-associated proteins.....	55
16. Neuroprotective effects of AP crude extracts against TNF- $\alpha$ -induced HT-22 hippocampal cells .....	55
16.1. Cytotoxicity of TNF- $\alpha$ and ergosterol against HT-22 cells .....	55
16.2. Neuroprotective effect of ergosterol on TNF- $\alpha$ -induced HT-22 cells .....	55
17. Antioxidative effects of AP crude extracts on HT-22 hippocampal cells .....	56
17.1. Protein expression of SOD-1, antioxidant enzyme .....	56
17.2. The antioxidant response element (ARE) activity .....	56

17.3. Intracellular ROS assay in HT-22 cells .....	56
18. Molecular mechanism of AP extracts against TNF- $\alpha$ -induced HT-22 hippocampal cells .....	57
18.1. Apoptosis antibody array.....	57
18.2. The expression of Akt/ GSK-3 $\beta$ signaling-associated proteins.....	58
18.3. The mRNA expression of NMDA receptors .....	58
18.4. The EGR-1 activity .....	59
18.5. EGR-1 overexpression in HT-22 hippocampal cells.....	59
18.6. Protein expression of NMDA receptor.....	60
18.7. Immunofluorescence staining of NR2B .....	60
19. Statistical analysis.....	61
CHAPTER IV RESULTS.....	62
1. Total phenolic and flavonoid contents present in AP crude extracts.....	62
2. Free radical scavenging activity of AP crude extracts.....	63
3. Effects of BPA on BV2 microglial cells.....	64
3.1. Cytotoxicity of BPA against BV2 microglial cells .....	64
3.2. Neuroinflammatory effects of BPA on BV2 microglial cells .....	65
4. Cytotoxicity of AP extracts against BV2 microglial cells .....	69
5. Anti-neuroinflammatory effects of AP extracts on BPA-induced BV2 microglial cell activation.....	70
6. The effects of AP extracts on NF- $\kappa$ B signaling pathway against BPA-induced BV2 microglial cell activation.....	75
7. Antioxidative and neuroprotective effects of AP extracts on BV2 cells .....	79
8. Neuroprotective effects of AP extracts against BV2-conditioned medium-exposed HT-22 hippocampal cell damage .....	81
9. Chemical compound isolation and identification .....	83
9.1. Column chromatography and crystalization.....	83
9.2. Thin layer chromatography (TLC) .....	84
9.3. Nuclear magnetic resonance (NMR) .....	85

10. The effects of ergosterol against BPA-induced BV2 microglial cell activation	86
11. Neuroprotective effect of ergosterol against the TNF- $\alpha$ -induced HT-22 cell death .....	87
12. Antioxidant activity of ergosterol on TNF- $\alpha$ -induced HT-22 cell injury .....	90
13. The molecular mechanism of ergosterol against TNF- $\alpha$ -induced HT-22 cell death .....	92
14. The effect of ergosterol on NMDA receptors in TNF- $\alpha$ -induced HT-22 cell death .....	96
CHAPTER V DISCUSSION .....	102
CHAPTER VI CONCLUSION .....	113
1. Conclusion .....	113
2. Limitation of the study.....	115
REFERENCES .....	116
APPENDIX.....	135
VITA.....	153



## LIST OF TABLES

	<b>Page</b>
Table 1 List of mushrooms containing ergosterol and their pharmaceutical properties .....	20
Table 2 Physicochemical properties of ergosterol .....	23
Table 3 Pharmacokinetic properties of ergosterol .....	23
Table 4 List of primers for pro-inflammatory cytokine gene expression .....	44
Table 5 Treatment conditions for investigation of the anti-neuroinflammatory effect of AP extracts on BPA-induced microglial cells .....	46
Table 6 Treatment conditions for investigation of the molecular mechanism of AP extracts on BPA-induced BV2 microglial activation.....	48
Table 7 Treatment conditions for investigation of the NF- $\kappa$ B p65 nuclear translocation of APE extract on BPA-induced BV2 microglial activation.....	49
Table 8 Treatment conditions for intracellular ROS assay in BV2 cells and BV2-conditioned medium preparation .....	50
Table 9 Treatment conditions for investigation of neuroprotective effects of BV2-conditioned medium against HT-22 hippocampal cell damage.....	51
Table 10 Treatment conditions for investigation of neuroprotective effects of BV2-conditioned medium against HT-22 hippocampal cell damage using the transwell co-culture system .....	52
Table 11 List of primers for glutamate ionotropic receptor NMDA type gene expression .....	59
Table 12 Antioxidant capacity and half-maximal effective concentration (EC <sub>50</sub> ) of free radical scavenging activity of AP crude extracts.....	64

## LIST OF FIGURES

	<b>Page</b>
Figure 1 Graphical abstract.....	4
Figure 2 Conceptual framework .....	6
Figure 3 Pathological hallmarks of Alzheimer’s disease (25) .....	7
Figure 4 Amyloid- $\beta$ formation (26) .....	8
Figure 5 Inflammation in Alzheimer’s disease (29) .....	8
Figure 6 Mechanism of microglial activation associated with neuronal death and neurodegeneration (33) .....	10
Figure 7 Structure of bisphenol A.....	11
Figure 8 Bisphenol A involves inflammation via the NF- $\kappa$ B pathway .....	13
Figure 9 The possible mechanism of actions regulated TNF- $\alpha$ signaling in neuronal cells (38).....	14
Figure 10 Structure of N-methyl-D-aspartate (NMDA) receptors (40).....	15
Figure 11 The effects of TNF- $\alpha$ on glutamate receptors in neuronal cells (6) .....	16
Figure 12 Medicinal properties of <i>Auricularia polytricha</i> extract .....	17
Figure 13 Chemical constituents found in <i>A. polytricha</i> extracts.....	19
Figure 14 Morphology of BV2 mouse microglial cells under normal (left) and inflammatory (right) conditions.....	25
Figure 15 Typical morphology of HT-22 mouse hippocampal cells.....	26
Figure 16 Experimental workflow .....	38
Figure 17 Schematic diagram showing the sequential maceration of <i>A. polytricha</i> ...40	
Figure 18 Schematic of transwell co-culture system between BV2 and HT-22 cells	52
Figure 19 Total (A) phenolic and (B) flavonoid contents exist in AP crude extracts.	62
Figure 20 Cytotoxicity of BPA in BV2 microglial cells at 24 and 48 h.....	65
Figure 21 Neuroinflammatory effects of BPA on BV2 microglial cells. ....	66
Figure 22 The mRNA expressions of pro-inflammatory cytokines: (A) TNF- $\alpha$ , (B) IL-1 $\beta$ , and (C) IL-6 in BPA-induced BV2 cells after 24 h of treatment.....	67

Figure 23 The levels of pro-inflammatory cytokines: (A) TNF- $\alpha$ , (B) IL-1 $\beta$ , and (C) IL-6 in BV2 cell culture media after the induction of BPA for 48 h. ....	69
Figure 24 Cytotoxicity of (A) APH, (B) APE, and (C) APW against BV2 microglial cells at 24 and 48 h.....	70
Figure 25 Anti-neuroinflammatory effects of AP extracts on BPA-induced BV2 microglial cell activation.....	71
Figure 26 The mRNA expressions of pro-inflammatory cytokines: (A) TNF- $\alpha$ , (B) IL-1 $\beta$ , and (C) IL-6 in co-treatment of BPA and AP extracts on BV-2 cells for 24 h. 73	
Figure 27 The levels of pro-inflammatory cytokines: (A) TNF- $\alpha$ , (B) IL-1 $\beta$ , and (C) IL-6 in BV2 cell culture media after co-treatment of BPA and AP extracts for 48 h. 75	
Figure 28 The effects of AP extracts on NF- $\kappa$ B signaling pathway against BPA-induced BV2 microglial cell activation. ....	76
Figure 29 Effects of AP extracts on NF- $\kappa$ B p65 nuclear translocation in BPA-induced BV2 microglial cell activation. ....	77
Figure 30 The protein expressions of iNOS and COX-2 in BV2 cells treated with BPA in the presence or absence of AP extracts for 24 h. ....	79
Figure 31 Antioxidative and neuroprotective effects of AP extracts on BV2 cells....	81
Figure 32 Neuroprotective effects of AP extracts against BV2 conditioned media-exposed HT-22 hippocampal cell damage.....	83
Figure 33 The isolation of chemical constituents from APE crude extracts. ....	84
Figure 34 Thin layer chromatography analysis of APH and APE-E1 developed in hexane/ ethyl acetate (80/ 20), visualizing under UV light at 254 and 365 nm, and iodine vapor staining.....	85
Figure 35 The $^1\text{H}$ NMR spectrum of APE-E1 and ergosterol structure. ....	85
Figure 36 Cytotoxicity of ergosterol against BV2 cells after exposure for 24 h. ....	86
Figure 37 The effects of ergosterol against BPA-induced BV2 cell activation.....	87
Figure 38 Cytotoxicity of (A) TNF- $\alpha$ and (B) ergosterol on HT-22 cells at 24 h. ....	88
Figure 39 Neuroprotective effect of ergosterol against TNF- $\alpha$ -induced HT-22 hippocampal cell death. ....	89
Figure 40 Antioxidant activity of ergosterol in the TNF- $\alpha$ -induced HT-22 hippocampal cell damage.....	91
Figure 41 Apoptosis-associated protein antibody array results after a 24-h treatment with TNF- $\alpha$ , in the presence or absence of ergosterol, in HT-22 cells. ....	93

Figure 42 The effect of ergosterol on the phosphorylation of Akt at Ser473 in TNF- $\alpha$ -treated HT-22 hippocampal cells. ....	94
Figure 43 The molecular mechanism of ergosterol associated with programmed cell death in TNF- $\alpha$ -treated HT-22 hippocampal cells. ....	96
Figure 44 The mRNA expressions of the glutamate ionotropic receptor NMDA type subunit 2A (Grin2a) and 2B (Grin2b) in TNF- $\alpha$ -treated HT-22 cells, in the presence or absence of ergosterol, after 24 h. ....	97
Figure 45 The effects of ergosterol on EGR-1 signaling in TNF- $\alpha$ -induced HT-22 hippocampal cells. ....	98
Figure 46 The effects of EGR-1 on NMDA receptors in HT-22 hippocampal cells. .	99
Figure 47 The effect of ergosterol on NMDA receptor expression in TNF- $\alpha$ -induced HT-22 hippocampal cells. ....	100
Figure 48 Schematic diagram showing the proposed mechanisms underlying anti-neuroinflammatory effects of <i>A. polytricha</i> extracts and ergosterol against BPA-induced microglial cell activation. ....	114
Figure 49 Schematic diagram showing the proposed mechanisms underlying neuroprotective effects of ergosterol against TNF- $\alpha$ -induced hippocampal cell damage. ....	115

# CHAPTER I

## INTRODUCTION

### 1. Background and significant

Bisphenol A (BPA) is an endocrine-disrupting compound used to synthesize phenol resins, polyacrylates, polyesters, epoxy resins, and polycarbonate plastics. These polymers are widely used in food and beverage packaging, as well as in dental sealing materials (1). However, BPA is found to contaminate food and the environment; moreover, it is detected in urine, feces, and serum. Toxicological studies indicate that BPA exposure has adverse effects, such as carcinogenesis, reproductive toxicity, inflammation, and neuronal toxicity (2). Several studies suggest that BPA is a neurotoxin that causes neurodegenerative diseases, including Alzheimer's disease (AD), by inducing amyloid  $\beta$  ( $A\beta$ ) formation (3) and neuroinflammation (4). In addition, prenatal exposure to BPA activated AD-associated gene and protein expression in offspring (5).

Neuroinflammation is characterized by elevating the levels of inflammatory mediators in the CNS.  $TNF-\alpha$  is one of the inflammatory mediators that is found to increase brain inflammation. The excess levels of  $TNF-\alpha$  lead to synaptic dysfunction and neuronal death, which can cause the development of neurodegenerative disorders (6).  $TNF-\alpha$  induces neuronal death through several molecular signaling pathways, namely, the activation of the nuclear factor kappa B ( $NF-\kappa B$ ) (7), the p38 mitogen-activated protein kinase (MAPK) (8), the c-Jun N-terminal kinase (JNK) (7), the



ceramide/sphingomyelinase (9), and the receptor-interacting protein kinase 1 (RIP1)/RIP3/ mixed lineage kinase domain-like (MLKL) (10, 11) pathways, as well as the suppression of the antioxidant pathway (11). Moreover, TNF- $\alpha$  potentiates the localization of ionotropic glutamate receptors, such as the  $\alpha$ -amino-3-hydroxy-5-methyl-4-isoxazole propionic acid (AMPA) and the *N*-methyl-D-aspartate (NMDA) receptors, thereby leading to excessive calcium entry into the cells that trigger neuronal excitotoxicity (12). The discovery of a potential therapeutic target associated with TNF- $\alpha$  signaling has been focused on relieving the progression of neurodegenerative disorders.

Natural products have been used in traditional and complementary alternative medicine to protect and treat several diseases. *Auricularia polytricha* (AP), known as cloud ear fungus, is an edible mushroom with an antioxidant (13), anti-tumor (14, 15), anti-hypercholesterolemic (16), anti-human immunodeficiency virus type-1 (17), and anti-inflammatory (18, 19) activities. Moreover, AP extract exhibited *in vitro* inhibitory activity on beta-site amyloid precursor protein cleaving enzyme 1 ( $\beta$ -secretase), an essential enzyme for A $\beta$  synthesis (20). Our previous study reported that AP hexane extract (APH) is a rich source of ergosterol and unsaturated fatty acids (17). Interestingly, ergosterol showed an anti-inflammatory effect on lipopolysaccharide (LPS)-induced microglial cells (21), one of the critical mechanisms in AD pathogenesis.

Therefore, in this context, AP seems to be a promising natural product with beneficial health effects against inflammatory responses and neurodegeneration. Although the anti-inflammatory effects of AP extracts have been studied, the effect

and molecular mechanism of AP extracts on BPA-induced neuroinflammation have not been investigated. Thus, we aimed to determine the anti-neuroinflammatory activity of the AP extracts. We hypothesized that AP extracts might be a good candidate as a food supplement that can attenuate neurodegenerative disorders by suppressing neuroinflammation caused by BPA exposure. This study investigated the *in vitro* anti-neuroinflammation effects and related molecular mechanisms of AP extracts in BPA-induced BV2 microglial cells. Besides, we aimed to evaluate the potential effects of ergosterol on the neuronal damage induced by exposure to TNF- $\alpha$ . The neuroprotective effect of the ergosterol was determined through cell viability MTS assays. The antioxidant effect of ergosterol was assessed by measuring the expression of superoxide dismutase-1 (SOD-1; a major antioxidant enzyme) and the accumulation of reactive oxygen species (ROS) in TNF- $\alpha$ -treated HT-22 cells. Moreover, the ability of ergosterol to suppress the expression of the NMDA receptor was determined through a reverse transcription polymerase chain reaction (RT-PCR), and it was found to be probably mediated by overexpression of the early growth response-1 (EGR-1) transcription factor. The results from this study provided valuable data of AP extracts and their isolated compounds, ergosterol, on anti-neuroinflammatory and neuroprotective activities.

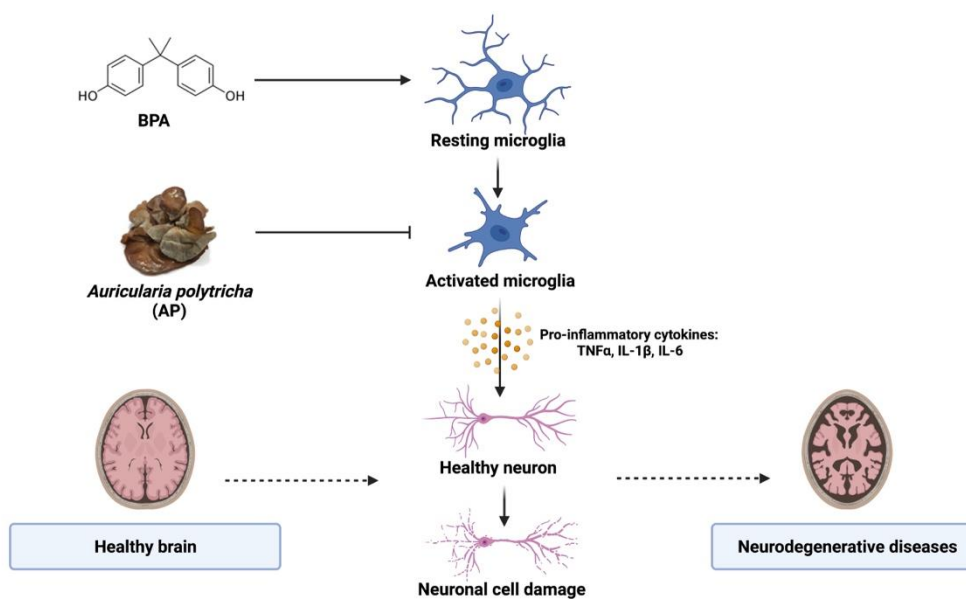


**Figure 1** Graphical abstract

## 2. Research questions

1. Do *Auricularia polytricha* crude extracts attenuate neuroinflammation of BPA-induced BV2 microglial cells?
2. Do *Auricularia polytricha* crude extracts protect HT-22 hippocampal cell toxicity against pro-inflammatory cytokine produced by BPA-induced BV2 microglial cells?
3. Do bioactive compounds isolated from *Auricularia polytricha* crude extracts provide anti-neuroinflammatory and neuroprotective effects?

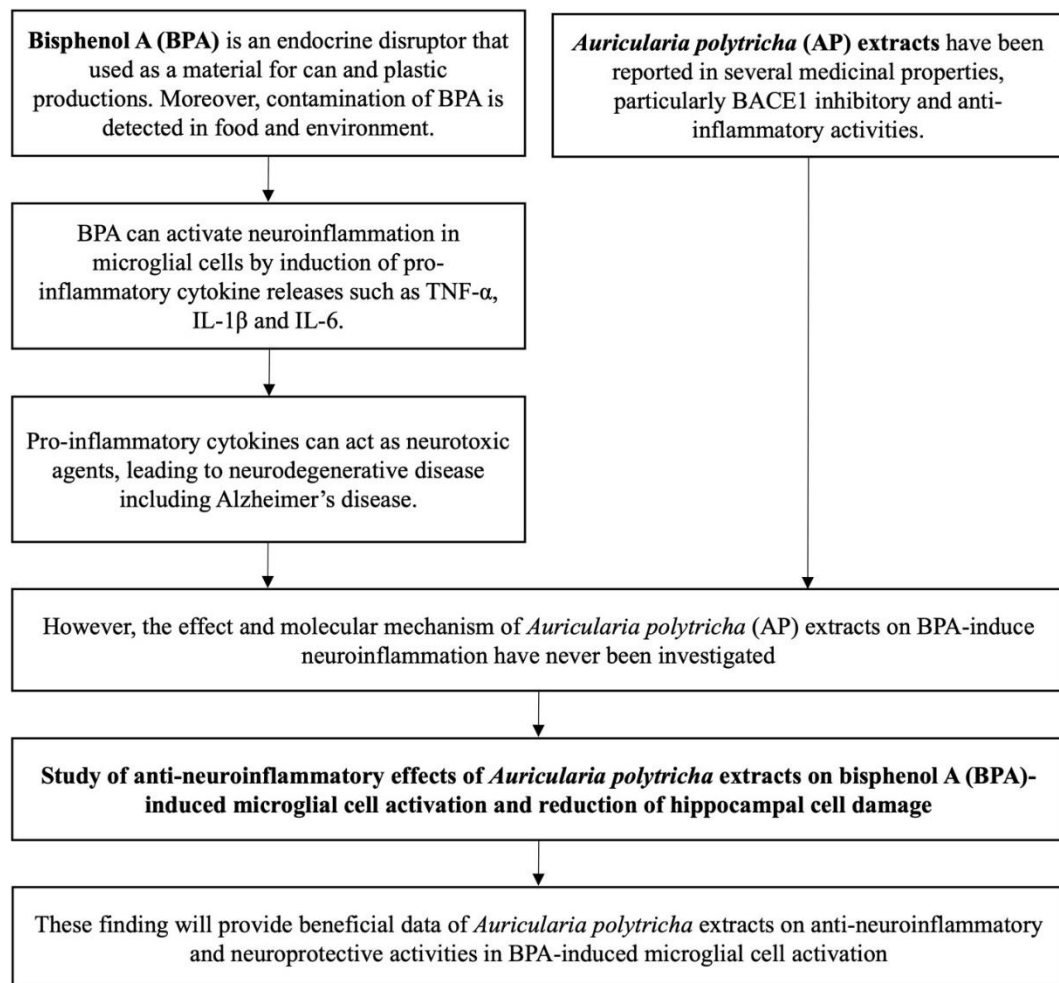
### 3. Research hypothesis

1. *Auricularia polytricha* crude extracts suppress neuroinflammation of BPA-induced BV2 microglial cells.
2. *Auricularia polytricha* crude extracts protect HT-22 hippocampal cell toxicity against pro-inflammatory cytokine produced by BPA-induced BV2 microglial cells.
3. Bioactive compounds isolated from *Auricularia polytricha* crude extracts provided anti-neuroinflammatory and neuroprotective effects.

### 4. Research objectives

1. To examine the anti-neuroinflammatory effect of *Auricularia polytricha* crude extracts in BPA-induced BV2 microglial cells
2. To determine the molecular mechanism of *Auricularia polytricha* crude extracts on anti-neuroinflammatory effect in BPA-induced BV2 microglial cells
3. To study the protective effect of *Auricularia polytricha* crude extracts on HT-22 hippocampal cells against pro-inflammatory cytokines produced by BPA-induced BV2 microglial cells
4. To isolate small molecules from *Auricularia polytricha* crude extracts and elucidate structures of the isolated compounds
5. To evaluate the anti-neuroinflammatory and neuroprotective effects of the isolated compound

## 5. Conceptual framework



จุฬาลงกรณ์มหาวิทยาลัย  
**Figure 2** Conceptual framework  
 CHULALONGKORN UNIVERSITY

## CHAPTER II

### LITERATURE REVIEW

#### 1. Alzheimer's disease

Alzheimer's disease (AD), a progressive brain disorder that slowly destroys memory is the most common cause of dementia in the elderly (22). Two major histopathological hallmarks of AD are characterized by intracellular neurofibrillary tangles and extracellular senile plaques, which are synthesized from the aggregation of phosphorylated tau protein and precipitation of amyloid- $\beta$  ( $A\beta$ ) protein, respectively (23, 24).

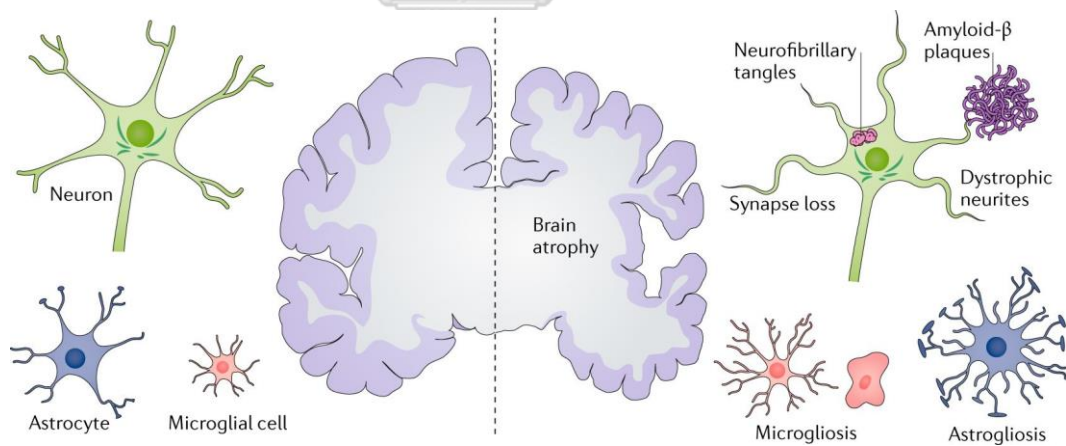


**Figure 3** Pathological hallmarks of Alzheimer's disease (25)

Amyloid- $\beta$  plaque is an aggregation of  $A\beta$ , which is a short peptide generated by sequential proteolytic cleavage of amyloid precursor protein (APP) using beta-site amyloid precursor protein cleaving enzyme 1 (BACE1,  $\beta$ -secretase) and  $\gamma$ -secretase,

leading to form A $\beta$  monomers, oligomers, and fibrils (26). A $\beta$  has several forms, including soluble monomer, soluble oligomer, insoluble fibril, and amyloid plaque (27). Many studies indicate that soluble A $\beta$  oligomer appeared to be the most neurotoxic form leading to AD by directly causing synaptic dysfunction, neuronal injury, and neuroinflammation (28).

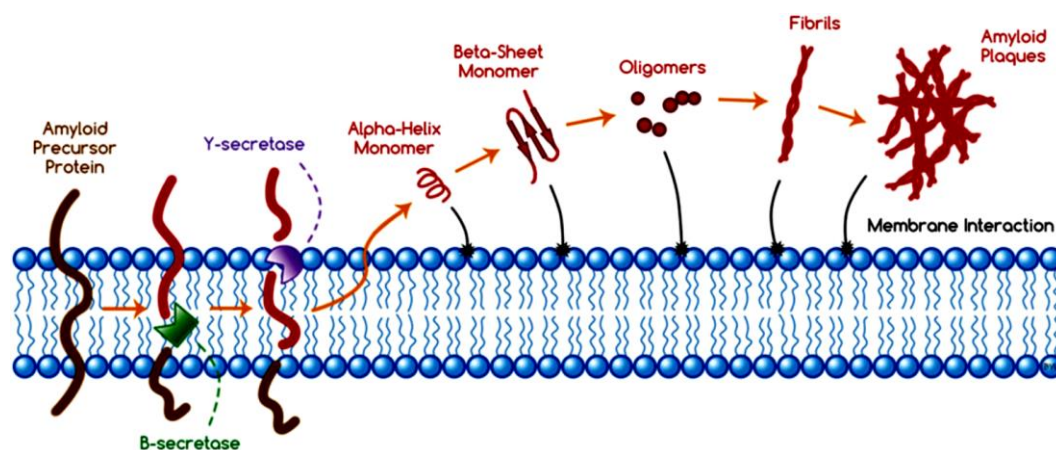


Figure 4 Amyloid- $\beta$  formation (26)

## 2. Neuroinflammation in Alzheimer's disease

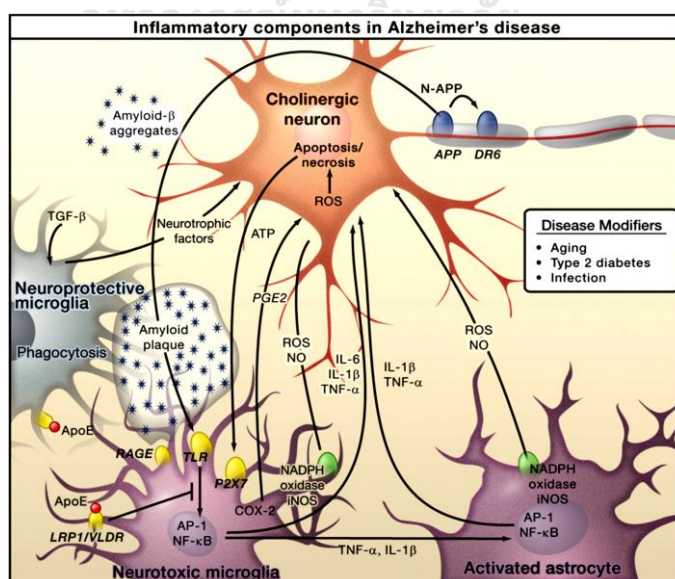
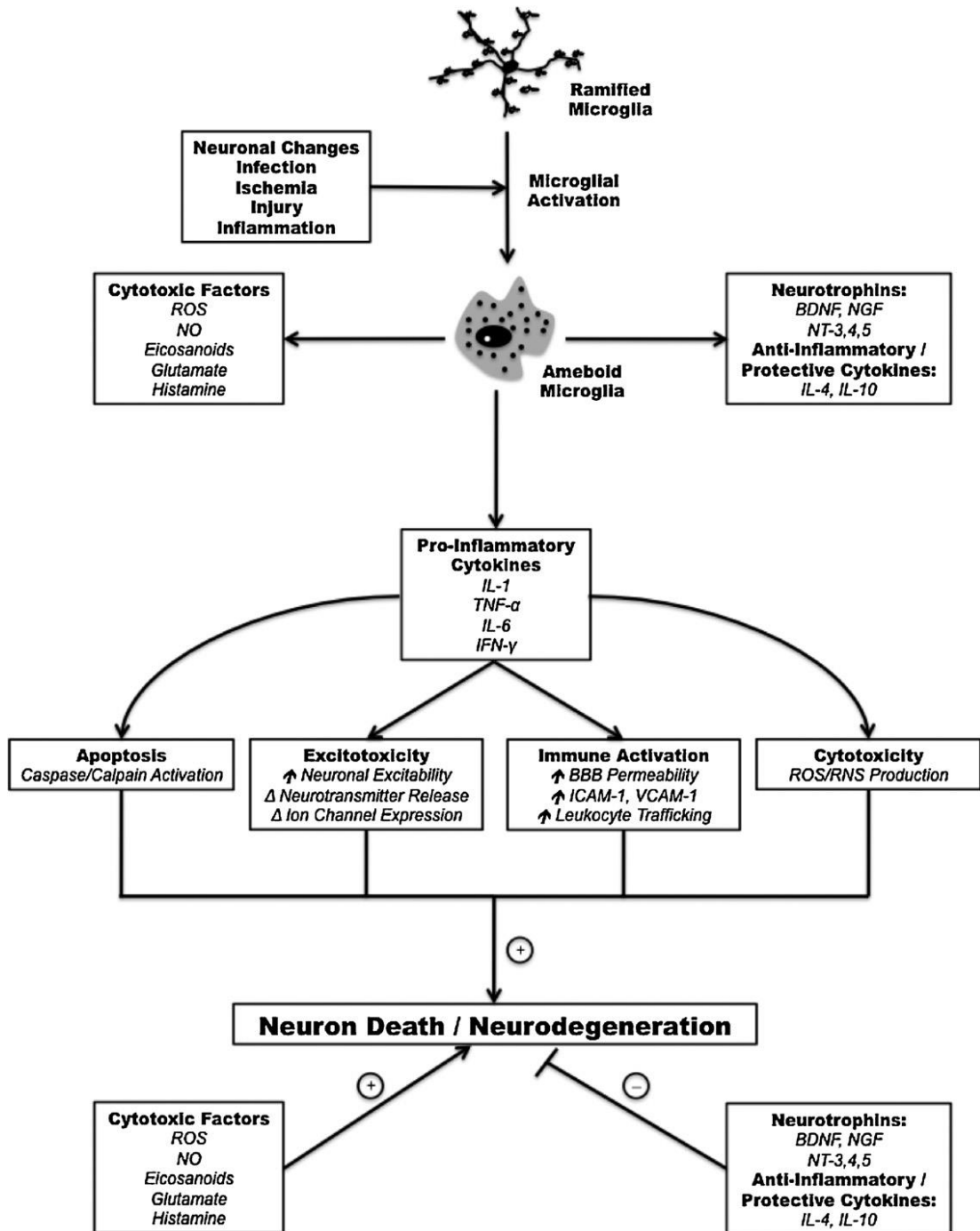


Figure 5 Inflammation in Alzheimer's disease (29)

Brain inflammation is a pathological hallmark of AD; it is characterized by an increased amount of activated microglial cells, the resident macrophages in the central nervous system (CNS). The activated cells markedly produce inflammatory substances such as pro-inflammatory cytokines (tumor necrosis factor-alpha (TNF- $\alpha$ , interleukin 1- $\beta$  (IL-1 $\beta$ ), IL-6, and interferon-gamma (IFN- $\gamma$ )), chemokines, prostaglandins, reactive oxygen species, nitric oxide, complement factors, and C-reactive protein (30). Accumulating data suggest that the inflammatory mediators could increase A $\beta$  production of neuronal cells; also, A $\beta$  could activate glial cell inflammation in a vicious circle (31). The previous study showed that the pro-inflammatory cytokines released from microglia act as a neurotoxin that causes neuronal injury and leads to AD (32). Accumulating evidence demonstrated that the pro-inflammatory cytokines might contribute to neurodegeneration by inducing apoptosis, excitotoxicity, immune activation, and cytotoxicity of the neuron (33). Therefore, inhibiting microglial cytokine production may be a potential target for treating neurodegenerative diseases, including AD.





**Figure 6** Mechanism of microglial activation associated with neuronal death and neurodegeneration (33)

### 3. Bisphenol A

Bisphenol A (BPA) or 4-[2-(4-hydroxyphenyl)propan-2-yl]phenol is an endocrine-disrupting compound commonly used to synthesize phenol resins, polyacrylates, polyesters, epoxy resins, and polycarbonate plastics. These polymers are utilized to produce food and beverage packaging and dental sealing material (1). Unfortunately, contamination of BPA is detected in food and the environment. Previous studies have reported that free BPA is observed in the urine (< 0.1 - 822 ng/ml; ca. 0.4 nM – 3.6  $\mu$ M), the serum of pregnant woman (< 0.1 – 154 ng/ml; ca. 0.4 – 674.6 nM), umbilical cord serum (< 0.05 - 52 ng/ml; ca. 0.2 – 227.8 nM), and breast milk (< 0.04 - 11 ng/ml; ca. 0.2 – 48.2 nM) (2). The US Food and Drug Administration and the European Food Safety Authority have determined that the safety levels of BPA exposure are lower than 50-4  $\mu$ g/kg body weight/day in animals and lower than 10  $\mu$ M in cell lines (34). Toxicological studies found that the doses of BPA that cause adverse health effects in animal models were lower than 1  $\mu$ g/kg body weight/day; however, the estimated daily intake of BPA by humans is lower than 1 to 5  $\mu$ g/kg body weight/day (2). Moreover, the accumulation of BPA in the body can cause adverse effects in several systems, such as the immune and nervous systems (2). BPA can stimulate these effects via estrogen receptor  $\beta$  (ER $\beta$ ) (4) and insulin receptor (IR) (3).

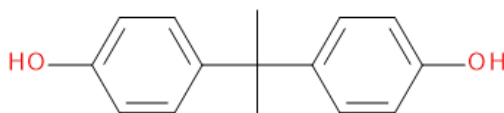


**Figure 7** Structure of bisphenol A

### 3.1. Effect of bisphenol A on amyloidosis

BPA is known as a neurotoxic agent; therefore, the study of the association between BPA and AD has been investigated. Wang T and colleagues found that BPA can induce AD-like neurotoxicity by increasing AD-associated pathological proteins, including BACE1, APP, C-terminal fragment-beta ( $\beta$ -CTF), C-terminal fragment-alpha ( $\alpha$ -CTF),  $A\beta_{1-42}$ , and phosphorylated tau proteins in SH-SY5Y and PC-12 cells (3). In addition, Thongkorn S *et al* indicated that the *Bace1* gene was upregulated in the hippocampal cells of prenatal BPA-exposed rats (5). Since we know that  $A\beta$  oligomers can induce the neuroinflammatory response of microglial cells, thus BPA might be an indirect inducer that causes neuroinflammation.

### 3.2. Effect of bisphenol A on neuroinflammation

Endocrine-disrupting compounds, including BPA, are the activator that can stimulate inflammation via estrogen receptors (ERs) in both  $ER\alpha$  and  $ER\beta$  (35). Interaction of BPA with  $ER\alpha$  shows both agonist and antagonist effects, while the binding of BPA to  $ER\beta$  exhibits agonist activity (36). Zhu J *et al* found that BPA at nanomole scale (10 – 1,000 nM) activated microglial inflammation by inducing morphologic changes and increased TNF- $\alpha$  and IL-1 $\beta$  inflammatory cytokine productions; moreover, the activation of c-Jun N-terminal protein kinase (JNK), extracellular signal-regulated kinases (ERK) mitogen-activated protein kinase (MAPK) and nuclear factor kappa-light-chain-enhancer of activated B cells (NF- $\kappa$ B) via  $ER\beta$  were observed in BPA-induced microglial cells (4). Sukjamnong S and colleagues reported that BPA-exposed maternal rats significantly increased the risk of AD pathological development in offspring by dysregulating genes associated with AD neuropathology and inflammation; moreover, they found that the expression of NF-

$\kappa$ B protein was significantly increased in the offspring hippocampus of BPA-exposed maternal rats (37).

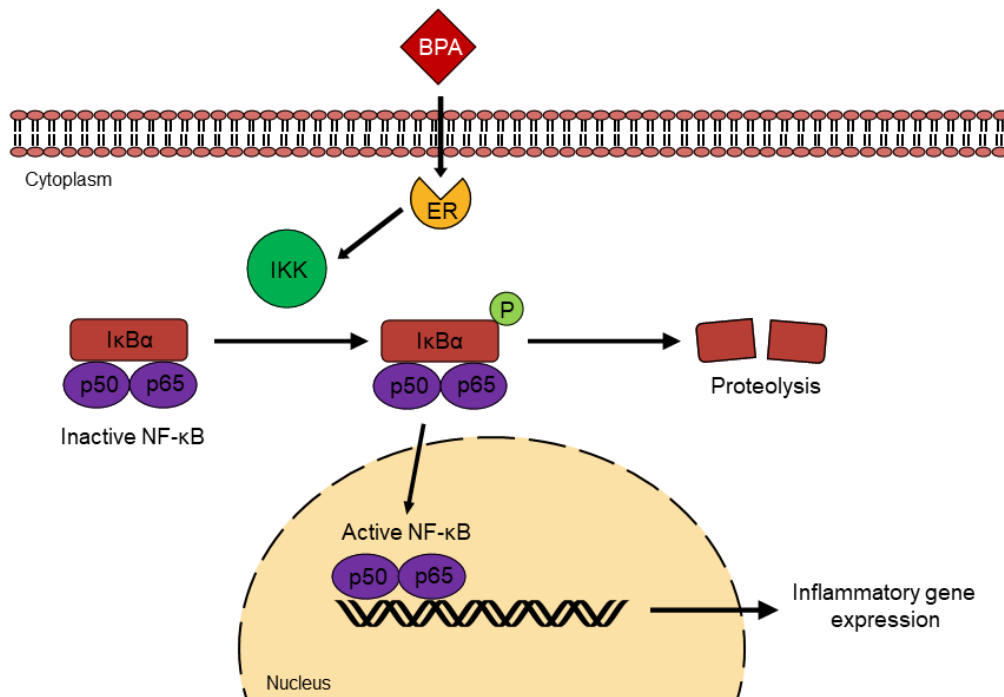


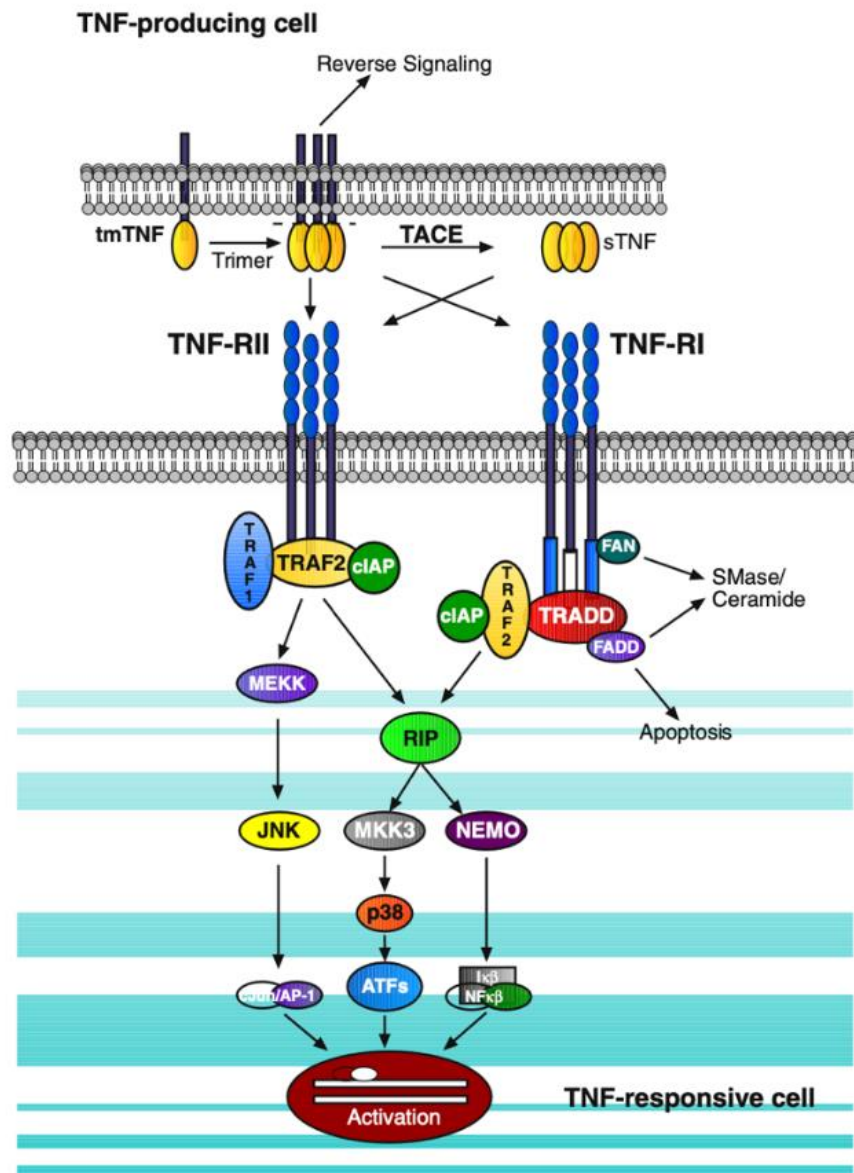
**Figure 8** Bisphenol A involves inflammation via the NF- $\kappa$ B pathway

จุฬาลงกรณ์มหาวิทยาลัย  
CHULALONGKORN UNIVERSITY

#### 4. Roles of TNF- $\alpha$ in neurodegenerative disorders

Tumor necrosis factor-alpha (TNF- $\alpha$ ) plays a crucial role in both the homeostatic and the degenerative processes within the central nervous system (CNS). In a healthy brain, TNF- $\alpha$  regulates synaptic plasticity, cognition, sleep, and food-water intake. In the pathological brain, excessive TNF- $\alpha$  is observed in neurodegenerative diseases such as Parkinson's disease, Alzheimer's disease, and multiple sclerosis (6). TNF- $\alpha$  induces neuronal death through several molecular signaling pathways, namely, the activation of the NF- $\kappa$ B (7), the p38 MAPK (8), the

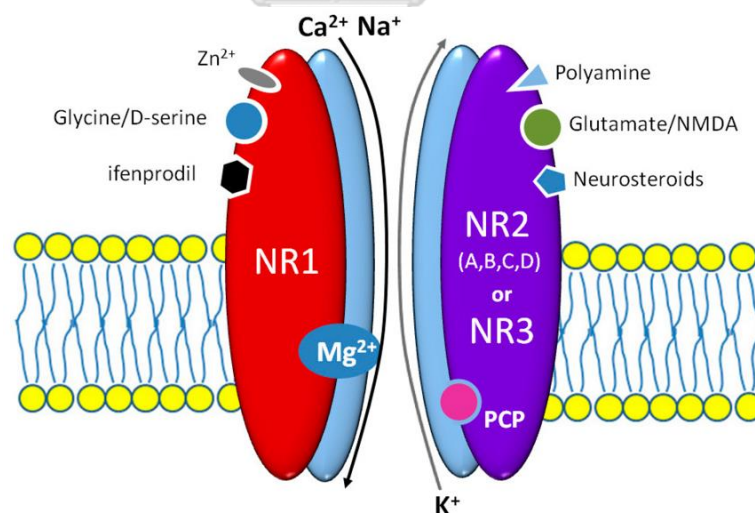
JNK (7), the ceramide/sphingomyelinase (9), and the RIP1/RIP3/MLKL (10, 11) pathways, as well as the suppression of the antioxidant pathway (11).



**Figure 9** The possible mechanism of actions regulated TNF- $\alpha$  signaling in neuronal cells (38)

## 5. The effects of TNF- $\alpha$ on ionotropic glutamate receptors in neurodegenerative disorders

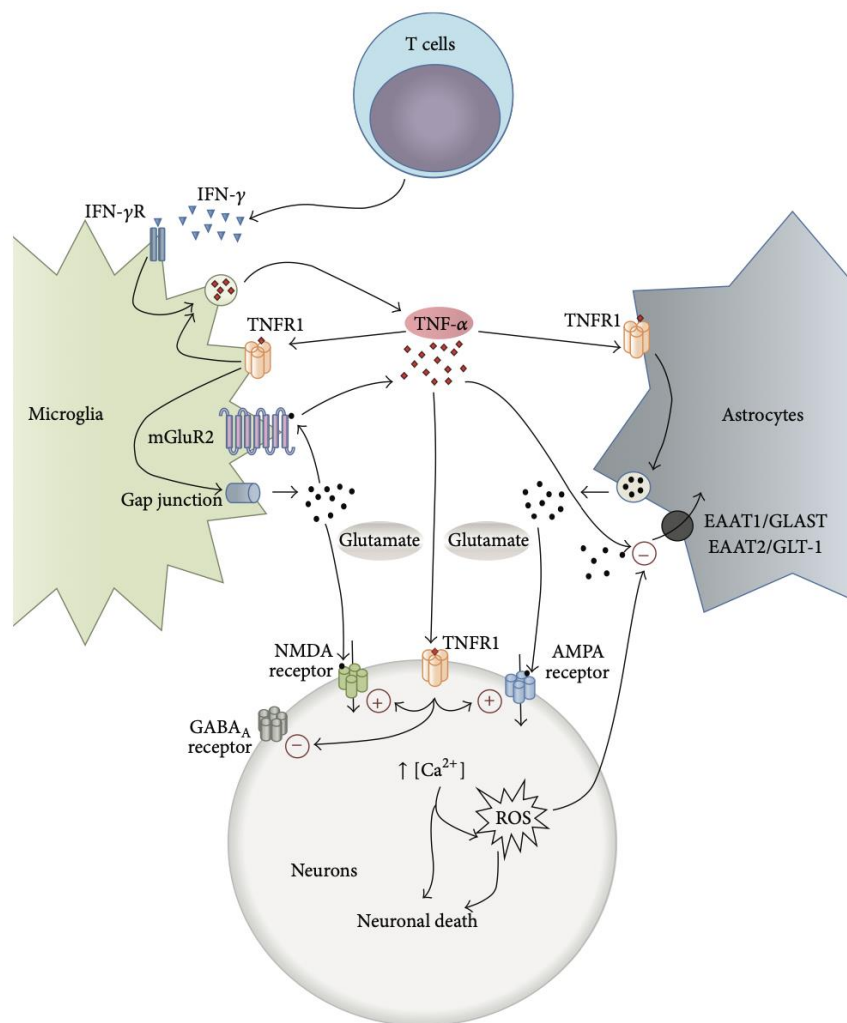
*N*-methyl-D-aspartate (NMDA) receptors are ionotropic glutamate receptors. Seven different subunits of NMDA receptors have been identified, including NR1, NR2A, NR2B, NR2C, NR2D, NR3A, and NR3B. Functional NMDA receptors are heterotetrameric proteins composed of two NR1 subunits and two NR2 or NR3 (39, 40). These four NMDA receptors form an ion channel pore selective for cations, including sodium ( $\text{Na}^+$ ), potassium ( $\text{K}^+$ ), and calcium ( $\text{Ca}^{2+}$ ) (41). NMDA receptors play a crucial role in neurotransmission that promotes synaptic plasticity and the survival of neuronal cells. However, high activation of NMDA receptor signaling leads to excitotoxicity and neuronal death (42, 43).



**Figure 10** Structure of N-methyl-D-aspartate (NMDA) receptors (40)

TNF- $\alpha$  potentiates the localization of the NMDA receptors (12). The overactivation of the ionotropic glutamate receptors dramatically increases the excitatory synaptic strength by inducing the  $\text{Ca}^{2+}$  influx, leading to ROS accumulation

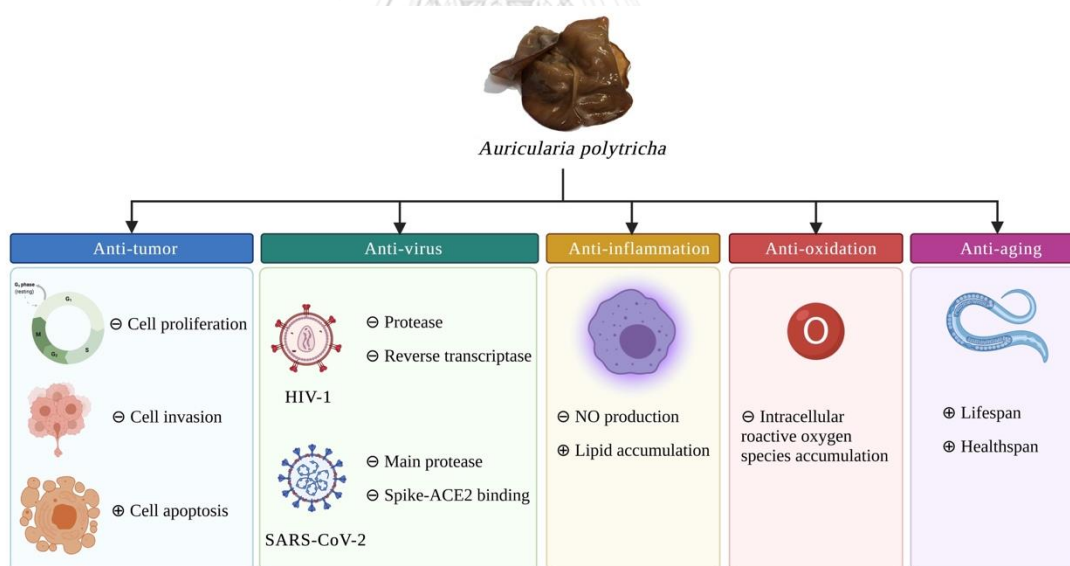
and neuronal death (6). Transcriptional expression of NMDA receptors is regulated by several transcription factors, including the NF- $\kappa$ B family, Jun and Fos families, and early growth response (EGR) family (44). Zhang W *et al* demonstrated that downregulation of EGR-1 expression via inhibiting NMDA receptor subunit 2B (NR2B) in the hippocampus of a mouse model exhibited an antidepressant effect (45).



**Figure 11** The effects of TNF- $\alpha$  on glutamate receptors in neuronal cells (6)

## 6. Medicinal properties of *Auricularia polytricha* (AP)

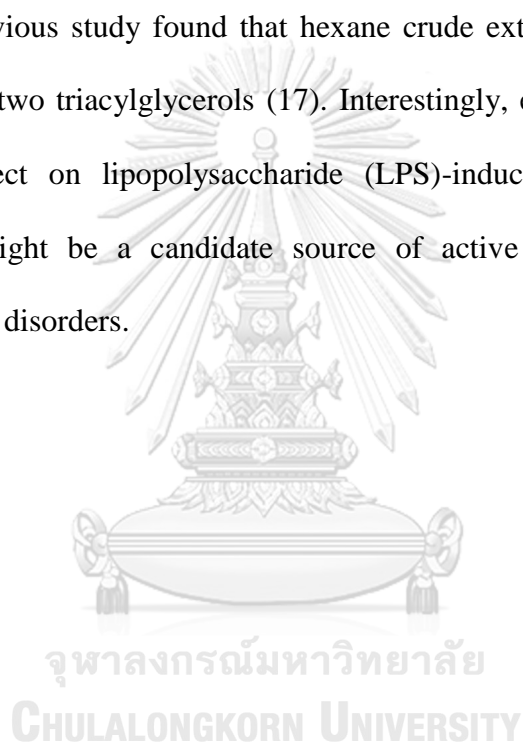
*Auricularia polytricha* (AP), an edible mushroom in the Auriculariaceae family, has been used as a medicinal food (46). Accumulating evidence demonstrated that AP has several medicinal properties such as antioxidant (13), anti-tumor (14, 15), anti-hypercholesterolemic (16), anti-human immunodeficiency virus type-1 (17), and anti-inflammatory (18) activities. Chiu WC *et al* reported that an aqueous extract of AP could protect against nonalcoholic fatty liver disease by attenuating inflammatory response in the rat (18). Our previous study showed that ethanol crude extract of AP ameliorated inflammation of mouse macrophage cell line (RAW264.7 cell line) by reducing nitric oxide production (19). Moreover, AP exhibited *in vitro* inhibition of  $\beta$ -secretase activity against AD (20).



**Figure 12** Medicinal properties of *Auricularia polytricha* extract



Chemical analysis exhibited that several active components were found in AP, such as the phenolics (47, 48), flavonoids (47), terpenoids (17), and polysaccharides (13), depending on the solvent of extraction. Ethanol crude extract is mainly composed of phenolic compounds such as gallic acid and vanillic acid (48). Koyama K and colleagues found cerebroside in methanol crude extract; moreover, they found ceramide, cerevisterol, and 9-hydroxycerevisterol in dichloromethane crude extract of AP (49). Our previous study found that hexane crude extract comprised ergosterol, linoleic acid, and two triacylglycerols (17). Interestingly, ergosterol showed an anti-inflammatory effect on lipopolysaccharide (LPS)-induced microglial cells (21). Therefore, AP might be a candidate source of active components that benefit neurodegenerative disorders.



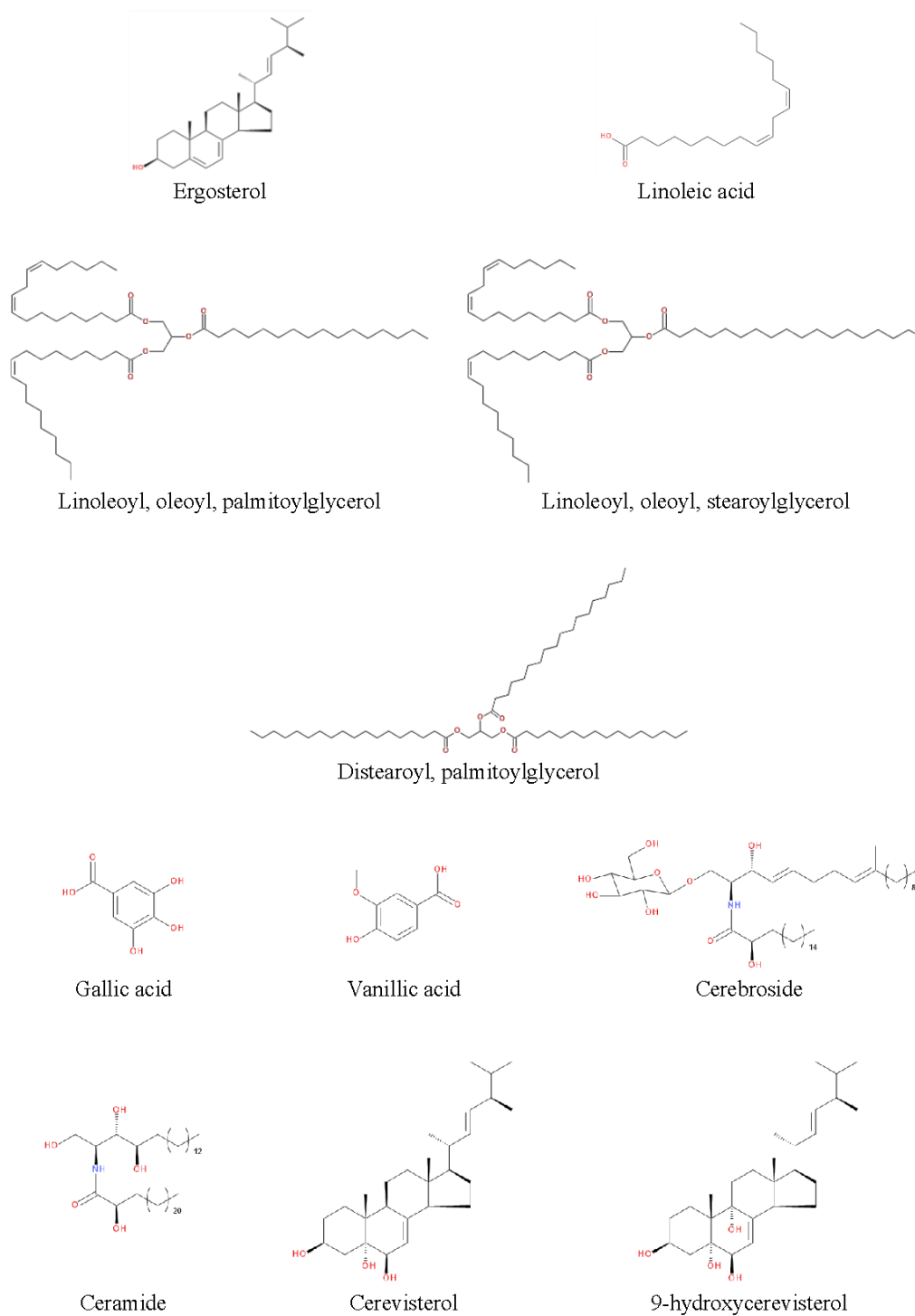


**Figure 13** Chemical constituents found in *A. polytricha* extracts

## 7. Ergosterol

Ergosterol or ergosta-5,7,22-trien-3 $\beta$ -ol is a steroidal triterpene, commonly found in natural sources, especially fungi (50). Ergosterol is the most sterol that existed in the cell membrane of the fungal family, including mushrooms (51, 52). Accumulating data reported that several mushrooms presented high content of ergosterol and provided pharmaceutical properties, as listed in **Table 1**.

**Table 1** List of mushrooms containing ergosterol and their pharmaceutical properties

<b>Mushroom species</b>	<b>Pharmaceutical property</b>	<b>Reference</b>
<i>Agaricus bisporus</i>	Antioxidant and anti-platelet aggregation	(53)
<i>Agaricus blazei</i>	Antioxidant and anti-microbial	(54)
<i>Auricularia auricularia-judae</i>	Antioxidant and anti-platelet aggregation	(53)
<i>Auricularia polytricha</i>	Anti-HIV-1	(17)
<i>Coprinus comatus</i>	Antioxidant and anti-platelet aggregation	(53)
<i>Ganoderma lucidum</i>	Antioxidant anti-platelet aggregation, and anti-cancer	(53, 55)
<i>Grifola frondosa</i>	Anti-allergy	(56, 57)
<i>Hericium erinaceus</i>	Antioxidant and anti-platelet aggregation	(53)
<i>Inonotus obliquus</i>	Anti-inflammation	(58)
<i>Lactarius deliciosus</i>	Antioxidant	(59)
<i>Lactarius sanguifluus</i>	Antioxidant	(59)
<i>Lactarius semisanguifluus</i>	Antioxidant	(59)
<i>Russula delica</i>	Antioxidant	(59)
<i>Lentinula edodes</i>	Antioxidant and anti-platelet aggregation, and anti-hypercholesterolemia	(53, 60)
<i>Monascus anga</i>	Antioxidant	(61)

<i>Neolentinus lepideus</i>	Antioxidant	(62)
<i>Pleurotus citrinopileatus</i>	Antioxidant and anti-hyperlipidemia	(63)
<i>Pleurotus eryngii</i>	Antioxidant and anti-platelet aggregation	(53)
<i>Pleurotus ostreatus</i>	Antioxidant and anti-platelet aggregation	(53)
<i>Pleurotus pulmonarius</i>	Antioxidant	(64, 65)
<i>Poria cocos Wolf</i>	Hepatoprotection	(66)
<i>Rhizopogon luteolus</i>	Antioxidant and anticholinesterase	(67)
<i>Sparassis crispa</i>	Antioxidant	(68)
<i>Suillus bellinii</i>	Antioxidant	(59)

### 7.1. Anti-inflammatory effect of ergosterol

Ergosterol has been reported as an inhibitor of inflammation. Nallathamby *et al* demonstrated that ergosterol could attenuate LPS-induced BV2 microglial cell inflammation by reducing the production of NO, which was generated by iNOS (21). Previous studies reported that ergosterol showed anti-inflammatory activity through NF- $\kappa$ B signaling in several cells, such as human bronchial epidermal cells (16HBE) (69), macrophages (58, 70), lung cells (69, 71), and renal cells (72). Sun *et al* reported that ergosterol exhibited an anti-inflammatory effect by inhibiting the production of inflammatory markers: NO, TNF- $\alpha$ , and IL-6 in cigarette smoke extract-induced 16HBE cells; moreover, ergosterol could reduce the number of inflammatory cells in bronchoalveolar lavage fluid of cigarette smoke extract-induced chronic obstructive pulmonary disease mice models (69). Besides, ergosterol inhibited NO production in LPS-induced macrophages by suppressing NF- $\kappa$ B activity (58). Kobori *et al.* showed that ergosterol could restore the level of TNF- $\alpha$  concentration by inhibiting NF- $\kappa$ B and CCAAT/enhancer binding protein  $\beta$  (C/EBP  $\beta$ ) transcriptional activities and MAPKs activation in LPS-induced macrophages (70). Ergosterol isolated from

*Scleroderma Polyrhizum* Pers., an edible fungus exhibited anti-inflammation in LPS-induced acute lung injury of mice via inhibiting of NF- $\kappa$ B/COX-2/iNOS pathway (71). Furthermore, Liu *et al* demonstrated that the treatment of ergosterol in mice model of diabetic nephropathy could attenuate renal inflammatory responses by reducing pro-inflammatory cytokine expressions in serum and renal tissues via regulation of NF- $\kappa$ B signaling pathway (72).

### **7.2. Antioxidative effect of ergosterol**

The mushroom's membrane is composed of ergosterol, which could be involved in fungi resistance to oxidative stress (73). Ergosterol isolated from *Monascus anka*, an edible mushroom showed anti-lipid peroxidation in hydrogen peroxide (H<sub>2</sub>O<sub>2</sub>)-induced human primary dermal fibroblast (PCS-201-012 cell line) injury (61). Moreover, ergosterol provided a cardioprotective effect in both *in vitro* and *in vivo* models by involving in antioxidative and anti-apoptotic activities through the Nrf2 signaling pathway (74, 75). Sun *et al* have evaluated the antioxidant activity of ergosterol against cigarette smoke extract-induced chronic obstructive pulmonary disease, and have found that ergosterol could increase the levels of certain antioxidant enzymes (such as SOD and catalase), and suppress the levels of malondialdehyde (a highly reactive compound) not only in human bronchial epithelial cells (16HBE cells), but also in BALB/c mice (69). Thus, ergosterol might be a good candidate to consider as a basis for the development of an antioxidant compound.

### **7.3. Drug-likeness and pharmacokinetic properties of ergosterol**

Drug-likeness and pharmacokinetic (ADMET: Absorption, Distribution, Metabolism, Excretion, and Toxicity) properties of ergosterol were computed using the pkCSM pharmacokinetics online server (<https://biosig.lab.uq.edu.au/pkcsm/>) (76).

The predicted values were tabulated in **Table 2 and 3**. According to Lipinski's rule (77), ergosterol was considered as drug-like compound (**Table 2**). Moreover, ergosterol probably crosses the blood-brain barrier (BBB) with predicted BBB permeability (logBB) at 0.767 (**Table 3**); compounds with logBB > 0.3 cross the BBB readily (78). Based on these *in silico* analyses, ergosterol could be used to protect/treat brain disease.

**Table 2** Physicochemical properties of ergosterol

Parameters	Value
Molecular Weight (g/mol)	396.659
LogP	7.3308
Number of rotatable Bonds	4
Number of H-bond acceptors	1
Number of H-bond donors	1
Surface Area	179.295

**Table 3** Pharmacokinetic properties of ergosterol

Property	Model Name	Predicted Value	Unit
<b>Absorption</b>	Water solubility	-6.947	Numeric (log mol/L)
	Caco2 permeability	1.236	Numeric (log Papp in 10 <sup>-6</sup> cm/s)
	Intestinal absorption (human)	95.197	Numeric (% Absorbed)
	Skin Permeability	-2.864	Numeric (log Kp)
	P-glycoprotein substrate	No	Categorical (Yes/No)
	P-glycoprotein I inhibitor	Yes	Categorical (Yes/No)
	P-glycoprotein II inhibitor	Yes	Categorical (Yes/No)

<b>Property</b>	<b>Model Name</b>	<b>Predicted Value</b>	<b>Unit</b>
<b>Distribution</b>	VD <sub>ss</sub> (human)	0.406	Numeric (log L/kg)
	Fraction unbound (human)	0	Numeric (Fu)
	BBB permeability	0.767	Numeric (log BB)
	CNS permeability	-1.705	Numeric (log PS)
<b>Metabolism</b>	CYP2D6 substrate	No	Categorical (Yes/No)
	CYP3A4 substrate	Yes	Categorical (Yes/No)
	CYP1A2 inhibitor	No	Categorical (Yes/No)
	CYP2C19 inhibitor	No	Categorical (Yes/No)
	CYP2C9 inhibitor	No	Categorical (Yes/No)
	CYP2D6 inhibitor	No	Categorical (Yes/No)
	CYP3A4 inhibitor	No	Categorical (Yes/No)
<b>Excretion</b>	Total Clearance	0.564	Numeric (log ml/min/kg)
	Renal OCT2 substrate	No	Categorical (Yes/No)
<b>Toxicity</b>	AMES toxicity	No	Categorical (Yes/No)
	Max. tolerated dose (human)	-0.511	Numeric (log mg/kg/day)
	hERG I inhibitor	No	Categorical (Yes/No)
	hERG II inhibitor	Yes	Categorical (Yes/No)
	Oral Rat Acute Toxicity (LD <sub>50</sub> )	2.05	Numeric (mol/kg)
	Oral Rat Chronic Toxicity (LOAEL)	0.909	Numeric (log mg/kg_bw/day)
	Hepatotoxicity	No	Categorical (Yes/No)
	Skin Sensitisation	No	Categorical (Yes/No)
	T.Pyriformis toxicity	0.639	Numeric (log ug/L)
	Minnow toxicity	-1.77	Numeric (log mM)

## 8. Cell models

### 8.1. Mouse microglial cell line (BV2 cell line)

BV2 is an immortalized microglial cell line derived from murine neonatal microglia and is generally used as a substitute for primary microglia to reduce animal experiments (79). This cell line is widely used as an *in vitro* model for neuroinflammatory research; many inflammatory inducers can activate inflammation of BV2 cells, such as LPS (80), A $\beta$  (32), and BPA (4). This cell line expresses ER $\beta$ , which can be activated by BPA induction (4). Activated microglia were observed in elongated morphology, while inactivated microglia were shown in short-round morphology (81).

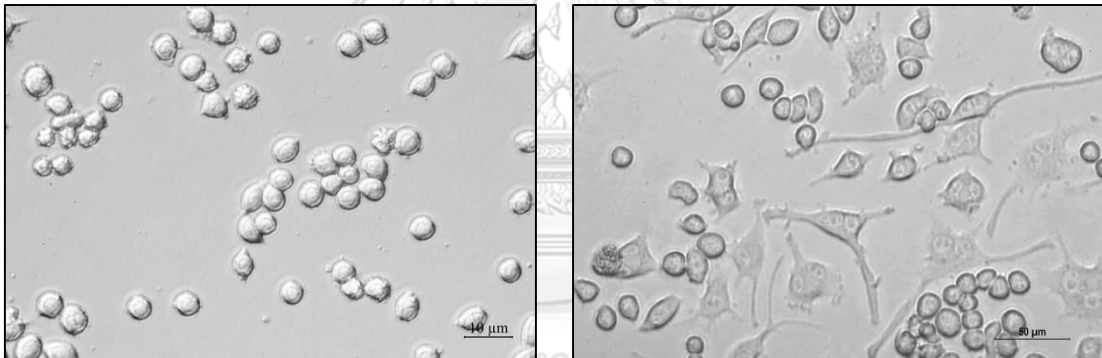


**Figure 14** Morphology of BV2 mouse microglial cells under normal (left) and inflammatory (right) conditions

### 8.2. Mouse hippocampal cell line (HT-22 cell line)

HT-22 cell line is a mouse hippocampal neuronal cell line derived from HT-4 primary mouse hippocampal neuronal tissue, which is immortalized by using a temperature-sensitive small virus-40 T antigen (82). It has been widely used as an *in vitro* model to study cellular processes of neurodegenerative diseases, including



Alzheimer's disease (83). This cell line is susceptible to glutamate; therefore, it is generally used to study glutamate-induced neuronal toxicity (83, 84). Moreover, HT-22 cells have been utilized to examine the toxicity of other neurotoxins such as BPA (85), A $\beta$  (86), and pro-inflammatory cytokines (32). Besides, the A $\beta$  synthesis of neuronal cells has been determined using this *in vitro* cell model (87). Generally, HT-22 cells lack NMDA receptors; however, the expression of NMDA receptors can be induced by using growth factors (88, 89).

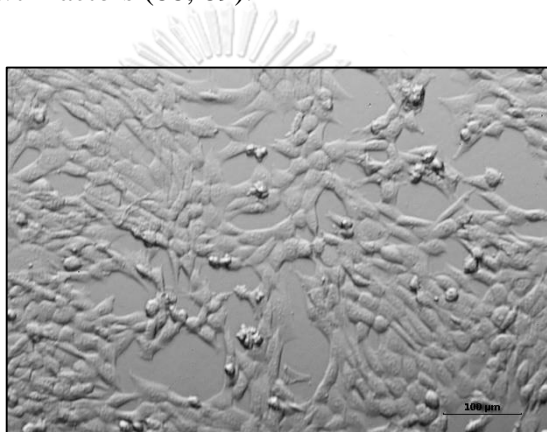


**Figure 15** Typical morphology of HT-22 mouse hippocampal cells

## CHAPTER III

### MATERIALS AND METHODS

#### 1. Laboratory instrument and equipment

-20°C freezer	Panasonic, Osaka, Japan
-80 °C freezer	Eppendorf, Hamburg, Germany
24-well cell culture plate	Corning, Corning, NY, USA
4 °C refrigerator	Sanyo, Osaka, Japan
48-well cell culture plate	Corning, Corning, NY, USA
500 MHz Agilent NMR spectrometer	Agilent Technologies, Santa Clara, CA, USA
6-well cell culture plate	Corning, Corning, NY, USA
96-well cell culture black plate	Corning, Corning, NY, USA
96-well cell culture plate	Corning, Corning, NY, USA
96-well white plate	Corning, Corning, NY, USA
Alliance Q9 mini	Uvitec, Cambridge, UK
Analytical balance	Mettler Toledo, Columbus, OH, USA
Autoclave	Hirayama, Tokyo, Japan
Autopipette 0.2-2 µL	Gilson, Middleton, WI, USA
Autopipette 1-10 µL	Gilson, Middleton, WI, USA
Autopipette 100-1,000 µL	Gilson, Middleton, WI, USA
Autopipette 2-20 µL	Gilson, Middleton, WI, USA

Autopipette 20-200 $\mu$ L	Gilson, Middleton, WI, USA
Beaker (50, 100, 250, 500, and 1,000 mL)	Pyrex, Corning, NY, USA
Biosafety cabinet class II	Labconco, Kansas City, MO, USA
Cell culture dish (35, 60, and 100 mm)	Corning, Corning, NY, USA
Cell culture flask (25 and 75 cm <sup>2</sup> )	Corning, Corning, NY, USA
Cell culture transwell inserts (0.4 $\mu$ m pore size, polyester (PET) membrane for the 24-well plate)	Corning, Corning, NY, USA
CellInsight CX7 HCS instrument	Thermo Fisher Scientific, Waltham, MA, USA
Centrifuge	Hettich, Tuttlingen, Germany
Centrifuge tube (15 and 50 mL)	SPL Life Sciences, Gyeonggi, South Korea
Chromatography glass column	Pyrex, Corning, NY, USA
CO <sub>2</sub> incubator	Thermo Scientific, Waltham, MA, USA
Confocal microscope (Axio Observer.Z1)	Zeiss, Oberkochen, Germany
Cryovial, 2 mL	Corning, Corning, NY, USA
Disposable pasture pipette (1 and 3 mL)	Nest Biotechnology, Wuxi, China
Disposable serological pipette (5, 10, 25, and 50 mL)	SPL Life Sciences, Gyeonggi, South Korea

Ductless fume cabinet	Esco Technologies, St. Louis, MO, USA
EnSpire Plate Reader	Perkin-Elmer, Waltham, MA, USA
Erlenmeyer flask (250, 500, and 1,000 mL)	Pyrex, Corning, NY, USA
Exicycler™ 96 real-time PCR	Bioneer, Daejeon, South Korea
Filtered pipette tip (10, 200, and 1,000 µL)	Corning, Corning, NY, USA
Fluorescence microscope (Axio Observer.A1)	Zeiss, Oberkochen, Germany
Freeze dryer	Thermo Fisher Scientific, Waltham, MA, USA
Fume hood	S.K.Powerable, Samut Sakhon, Thailand
Gas chromatography-Mass spectrometry	Agilent Technologies, Santa Clara, CA, USA
Glass bottle (100, 250, 500, and 1,000 mL)	Pyrex, Corning, NY, USA
Glass cover slip	Paul Marienfeld, Lauda-Königshofen, Germany
Hemocytometer	HBG, Nordrhein-Westfalen, Germany
Hot air oven	Memmert, Schwabach, Germany

Inverted light microscope (Eclipse TS100)	Nikon, Tokyo, Japan
Light microscope (CH30)	Olympus, Tokyo, Japan
Microcentrifuge tube, 1.7 mL	Axygen, Corning, NY, USA
Microscope glass slide	Paul Marienfeld, Lauda-Königshofen, Germany
Mini shaker	Biosan, Riga, Latvia
Mini Trans-Blot <sup>®</sup> Cell	Bio-Rad Laboratories, Hercules, CA, USA
MiniAmp <sup>™</sup> Plus Thermal Cycler	Thermo Fisher Scientific, Waltham, MA, USA
Multichannel pipette (20-200 $\mu$ L)	Gilson, Middleton, WI, USA
Multiskan <sup>™</sup> FC Microplate Photometer	Thermo Scientific, Waltham, MA, USA
Nanodrop 1000 spectrophotometer	Thermo Fisher Scientific, Waltham, MA, USA
Optical sealing film	Bioneer, Daejeon, South Korea
PCR cabinet	Esco Technologies, St. Louis, MO, USA
PCR tube	Bioneer, Daejeon, South Korea
Pipette tip (10, 200, and 1,000 $\mu$ L)	Nest Biotechnology, Wuxi, China
PowerPac <sup>™</sup> HC Power Supply	Bio-Rad Laboratories, Hercules, CA, USA

Rotary evaporator	Heidolph Instruments, Schwabach, Germany
Shaking incubator	Labwit Scientific, Victoria, Australia
Spectroline CM UV-viewing cabinet	Fisher Scientific, Hampton, NH, USA
Sterile syringe filter (0.2 and 0.45 $\mu\text{m}$ )	Corning, Corning, NY, USA
Synergy HTX Multi-Mode Microplate Reader	BioTek, Winooski, VT, USA
Syringe (1, 5, 10, and 20 mL)	Nipro, Mechelen, Belgium
TLC plate silica gel	Merck, Darmstadt, Germany
Ultrapure water system	Merck, Darmstadt, Germany
Vortex mixer	FinePCR, Gyeonggi, South Korea
Water bath	Memmert, Schwabach, Germany

## 2. Chemicals and reagents

1 M Tris-HCl, pH 6.8	Biosesang, Gyeonggi, South Korea
1.5 M Tris-HCl, pH 8.8	Biosesang, Gyeonggi, South Korea
10% SDS Solution	Biosesang, Gyeonggi, South Korea
2,2-Diphenyl-1-picrylhydrazyl (DPPH)	Sigma-Aldrich, St. Louis, MO, USA
2,2'-Azino-bis (3-ethylbenzothiazoline-6-sulfonic acid) diammonium salt (ABTS)	Sigma-Aldrich, St. Louis, MO, USA

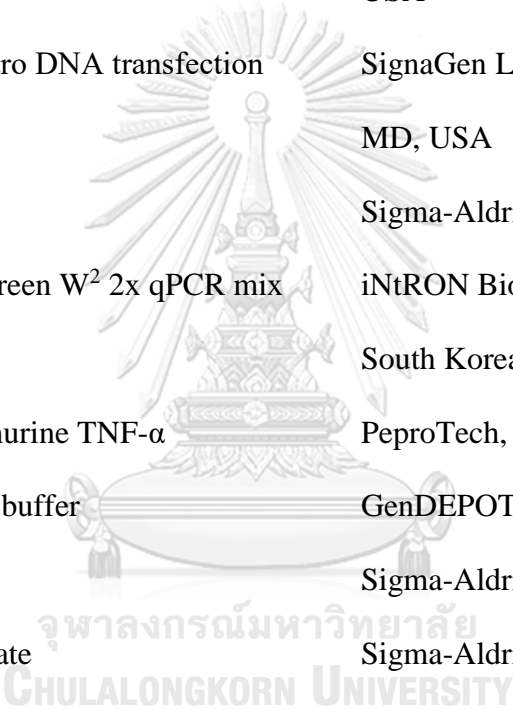
2', 7'-dichlorodihydrofluorescein diacetate (H <sub>2</sub> DCFDA)	Molecular Probes, Eugene, OR, USA
3-(4,5-dimethylthiazol-2-yl)-5-(3-carboxymethoxyphenyl)-2-(4-sulfophenyl)-2H-tetrazolium (MTS) solution	Promega, Madison, WI, USA
3-(4,5-dimethylthiazol-2-yl)-2,5-diphenyltetrazoliumbromide (MTT)	Bio Basic, Markham, ON, Canada
30% Polyacrylamide	Bio-Rad Laboratories, Hercules, CA, USA
4% Paraformaldehyde	Biosesang, Gyeonggi, South Korea
Acetonitrile	Merck, Darmstadt, Germany
Aluminum chloride	Sigma-Aldrich, St. Louis, MO, USA
Ammonium persulfate	Sigma-Aldrich, St. Louis, MO, USA
Anti-actin antibody (C-2) (Cat. #SC-8432)	Santa Cruz Biotechnology, Dallas, TX, USA
Anti-Akt antibody (Cat. #9272S)	Cell Signaling Technology, Danvers, MA, USA
Anti-COX-2 antibody (D-12) (Cat. #SC-166475)	Santa Cruz Biotechnology, Dallas, TX, USA
Anti-CU/ZN SOD rabbit antibody (Cat. #RDI-SODabRx)	Fitzgerald Industries International, Acton, MA, USA

Anti-EGR-1 antibody (588) (Cat. #SC-110)	Santa Cruz Biotechnology, Dallas, TX, USA
Anti-iNOS (D6B6S) rabbit mAb (Cat. #13120S)	Cell Signaling Technology, Danvers, MA, USA
Anti-I $\kappa$ B $\alpha$ (L35A5) mouse mAb (amino-terminal antigen) (Cat. #4814P)	Cell Signaling Technology, Danvers, MA, USA
Anti-NAG-1 polyclonal antibody	Laboratory of signal transduction, College of Veterinary Medicine, Seoul National University, Korea
Anti-NF $\kappa$ B p65 antibody (F-6) (Cat. #SC-8008)	Santa Cruz Biotechnology, Dallas, TX, USA
Anti-NR2B antibody (Cat. #06-600)	Sigma-Aldrich, St. Louis, MO, USA
Anti-phospho-Akt (Ser473) antibody (Cat. #9271S)	Cell Signaling Technology, Danvers, MA, USA
Anti-phospho-I $\kappa$ B $\alpha$ (Ser32) (14D4) rabbit mAb (Cat. #2859P)	Cell Signaling Technology, Danvers, MA, USA
Anti-phospho-GSK-3 $\alpha/\beta$ (Ser21/9) antibody (Cat. #9331S)	Cell Signaling Technology, Danvers, MA, USA
Anti-Rictor (53A2) antibody (Cat. #2114T)	Cell Signaling Technology, Danvers, MA, USA
Ascorbic acid	Sigma-Aldrich, St. Louis, MO, USA
Bisphenol A (BPA)	Sigma-Aldrich, St. Louis, MO, USA
Bovine Serum Albumin	Sigma-Aldrich, St. Louis, MO, USA



Chloroform	Merck, Darmstadt, Germany
Dako Fluorescence Mounting Medium	Dako North America, Carpinteria, CA, USA
DAPI	Sigma-Aldrich, St. Louis, MO, USA
Dimethyl sulfoxide (DMSO)	RCI Labscan, Bangkok, Thailand
Dual luciferase <sup>®</sup> reporter assay system kit	Promega, Madison, WI, USA
Dulbecco's Modified Eagle's Medium (DMEM)	Thermo Scientific HyClone, Logan, UT, USA
Ergosterol	Sigma-Aldrich, St. Louis, MO, USA
Ethanol	Merck, Darmstadt, Germany
Ethyl acetate	Merck, Darmstadt, Germany
Fetal bovine serum (FBS)	Thermo Scientific HyClone, Logan, UT, USA
FITC-conjugated goat anti-mouse IgG secondary antibody	Invitrogen, Eugene, OR USA
Follin-Ciocalteu phenol reagent	Sigma-Aldrich, St. Louis, MO, USA
Gallic acid	Sigma-Aldrich, St. Louis, MO, USA
Glycine	LPS Solution, Daejeon, South Korea
Goat anti-mouse IgG (H+L) secondary antibody, HRP	Invitrogen, Rockford, IL, USA
Goat anti-rabbit IgG (H+L) secondary antibody, HRP	Invitrogen, Rockford, IL, USA

GoTaq <sup>®</sup> Green Master Mix reagent	Promega, Madison, WI, USA
Hanks' Balanced Salt solution (HBSS)	Thermo Scientific HyClone, Logan, UT, USA
Hexane	Merck, Darmstadt, Germany
HiQ Blueye protein ladder	Bio D, Gyeonggi, South Korea
Hoechst 33342	Sigma-Aldrich, St. Louis, MO, USA
HRP-conjugated anti-GAPDH antibody (G-9) (Cat. #SC-365062 HRP)	Santa Cruz Biotechnology, Dallas, TX, USA
HRP-conjugated anti- $\beta$ -actin antibody (C4) (Cat. #SC-47778 HRP)	Santa Cruz Biotechnology, Dallas, TX, USA
Isopropanol	Merck, Darmstadt, Germany
L-glutamic acid	Sigma-Aldrich, St. Louis, MO, USA
Linoleic acid	Sigma-Aldrich, St. Louis, MO, USA
Lipopolysaccharide (LPS) from Escherichia coli O55:B5	Sigma-Aldrich, St. Louis, MO, USA
Maxime RT PreMix Oligo (dT) <sub>18</sub> Primer kit	iNtRON Biotechnology, Gyeonggi, South Korea
Mouse Apoptosis Signaling Pathway Array C1	RayBiotech, Peachtree Corners, GA, USA
Mouse IL-1 beta uncoated ELISA kit	Invitrogen, Waltham, MA, USA
Mouse IL-6 uncoated ELISA kit	Invitrogen, Waltham, MA, USA
Mouse TNF- $\alpha$ uncoated ELISA kit	Invitrogen, Waltham, MA, USA
N-Acetyl cysteine	Sigma-Aldrich, St. Louis, MO, USA



Penicillin-Streptomycin solution	Gibco, Waltham, MA, USA
Phosphate buffered saline (PBS)	Thermo Scientific HyClone, Logan, UT, USA
Pierce™ BCA protein assay kit	Thermo Scientific, Rockford, IL, USA
Pierce™ ECL Western blotting substrate	Thermo Scientific, Rockford, IL, USA
PolyJet™ in vitro DNA transfection reagent	SignaGen Laboratories, Frederick, MD, USA
Quercetin	Sigma-Aldrich, St. Louis, MO, USA
RealMOD™ Green W <sup>2</sup> 2x qPCR mix	iNtRON Biotechnology, Gyeonggi, South Korea
Recombinant murine TNF- $\alpha$	PeptoTech, Cranbury, NJ, USA
RIPA cell lysis buffer	GenDEPOT, Katy, TX, USA
Sodium acetate	Sigma-Aldrich, St. Louis, MO, USA
Sodium carbonate	Sigma-Aldrich, St. Louis, MO, USA
Sodium dodecyl sulfate	Thermo Scientific, Rockford, IL, USA
SuperSignal™ West Femto maximum sensitivity substrate	Thermo Scientific, Rockford, IL, USA
Tetramethylethylenediamine (TEMED)	Biosesang, Gyeonggi, South Korea
Tumor necrosis factor alpha (TNF- $\alpha$ )	PeptoTech, Rocky Hill, NJ, USA

Tris (hydroxymethyl) aminomethane (TRIS)	Biopure Reagents, Seoul, South Korea
Trizol reagent	Invitrogen, Carlsbad, CA, USA
Trypsin-EDTA (0.25%)	Gibco, Waltham, MA, USA
Universal protease inhibitor	Biomax, Seoul, South Korea
Verso cDNA Synthesis kit	Thermo Fisher Scientific, Waltham, MA, USA



### 3. Experimental workflow

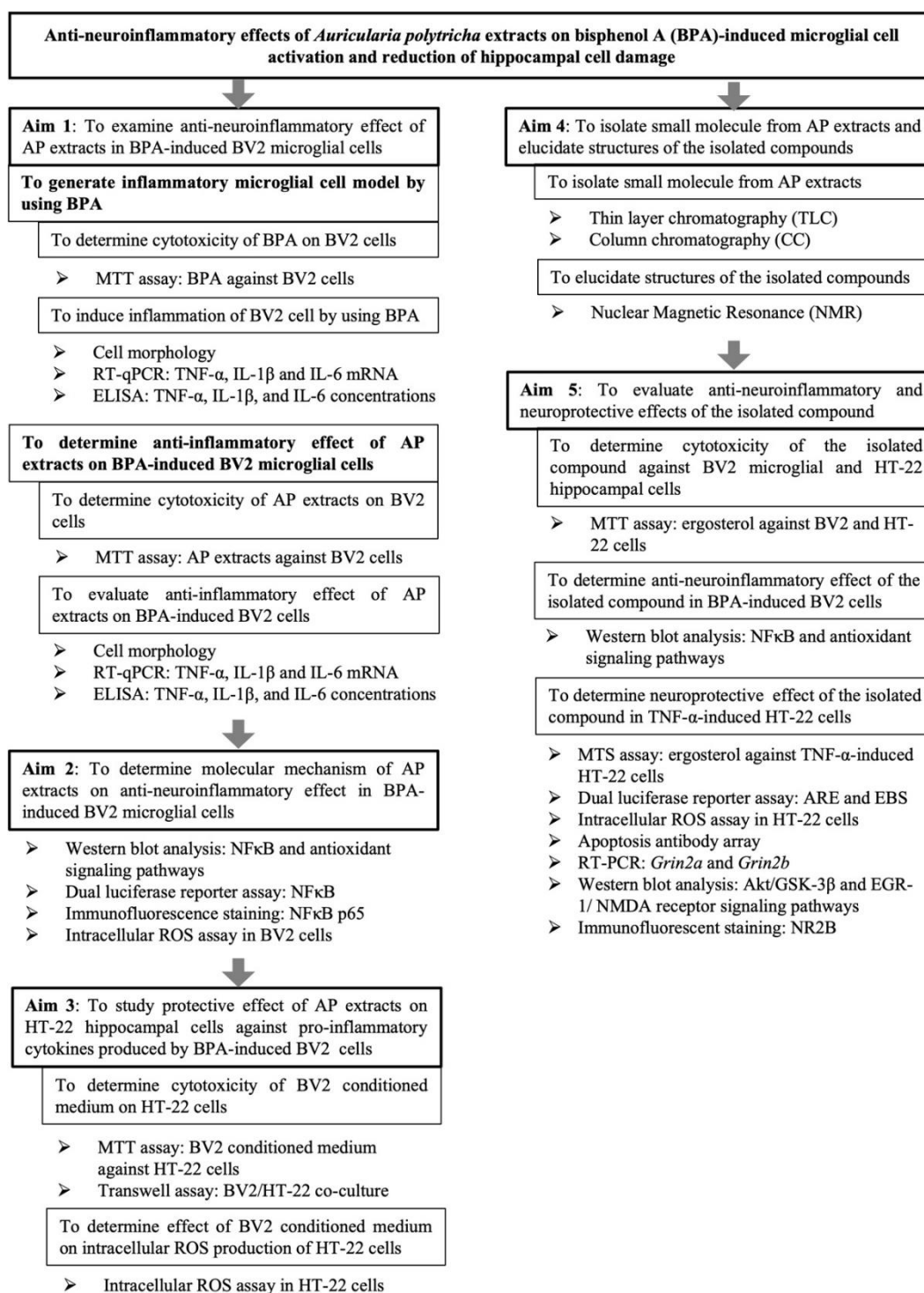


**Figure 16** Experimental workflow

#### 4. Mushroom extract preparation

*Auricularia polytricha* (AP) crude extracts: hexane (APH), ethanol (APE), and water (APW) crude extracts were obtained from our previous study (17). Briefly, the AP mushrooms were grown in the Chang Daeng mushroom farm, Samutprakarn, Thailand (latitude, longitude: 13.68459, 100.58189). The mushroom was identified species by comparing the nucleotide sequence at the internal transcribed spacer (ITS) region to GenBank online database. The fresh AP fruiting bodies were dried and ground into powder. As illustrated in **Figure 17**, the AP powder was extracted by sequential maceration using hexane, ethanol, and water, respectively. The hexane and ethanol extractions were performed at room temperature for 72 h, while the water extraction was conducted at 4 °C for 72 h. APH and APE were concentrated using a rotary evaporator; APW was dried using a freeze dryer. The concentrated AP extracts were aliquoted and stored at -80 °C to avoid the degradation of the extract components.

The extracts were prepared as stock solutions at a concentration of 100 mg/mL, APH and APE were dissolved in absolute dimethyl sulfoxide (DMSO), while APW was prepared in PBS. The dissolved extracts were filtered pass through 0.22 µm of a sterile filter. All prepared extracts were kept at -20 °C until use.

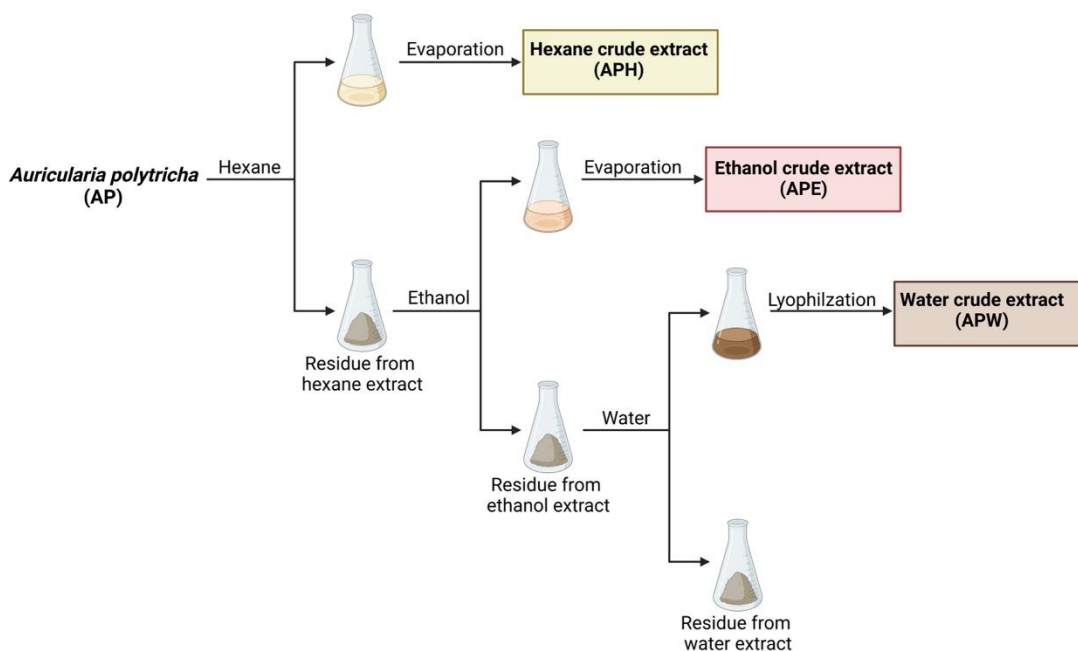


**Figure 17** Schematic diagram showing the sequential maceration of *A. polytricha*

## 5. *In vitro* non-cell-based antioxidant assays

### 5.1. Total phenolic content analysis

The total phenolic content of AP extracts was determined by the Folin-Ciocalteu method (83). Briefly, the extract at 1 mg/mL (50  $\mu$ L) was mixed with the Folin-Ciocalteu's phenol reagent (10%, v/v; 50  $\mu$ L) in a 96-well plate, and then the mixture was incubated in the dark at room temperature for 20 min. Next, 7.5% (w/v) of sodium carbonate ( $\text{Na}_2\text{CO}_3$ , 50  $\mu$ L) was added and further incubated for 20 min. The absorbance at 760 nm was measured by using a microplate reader. Gallic acid was used as a standard compound, and the various concentrations of gallic acid were tested to generate a standard calibration curve. The extract's total phenolic content was calculated using the calibration curve and reported in mg of gallic acid equivalent (GAE)/g dry weight.

## 5.2. Total flavonoid content analysis

Total flavonoid content was examined by the colorimetric aluminium chloride method (83). The extract at 1 mg/mL (50  $\mu$ L) was mixed with 10% (v/v) aluminium chloride ( $\text{AlCl}_3$ , 10  $\mu$ L), 1 M sodium acetate (NaOAc, 10  $\mu$ L), and 95% (v/v) ethanol (150  $\mu$ L). The mixture was incubated in the dark at room temperature for 40 min. Then, the absorbance at 415 nm was measured by using a microplate reader. The total flavonoid content of the extracts was calculated by comparing to the quercetin standard calibration curve. The result was reported in mg of quercetin equivalent (QE)/g dry weight.

## 5.3. Free radical scavenging assays

### 5.3.1. ABTS assay

ABTS solution was prepared by mixing 7 mM of ABTS and 2.45 mM potassium persulfate ( $\text{K}_2\text{S}_2\text{O}_8$ ) and incubated overnight to generate the stable free radical cation ( $\text{ABTS}^{\bullet+}$ ). Then, the 20  $\mu$ L of AP crude extracts (0, 0.5, 1, 2, 4, and 8 mg/mL) was added to 180  $\mu$ L of ABTS solution and placed in the dark for 20 min. The  $\text{ABTS}^{\bullet+}$  was decolorized from green to colorless as the reaction continued, and a microplate reader measured the absorbance at wavelength 734 nm.

### 5.3.1. DPPH assay

DPPH, the stable free radical ( $\text{DPPH}^{\bullet}$ ), was prepared at a 0.2 mM solution in ethanol. After adding the 20  $\mu$ L of sample to 180  $\mu$ L of DPPH solution for 20 min in the dark, the purple DPPH solution was neutralized to yellow. The color reaction was read the absorbance at 517 nm.



The antioxidant capacity of AP crude extracts was calculated by comparing it to the vitamin C calibration curve. The results were expressed in mg of vitamin C equivalent antioxidant capacity (VCEAC)/g dry weight. Various concentrations of AP crude extracts were tested to determine the half-maximal effective concentration (EC<sub>50</sub>) value.

## 6. Cytotoxicity of BPA against BV2 microglial cells

BV2 cells ( $1 \times 10^4$  cells/well) were cultured on a 96-well plate overnight and then treated with BPA at 0.01, 0.1, 1, 10, and 100  $\mu\text{M}$ ; the final volume of culture media was 200  $\mu\text{L}$ . After 24 and 48 h of incubation, MTT (20  $\mu\text{L}$ ) was added to each well of the 96-well plate and further incubated for 3 h. Next, all culture media was removed, and absolute DMSO (200  $\mu\text{L}$ ) was added to dissolve formazan crystal as a final product of the MTT assay. The absorbance at 570 nm was measured by using a microplate reader. The percentage of cell viability was calculated compared to cell control (untreated cell). Ethanol (0.1%, v/v), a solvent used to prepare the BPA stock solution, was tested as vehicle control. The concentrations that do not harm BV2 cell viability (% cell viability > 80%) were used in the following experiments.

$$\% \text{ Cell viability} = \frac{\text{Absorbance of treatment}}{\text{The absorbance of untreated cell control}} \times 100$$

## 7. Neuroinflammatory effects of BPA on BV2 microglial cells

### 7.1. BV2 microglial cell morphological changes against BPA induction

BV2 cells ( $3 \times 10^5$  cells/well) were cultured on a 6-well plate overnight. After that, the cells were treated with BPA at concentrations of 2.5, 5, and 10  $\mu\text{M}$  for 24 h. Cell culture media, ethanol (0.1 %, v/v), and LPS (1  $\mu\text{g}/\text{mL}$ ) were used as untreated, vehicle, and positive controls, respectively. Cell morphological changes were detected under a phase-contrast microscope. Activated microglial cells were observed in ameboid shape, while inactivated microglial cells were shown in round morphology. Numbers of activated and inactivated microglia were counted and reported in the percentage of microglial activation.

$$\% \text{ Microglial activation} = \frac{\text{Number of activated microglia}}{\text{Number of activated microglia} + \text{Number of inactivated microglia}}$$

### 7.2. Pro-inflammatory cytokine mRNA expression of BPA-induced BV2 microglial cells

BV2 cells ( $3 \times 10^5$  cells/well) were grown in a 6-well plate overnight and then treated with BPA (2.5, 5, and 10  $\mu\text{M}$ ) for 24 h. Culture media, ethanol (0.1 %, v/v), and LPS (1  $\mu\text{g}/\text{mL}$ ) were utilized as the untreated, vehicle, and positive controls, respectively. The treated cells were harvested, and total RNA was extracted using Trizol reagent (Invitrogen) following the manufacturer's instruction. The amount of total RNA was measured by using a NanoDrop spectrophotometer (Thermo Scientific™ NanoDrop1000, Waltham, MA, USA). Next, the extracted RNA was

converted to complementary DNA (cDNA) by reverse transcription using the Maxime RT PreMix Oligo (dT)<sub>18</sub> Primer kit (iNtRON Biotechnology). Quantitative real-time PCR (qPCR) was performed using RealMOD™ Green W<sup>2</sup> 2x qPCR mix (iNtRON Biotechnology) by an Exicycler™ 96 (Bioneer). The temperature profile was set as follows: initial denaturation at 95 °C for 10 min, 40 cycles of PCR step at 95 °C for 20 s, and then 58 °C for 40 s. Relative quantification of pro-inflammatory cytokine genes: TNF- $\alpha$ , IL-1 $\beta$ , and IL-6 were calculated using the delta-delta Ct method compared to  $\beta$ -actin, an internal control. All primer sequences used in this study are tabulated in the following table.

**Table 4** List of primers for pro-inflammatory cytokine gene expression

Gene	Nucleotide sequence	Product size (bp)
TNF- $\alpha$ forward	5'-GATCGGTCCCCAAAGGGATG-3'	275
TNF- $\alpha$ reverse	5'-TAGCAAATCGGCTGACGGTG-3'	
IL-1 $\beta$ forward	5'-GAAATGCCACCTTTTGACAGTG-3'	117
IL-1 $\beta$ reverse	5'-CTGGATGCTCTCATCAGGACA-3'	
IL-6 forward	5'-TCTTGGGACTGATGCTGGTG-3'	93
IL-6 reverse	5'-CAGGTCTGTTGGGAGTGGTA-3'	
$\beta$ -actin forward	5'-GGCTGTATTCCCCTCCATCG-3'	154
$\beta$ -actin reverse	5'-CCAGTTGGTAACAATGCCATGT-3'	

### 7.3. Pro-inflammatory cytokine secretion of BPA-induced BV2 microglial cells

To determine the soluble marker of microglia cell activation, the production of pro-inflammatory cytokine was measured using enzyme-linked immunosorbent assay (ELISA). BV2 cells were seeded at a cell density of  $6 \times 10^5$  cells/well in a 6-well plate for 24 h and then treated with the same conditions as the RT-qPCR assay. After 48 h

of treatment, the cell culture media was collected and centrifuged at  $10,000\times g$  for 10 min. Then the culture media was filtered through a  $0.45\ \mu\text{m}$  syringe filter to eliminate the cell debris. The filtered media was used to determine the concentrations of TNF- $\alpha$ , IL-1 $\beta$ , and IL-6 using mouse TNF- $\alpha$ , IL-1 $\beta$ , and IL-6 uncoated ELISA kits (Invitrogen, Thermo Fisher Scientific, Waltham, MA, USA), respectively. These assays were performed according to the manufacturer's instructions.

## **8. Cytotoxicity of AP extracts against BV2 microglial cells**

BV2 cells ( $1\times 10^4$  cells/well) were plated on a 96-well plate overnight and treated with APH, APE, and APW crude extracts at various concentrations: 2.5, 5, 10, and 20  $\mu\text{g/ml}$  for 24 and 48 h. To evaluate the BV2 cell viability, an MTT assay was performed following the above procedure. DMSO (0.1%, v/v) was used as vehicle control for APH and APE extracts. While PBS (0.1%, v/v) was utilized as vehicle control for APW extract. The non-toxic concentrations (cell viability greater than 80%) of AP extracts were selected to test in further experiments.

## **9. Anti-neuroinflammatory effects of AP extracts on BPA-induced BV2 microglial cells**

### **9.1. The effect of AP extracts on BPA-induced BV2 microglial cell morphological changes**

BV2 cells ( $3\times 10^5$  cells/well) were cultured on a 6-well plate overnight. Afterward, the cells were co-treated with BPA and AP extracts (**Table 5**) for 24 h. Cell culture media, BPA (5  $\mu\text{M}$ ), DMSO (0.1%, v/v), and quercetin (0.4 and 0.8  $\mu\text{M}$ )

were tested as untreated, BPA, vehicle, and natural product positive (anti-inflammation) controls, respectively. Cell morphological changes were observed under a phase-contrast microscope.

**Table 5** Treatment conditions for investigation of the anti-neuroinflammatory effect of AP extracts on BPA-induced microglial cells

<b>Condition</b>	<b>Treatment</b>
<b>Untreated cell control</b>	Cell culture media
<b>BPA and vehicle control</b>	BPA (5 $\mu$ M) + DMSO (0.1 %, v/v)
<b>Positive control</b>	BPA (5 $\mu$ M) + Quercetin (0.4 and 0.8 $\mu$ M)
<b>Test</b>	BPA (5 $\mu$ M) + APH (5 and 10 $\mu$ g/mL) BPA (5 $\mu$ M) + APE (2.5 and 5 $\mu$ g/mL) BPA (5 $\mu$ M) + APW (2.5 and 5 $\mu$ g/mL)

### **9.2. The effect of AP extracts on pro-inflammatory cytokine mRNA expression in BPA-induced BV2 microglial cells**

BV2 cells ( $3 \times 10^5$  cells/well) were cultured in a 6-well plate, then treated with AP extracts and BPA (**Table 5**) for 24 h. After that, TNF- $\alpha$ , IL-1 $\beta$ , and IL-6 mRNA expressions were determined by RT-qPCR according to the method previously mentioned.

### **9.3. The effect of AP extracts on pro-inflammatory cytokine secretion in BPA-induced BV2 microglial cells**

BV2 cells ( $6 \times 10^5$  cells/well) were treated following the conditions presented in **Table 5**. After 48 h, the levels of TNF- $\alpha$ , IL-1 $\beta$ , and IL-6 secretion in cell culture supernatant were examined by commercial ELISA kits.

Taken together, the extracts that significantly decrease BPA-induced BV2 microglial cell activation were chosen to study molecular mechanisms furthermore.

## **10. Molecular mechanisms of AP extracts on BPA-induced BV2 microglial activation**

### **10.1. The expression of NF- $\kappa$ B signaling-associated proteins**

The levels of p-I $\kappa$ B $\alpha$ , I $\kappa$ B $\alpha$ , iNOS, COX-2, and  $\beta$ -actin expressions were determined by Western blot analysis. BV2 cells ( $8 \times 10^5$  cells in a 60-mm cell culture dish) were treated with the AP extracts and BPA (**Table 6**) for the optimal time of each protein expression (6 h for p-I $\kappa$ B $\alpha$  and I $\kappa$ B $\alpha$ ; 24 h for iNOS and COX-2). After that, the treated cells were harvested then the total protein was isolated by using a RIPA lysis buffer. The isolated protein concentration was measured by BCA assay. An equal amount of each protein condition was electrophoresed and transferred to the polyvinylidene fluoride (PVDF, 0.22  $\mu$ m of pore size) membrane. The immunoblot was incubated overnight with specific primary antibodies at 4 °C. After that, the HRP-conjugated secondary antibody was probed for an hour at room temperature. The signal was detected using a chemiluminescence substrate and visualized by Alliance Q9 mini (Cambridge, UK). The intensity of target proteins was normalized to  $\beta$ -actin as a loading control.

**Table 6** Treatment conditions for investigation of the molecular mechanism of AP extracts on BPA-induced BV2 microglial activation

<b>Condition</b>	<b>Treatment</b>
<b>Untreated cell control</b>	Cell culture media
<b>BPA and vehicle control</b>	BPA (5 $\mu$ M) + DMSO (0.1 %, v/v)
<b>Positive control</b>	BPA (5 $\mu$ M) + Quercetin (0.4 $\mu$ M)
<b>Test</b>	BPA (5 $\mu$ M) + APH (5 and 10 $\mu$ g/mL) BPA (5 $\mu$ M) + APE (2.5 and 5 $\mu$ g/mL)

### 10.2. Dual luciferase assay of NF- $\kappa$ B activity

BV2 cells ( $5 \times 10^4$  cells/well) were cultured in completed media on a 24-well plate for 24 h. The cultured media was replaced with fresh completed media for an hour prior to the cell transfection process. The cells were transfected with pNF- $\kappa$ B-Luc (500 ng) and pRL-null (50 ng) plasmids using PolyJet™ in vitro DNA transfection reagent for 18 hours. All solution was replaced with fresh completed media and the transfected cells were continuously incubated for 24 h. The transfected cells were co-treated with BPA and AP extracts (**Table 6**) for 6 h. Total protein was harvested, and luciferase assay was performed using a dual luciferase® reporter assay system kit (Promega, WI, USA), according to the manufacturer's protocol.

### 10.3. Nuclear translocation of NF- $\kappa$ B p65

BV2 cells were cultured on  $18 \times 18$  mm cover glass and placed on a 6-well plate at a cell confluence of  $6 \times 10^5$  cells/well for overnight. The cells were exposed to the designed treatments (**Table 7**) for 6 h and then fixed with 4% paraformaldehyde at room temperature for 20 min. The cells were permeabilized by treating with 0.3% Triton X-100 at room temperature for 10 min, followed by a blocking step using 1%

bovine serum albumin (BSA) for an hour. The prepared cells were incubated with anti-NF- $\kappa$ B p65 antibody (1:500), overnight at 4 °C. After that, the slides were incubated with FITC-conjugated goat anti-mouse IgG secondary antibody (1:1,000) prior to DAPI counterstaining. The stained coverslip was mounted with a mounting medium on a glass slide and observed under a confocal microscope. The quantitative ratio of nuclear /cytoplasmic fluorescence intensity was analyzed according to the previous recommendation method using ImageJ software (90).

**Table 7** Treatment conditions for investigation of the NF- $\kappa$ B p65 nuclear translocation of APE extract on BPA-induced BV2 microglial activation

Condition	Treatment
Untreated cell control	Cell culture media
BPA and vehicle control	BPA (5 $\mu$ M) + DMSO (0.1 %, v/v)
Test	BPA (5 $\mu$ M) + APE (5 $\mu$ g/mL)

## 11. Antioxidative effects of AP crude extracts on BV2 microglial cells

### 11.1. Protein expression of SOD-1, antioxidant enzyme

BV2 cells were plated on a 60-mm cell culture dish at a cell density of  $8 \times 10^5$  cells. After growing the cells overnight, the cells were exposed to AP extracts (APH, 5 and 10  $\mu$ g/ mL; APE 2.5 and 5  $\mu$ g/ mL) for 18 h. The total protein was harvested and determined the levels of SOD-1 and  $\beta$ -actin by the Western blotting procedure as described above.

### 11.2. Intracellular reactive oxygen species (ROS) in BV2 cells

BV2 cells ( $1 \times 10^4$  cells/well) were seeded on a 96-well black-plate with clear bottom and cultured overnight then treated with AP extracts in the presence of BPA



(**Table 8**) for 14 h. The treated cells were incubated with H<sub>2</sub>DCFDA (10  $\mu$ M) for 30 min, followed by washing with HBSS. The fluorescence intensity (excitation/emission = 485/535 nm) was measured by using an EnSpire Plate Reader (Perkin-Elmer). Besides, the images of DCF fluorescence were captured by a fluorescence microscope.

**Table 8** Treatment conditions for intracellular ROS assay in BV2 cells and BV2-conditioned medium preparation

Condition	Treatment
Untreated cell control	Cell culture media
BPA/ vehicle control	BPA (5 $\mu$ M) + DMSO (0.1 %, v/v)
Test	BPA (5 $\mu$ M) + APH (5 and 10 $\mu$ g/mL)
	BPA (5 $\mu$ M) + APE (2.5 and 5 $\mu$ g/mL)

## 12. Neuroprotective effects of AP extracts on HT-22 hippocampal cell damage

Previous studies showed that pro-inflammatory cytokines released from microglial cells may contribute to neurodegeneration by inducing apoptosis and cytotoxicity of the neuron (33). Therefore, in this study, we examined the protective effect of AP extracts on HT-22 hippocampal cells against pro-inflammatory cytokine produced by BPA-induced BV2 microglial cells.

### 12.1. Conditioned medium preparation

To prepare BV2 conditioned medium, BV2 cells ( $6 \times 10^5$  cells/well in 6-well plate) were treated with AP extracts and BPA (**Table 8**) for 48 h. The BV2 cell culture supernatant (BV2-conditioned medium) was collected and centrifuged at  $10,000 \times g$ , 4°C for 10 min, and filtered through a 0.45  $\mu$ m syringe filter to remove

cells and cell debris. The BV2-conditioned medium was further used to treat HT-22 hippocampal cells.

### 12.2. HT-22 hippocampal cell viability

HT-22 cells ( $5 \times 10^3$  cells/well) were plated on a 96-well plate overnight then the cells were treated with BV2-conditioned medium for 24 h. After that, HT-22 cell viability was determined by MTT assay.

**Table 9** Treatment conditions for investigation of neuroprotective effects of BV2-conditioned medium against HT-22 hippocampal cell damage

Condition	Treatment	
<b>HT-22 direct treatment</b>	Untreated cell control	Cell culture media
	BPA/ vehicle control	BPA (5 $\mu$ M) + DMSO (0.1 %, v/v)
	Test	BPA (5 $\mu$ M) + APH (5 and 10 $\mu$ g/mL) BPA (5 $\mu$ M) + APE (2.5 and 5 $\mu$ g/mL)
<b>BV2 conditioned medium</b>	Untreated cell control	Cell culture media
	BPA/ vehicle control	BPA (5 $\mu$ M) + DMSO (0.1 %, v/v)
	Test	BPA (5 $\mu$ M) + APH (5 and 10 $\mu$ g/mL) BPA (5 $\mu$ M) + APE (2.5 and 5 $\mu$ g/mL)

### 12.3. Co-culture of BV2 microglial and HT-22 hippocampal cells

To confirm the results of the BV-conditioned medium treatment, we used a transwell co-culture system that allows diffusion of soluble molecules between BV2 cells and HT-22 cells without direct cell-cell contact. HT-22 cells were plated on a 24-well plate at a cell density of  $2 \times 10^4$  cells/well. Next, BV2 cells ( $1 \times 10^5$  cells/well) were seeded in the cell culture transwell inserts (0.4  $\mu$ m pore size, polyester (PET) membrane for the 24-well plate) that were placed on the HT-22 culture plate. The

cells were treated with the conditions shown in **Table 7**. After 24 of treatment, the HT-22 cell viability was determined by MTT assay.

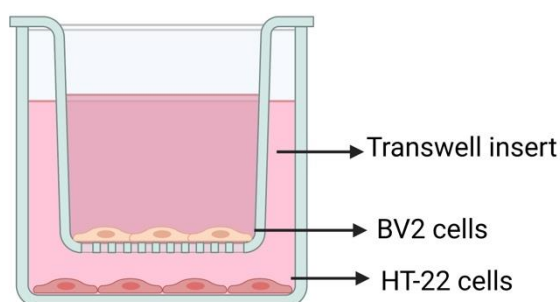


**Figure 18** Schematic of transwell co-culture system between BV2 and HT-22 cells

**Table 10** Treatment conditions for investigation of neuroprotective effects of BV2-conditioned medium against HT-22 hippocampal cell damage using the transwell co-culture system

Condition		Treatment
<b>HT-22 cells</b>	Untreated cell control	Cell culture media
	BPA/ vehicle control	BPA (5 $\mu$ M) + DMSO (0.1 %, v/v)
	Test	BPA (5 $\mu$ M) + APH (10 $\mu$ g/mL)
		BPA (5 $\mu$ M) + APE (5 $\mu$ g/mL)
<b>BV2/ HT-22 cell co-culture</b>	Untreated cell control	Cell culture media
	BPA/ vehicle control	BPA (5 $\mu$ M) + DMSO (0.1 %, v/v)
	Test	BPA (5 $\mu$ M) + APH (10 $\mu$ g/mL)
		BPA (5 $\mu$ M) + APE (5 $\mu$ g/mL)

#### 12.4. Intracellular ROS in HT-22 hippocampal cells

Accumulating data demonstrated that pro-inflammatory cytokines produced from microglial activation may upregulate a production of intracellular reactive

oxygen species (ROS) that can induce neuronal death (33). Herein, we studied an inhibitory effect of AP extracts on the ROS production in HT-22 cells activated by pro-inflammatory cytokines released from BPA-induced BV2 cells. HT-22 cells ( $1 \times 10^4$  cells/well) were seeded on a 96-well black plate with clear bottom and cultured overnight. The cultured cells were treated with a BV2-conditioned medium (**Table 8**) for 14 h. After treatments, the level of intracellular ROS in HT-22 cells was examined by using H<sub>2</sub>DCFDA, according to the protocol mentioned above.

### **13. Chemical compound isolation**

#### **13.1. Thin-layer chromatography (TLC)**

APE crude extract was dissolved in DMSO, then applied on a TLC plate (silica gel 60 F<sub>254</sub> aluminum sheet). The TLC plate was run in hexane: ethanol (100: 0 to 50: 50) to develop an optimal mobile phase system. The isolated spots were visualized under UV light (254 and 365 nm) and iodine vapor staining.

#### **13.2. Column chromatography (CC)**

Chemical constituents in APE crude extracts were separated by column chromatography using silica gel 60 (0.063 – 0.200 mm). The sample was eluted with gradient mobile system of hexane/ethyl acetate (80/20) to ethanol/DMSO (20/80). The eluents were collected in the test tube, then the collected eluents were screened the purity by TLC. The fractions that contained the same eluted compound were pooled and concentrated by the rotary evaporator.

### 13.3. Crystallization

The fraction E was crystallized by absolute hexane at room temperature to get fraction E1 (APE-E1) as a white needle crystal.

## 14. Chemical compound identification

### 14.1. Thin-layer chromatography (TLC) of APH and APE-1

According to our previous study, chemical constituents in APH were fully identified (17). Therefore, the TLC profile of APE-E1 was performed using silica gel 60 F254 aluminum sheet and developed in hexane/ethyl acetate (80/20) comparing to the TLC profile of APH.

### 14.2. Nuclear magnetic resonance (NMR)

The  $^1\text{H}$  NMR spectroscopy of the isolated compound was performed using a 500 MHz Agilent NMR spectrometer. The compound was dissolved in deuterated chloroform ( $\text{CDCl}_3$ ), and tetramethylsilane (TMS) was used as an internal reference.

จุฬาลงกรณ์มหาวิทยาลัย  
CHULALONGKORN UNIVERSITY

## 15. Anti-neuroinflammatory effects of ergosterol against BPA-induced BV2 cells

### 15.1. Cytotoxicity of ergosterol against BV2 microglial cells

BV2 cells ( $1 \times 10^4$  cells/well) were plated on a 96-well plate overnight and treated with ergosterol at concentrations of 25, 50, 100, and 200 nM for 24. After incubation, an MTT assay was performed following the procedure described above.

### **15.2. The expression of NF- $\kappa$ B signaling-associated proteins**

BV2 cells were plated on a 60 mm cell culture dish at a cell density of  $8 \times 10^5$  cells. The cells were exposed to BPA in the presence or absence of ergosterol (25 and 50 nM) for 6 and 24 h to determine the protein levels of p-I $\kappa$ B $\alpha$ /I $\kappa$ B $\alpha$  and iNOS, respectively. Western blot analysis was performed according to previously mentioned protocol.

## **16. Neuroprotective effects of AP crude extracts against TNF- $\alpha$ -induced HT-22 hippocampal cells**

### **16.1. Cytotoxicity of TNF- $\alpha$ and ergosterol against HT-22 cells**

HT-22 cells ( $5 \times 10^3$  cells/well) were plated on 96-well plates overnight before them being treated with TNF- $\alpha$  (1, 10, and 100 ng/mL) or ergosterol (0.01, 0.1, 1, and 10  $\mu$ M) for 24 h. After treatment, the cells were incubated with the MTS reagent for 1 h, and then the absorbance was measured at 490 nm by using a microplate reader (Multiskan<sup>TM</sup> FC Microplate Photometer, Thermo Scientific, Waltham, MA, USA).

### **16.2. Neuroprotective effect of ergosterol on TNF- $\alpha$ -induced HT-22 cells**

HT-22 cell were cultured on 96-well plates at cell density of  $5 \times 10^3$  cells/well overnight. The cells were exposed to TNF- $\alpha$  (1 ng/mL) in the presence or absence of ergosterol (0.01, 0.1, and 1  $\mu$ M) for 24 h. After treatments, the HT-22 cell viability was determined by MTS assay.

## **17. Antioxidative effects of AP crude extracts on HT-22 hippocampal cells**

### **17.1. Protein expression of SOD-1, antioxidant enzyme**

HT-22 cells ( $5 \times 10^5$  cells) were seeded on 60-mm cell culture dishes overnight. The cells were treated with TNF- $\alpha$  (1 ng/mL) in the presence or absence of ergosterol (100 nM). After 18 h of incubation, total protein was harvested, and the level of SOD-1 expression was measured by Western blot analysis.

### **17.2. The antioxidant response element (ARE) activity**

HT-22 cells were cultured overnight in a complete medium, in 24-well plates, at a cell density of  $1 \times 10^4$  cells/well. Before transfection, the culture medium was replaced with fresh medium for 1 h. HT-22 cells were co-transfected with pARE-Luc and pRL *Renilla* Luciferase control reporter (pRL-null) plasmids by using the PolyJet™ *in vitro* DNA transfection reagent (SignaGen Laboratories, Frederick, MD, USA). After 18 h of transfection, the transfected solution was replaced with fresh medium, and then the cells were further incubated for 6 h. The transfected HT-22 cells were treated with TNF- $\alpha$  (1 ng/mL) in the presence or absence of ergosterol (100 nM) for 24 h. The total protein was extracted, and the luminescence intensity was detected by using a Dual-Luciferase® Reporter Assay System kit (Promega, Madison, WI, USA). The luminescence intensity of the target (firefly luciferase) was normalized with the luminescence intensity of the control reporter (*Renilla* luciferase), and the luminescence was measured by using a luminometer (Synergy HTX Multi-Mode Microplate Reader, BioTek, Winooski, VT, USA).

### **17.3. Intracellular ROS assay in HT-22 cells**

HT-22 cells were plated on 96-well black plates at a cell density of  $1 \times 10^4$

cells/well, and were allowed to grow overnight. The cells were then treated with TNF- $\alpha$  (1 ng/mL) in the presence or absence of ergosterol (100 nM) for 14 h. The treated cells were washed with HBSS, and were subsequently incubated with H<sub>2</sub>DCFDA (10  $\mu$ M) in serum-free medium, for 30 min. The cells were washed with HBSS twice and their fluorescence intensity was measured at 485/535 nm (excitation/emission) by using a Synergy HTX Multi-Mode Microplate Reader (BioTek, Winooski, VT, USA).

A high-content screening (HCS) platform was used to visualize and analyze the HT-22 cells' intracellular ROS. The cells were cultured on a 48-well plate and were then treated with TNF- $\alpha$  (1 ng/mL) in the presence or absence of ergosterol (100 nM) for 14 h. Subsequently, the cells were stained with H<sub>2</sub>DCFDA (10  $\mu$ M) and Hoechst 33342 (10  $\mu$ g/mL) for 30 min. The stained cells were captured and analyzed by using the CellInsight CX7 HCS instrument (Thermo Fisher Scientific, Waltham, MA, USA).

## **18. Molecular mechanism of AP extracts against TNF- $\alpha$ -induced HT-22 hippocampal cells**

### **18.1. Apoptosis antibody array**

HT-22 cells were seeded on 60-mm dishes at a cell density of  $5 \times 10^5$  cells. After allowing the cells to grow overnight, the cells were treated with TNF- $\alpha$  (1 ng/mL) in the presence or absence of ergosterol (100 nM) for 24 h. The treated cells were lysed with a lysis buffer containing a protease inhibitor cocktail and a phosphatase inhibitor cocktail, and the total protein was collected. The assay was performed by using the Mouse Apoptosis Signaling Pathway Array C1 (RayBiotech,



Peachtree Corners, GA, USA) according to the manufacturer's protocol. The chemiluminescence signal was detected by using the Alliance Q9 mini imager (Cambridge, UK).

### **18.2. The expression of Akt/ GSK-3 $\beta$ signaling-associated proteins**

HT-22 cells ( $5 \times 10^5$  cells) were seeded on 60-mm cell culture dishes overnight. The cells were treated with TNF- $\alpha$  (1 ng/mL) in the presence or absence of ergosterol (100 nM). After 24 h of incubation, total protein was harvested, and the levels of pAkt (S473), Akt, RICTOR, GSK-3 $\beta$  (S9), NAG-1, and  $\beta$ -actin expressions was measured by Western blot analysis.

### **18.3. The mRNA expression of NMDA receptors**

HT-22 cells ( $1 \times 10^5$  cells/well) were plated on 6-well plates overnight. The cells were treated with TNF- $\alpha$  (1 ng/mL) in the presence or absence of ergosterol (100 nM) for 24 h. The total mRNA was extracted by using the TRIZol reagent according to the manufacturer's instructions. After that, the mRNA was converted to cDNA by using a Verso cDNA Synthesis Kit (Thermo Fisher Scientific, Waltham, MA, USA). The glutamate ionotropic receptor NMDA type subunit 2A (*Grin2a*) and 2B (*Grin2b*) genes were amplified using the primer pairs listed in **Table 11**. Moreover, the glyceraldehyde 3-phosphate dehydrogenase (*Gapdh*) gene was used as a reference gene. The RT-PCR was performed by using the GoTaq<sup>®</sup> Green Master Mix reagent (Promega, Madison, WI, USA) and the MiniAmp<sup>™</sup> Plus Thermal Cycler (Thermo Fisher Scientific, Waltham, MA, USA).

**Table 11** List of primers for glutamate ionotropic receptor NMDA type gene expression

Gene	Nucleotide sequence	Product size (bp)
<i>Grin2a</i> forward	5'-TTGAACTACAAGGCCGGGAG-3'	546
<i>Grin2a</i> reverse	5'-GTCCATTCGCGAGGAGTTCA-3'	
<i>Grin2b</i> forward	5'-GGGTCACGCAAACCCTTTC-3'	591
<i>Grin2b</i> reverse	5'-ACTGAGGCCCGTTCTATCCT-3'	
<i>Gapdh</i> forward	5'-GACCACAGTCCATGCCATCACT-3'	453
<i>Gapdh</i> reverse	5'-TCCACCACCCTGTTGCTGTAG-3'	

#### 18.4. The EGR-1 activity

To determine the EGR-1 activity, dual luciferase reporter assay was performed by using a luciferase construct containing an EGR-1 binding site (EBS). Briefly, HT-22 cells were cultured overnight in a complete medium, in 24-well plates, at a cell density of  $1 \times 10^4$  cells/well. Before transfection, the culture medium was replaced with fresh medium for 1 h. HT-22 cells were co-transfected with pEBS-Luc and pRL *Renilla* Luciferase control reporter (pRL-null) plasmids by using the PolyJet™ *in vitro* DNA transfection reagent (SignaGen Laboratories, Frederick, MD, USA). After 18 h of transfection, the transfected solution was replaced with fresh medium, and then the cells were further incubated for 6 h. The transfected HT-22 cells were treated with TNF- $\alpha$  (1 ng/mL) in the presence or absence of ergosterol (100 nM) for 24 h. Then, the dual luciferase reporter assay was performed following the procedure mentioned above.

#### 18.5. EGR-1 overexpression in HT-22 hippocampal cells

HT-22 cells were seeded on 6-well plates at a cell density of  $1 \times 10^5$  cells/well, and were allowed to grow overnight. The cells were transfected with a

pCDNA3.1/V5-His EGR1 plasmid by using a PolyJet™ *in vitro* DNA transfection reagent (SignaGen Laboratories, Frederick, MD, USA). The pLacZ plasmid was used as a negative plasmid control. After 18 h of transfection, the transfected mixture was replaced with fresh complete medium, and the cells were further incubated for 30 h. The expression of EGR-1 was determined by Western blotting with the help of an anti-EGR-1 antibody. The following primers were used for the determination of the EGR-1 gene expression with the use of RT-PCR: 5'-ACCCCTTGCTCCCTTCAATG-3' (forward) and 5'-GGTGAGCATGTCCCTCACAA-3' (reverse).

#### **18.6. Protein expression of NMDA receptor**

HT-22 cells ( $5 \times 10^5$  cells) were seeded on 60-mm cell culture dishes overnight. The cells were treated with TNF- $\alpha$  (1 ng/mL) in the presence or absence of ergosterol (100 nM). After 24 h of incubation, total protein was harvested, and the levels of NR2B and  $\beta$ -actin expressions was measured by Western blot analysis.

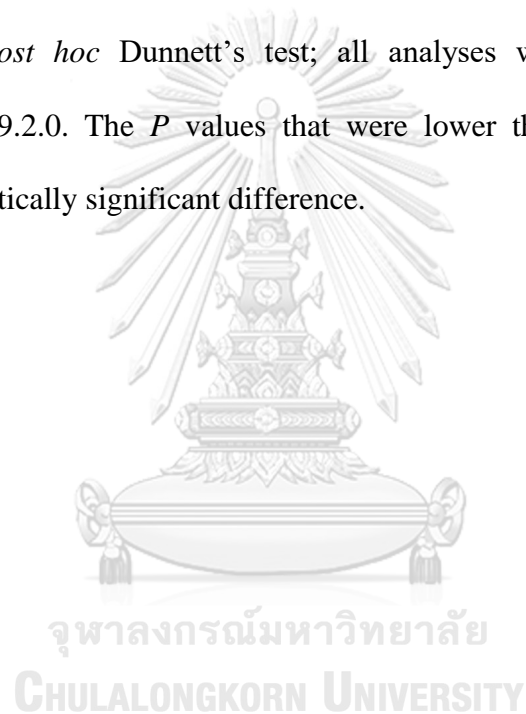
#### **18.7. Immunofluorescence staining of NR2B**

HT-22 cells were cultured on  $18 \times 18$  mm cover glass and placed on a 6-well plate at a cell density of  $1 \times 10^5$  cells/well overnight. The cells were exposed to the TNF- $\alpha$  (1 ng/mL) in the presence or absence of ergosterol (100 nM) for 24 h and then fixed with 4% paraformaldehyde at room temperature for 20 min. The cells were permeabilized by treatment with 0.3% Triton X-100 at room temperature for 10 min, followed by blocking with 1% bovine serum albumin for an hour. The prepared cells were incubated with anti-NR2B antibody (1:500) overnight at 4 °C. The slides were then incubated with FITC-conjugated goat anti-mouse IgG secondary antibody

(1:1,000) prior to DAPI counterstaining. The stained coverslips were mounted on a glass slide with a mounting medium and observed under a confocal microscope.

## 19. Statistical analysis

The results are presented as the mean  $\pm$  standard error mean (SEM) of three independent experiments. Statistical significance was analyzed by one-way ANOVA, followed by a *post hoc* Dunnett's test; all analyses were performed by using GraphPad Prism 9.2.0. The *P* values that were lower than 0.05 were considered indicative of statistically significant difference.



## CHAPTER IV

### RESULTS

#### 1. Total phenolic and flavonoid contents present in AP crude extracts

AP was extracted by sequential maceration using solvents in increasing polarity; three crude extracts were obtained, including hexane (APH), ethanol (APE), and water (APW) crude extracts (17). The total phenolic and flavonoid contents in these three crude extracts were analyzed using Folin-Ciocalteu and aluminium chloride methods, respectively. The phenolic content analysis indicated that APW ( $33.66 \pm 0.14$  mg GAE/g dry weight) contained the highest level of phenolic compounds, followed by APE ( $12.95 \pm 0.12$  mg GAE/g dry weight) and APH ( $1.90 \pm 0.03$  mg GAE/g dry weight), respectively (**Figure 19A**). APE ( $4.01 \pm 0.75$  mg QE/g dry weight) exhibited the highest quantity of flavonoid content. In contrast, the flavonoid content was almost undetectable in APH and APW (**Figure 19B**).

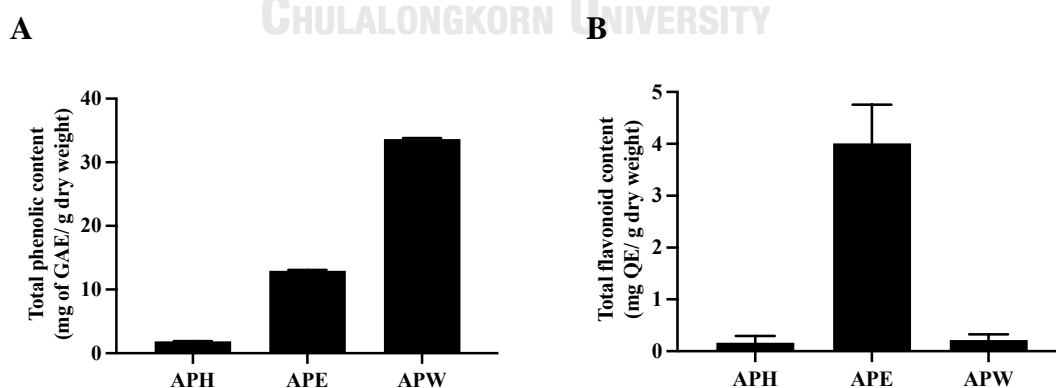


**Figure 19** Total (A) phenolic and (B) flavonoid contents exist in AP crude extracts. All data are shown as the mean  $\pm$  SEM of triplicate values.

## 2. Free radical scavenging activity of AP crude extracts

The antioxidant properties of AP crude extracts were studied by using ABTS and DPPH assays. Both assays relied on the capacity of the extracts to scavenge the free radicals and neutralize the reaction. As shown in **Table 12**, APH, APE, and APW had antioxidant capacity values of  $0.92 \pm 0.12$ ,  $1.57 \pm 0.04$ , and  $2.47 \pm 0.06$  mg VCEAC/g dry weight in ABTS assay, respectively. Statistical analysis indicated that APW had significantly higher ABTS scavenging activity compared to APH. Besides, APW showed the highest DPPH scavenging activity ( $1.88 \pm 0.25$  mg VCEAC/g dry weight), followed by APE ( $1.27 \pm 0.04$  mg VCEAC/g dry weight) and APH ( $0.99 \pm 0.08$  mg VCEAC/g dry weight). All extracts exhibited significant differences in DPPH scavenging activity compared to each extract.

The half-maximal effective concentration ( $EC_{50}$ ) values of APE and APW in the ABTS assay were  $3.11 \pm 0.05$  and  $1.06 \pm 0.04$  mg/mL, respectively. For the DPPH assay,  $EC_{50}$  values of APE and APW were  $12.61 \pm 3.47$  and  $3.62 \pm 0.35$  mg/mL, respectively. However, at up to 8 mg/ml, APH showed no activity in both assays. Its accurate  $EC_{50}$  was not obtainable. In comparison, APW is the most potent extract among the three AP extracts.

**Table 12** Antioxidant capacity and half-maximal effective concentration (EC<sub>50</sub>) of free radical scavenging activity of AP crude extracts.

Crude extract	ABTS scavenging activity		DPPH scavenging activity	
	mg VCEAC/g dry weight	EC <sub>50</sub> (mg/mL)	mg VCEAC/g dry weight	EC <sub>50</sub> (mg/mL)
	APH	0.92 ± 0.12 <sup>a</sup>	> 8	0.99 ± 0.08 <sup>a, b</sup>
APE	1.57 ± 0.04	3.11 ± 0.05	1.27 ± 0.04 <sup>a, c</sup>	12.61 ± 3.47
APW	2.47 ± 0.06 <sup>a</sup>	1.06 ± 0.04	1.88 ± 0.25 <sup>b, c</sup>	3.62 ± 0.35

The data are expressed as mean ± SEM (n = 3). The same superscript letters in the same column indicate a significant difference between the means by one-way ANOVA ( $P < 0.05$ ).

### 3. Effects of BPA on BV2 microglial cells

#### 3.1. Cytotoxicity of BPA against BV2 microglial cells

An optimal dose of BPA on the cell model was determined by testing the cytotoxicity of BPA against mouse microglia BV2 cells at a range of concentrations (0.1-100 μM) of BPA using MTT assay. The results showed that 100 μM BPA significantly decreased BV2 cell viability after treatment for 24 and 48 h. However, BPA concentrations ranging from 0.1 μM to 10 μM did not have any significant effect on BV2 cells, and they exhibited cell viability of greater than 80% (**Figure 20**). Therefore, BPA concentrations lower than or equal to 10 μM were used in the subsequent experiments.

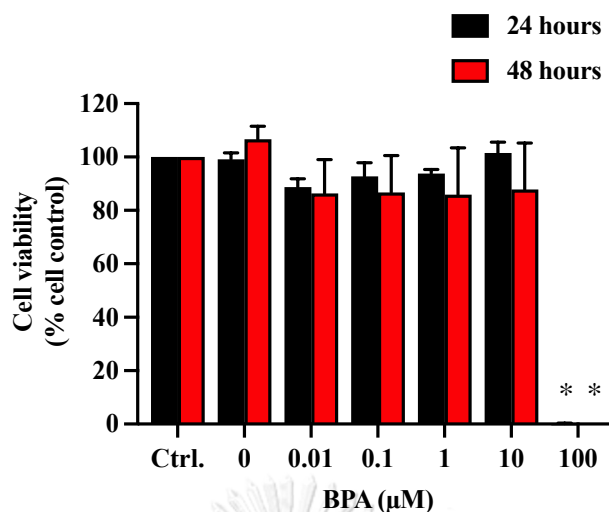


**Figure 20** Cytotoxicity of BPA in BV2 microglial cells at 24 and 48 h.

All data are shown as the mean  $\pm$  SEM of triplicate values. Statistical significance was analyzed by one-way ANOVA, Dunnett's test. \*  $P < 0.05$  versus the media control.

### 3.2. Neuroinflammatory effects of BPA on BV2 microglial cells

BV2 cells were treated with BPA (2.5, 5, and 10  $\mu$ M) for 24 h, and then changes in cell morphology were observed under a phase-contrast microscope. Short-round morphology and elongated morphology indicate inactivated and activated BV2 cells, respectively (81). Cells in the media control exhibited mostly round cell morphology, while LPS (1  $\mu$ g/mL) control showed an increase in the number of elongated cells. In addition, 5 and 10  $\mu$ M BPA significantly increased the number of elongated cells compared to the media control (**Figure 21A and 21B**). These results suggest that BPA at 5 and 10  $\mu$ M concentrations could induce microglial cell activation.



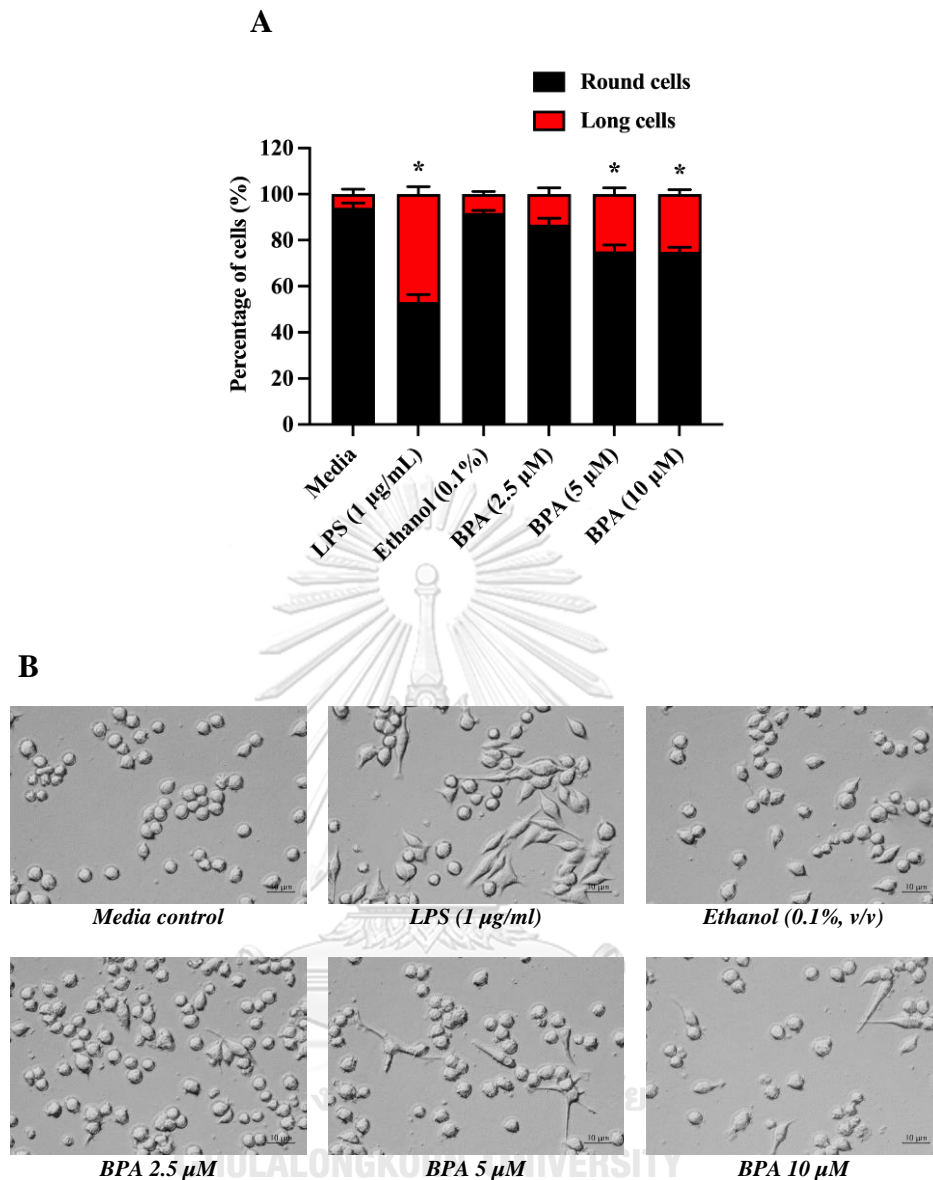


**Figure 21** Neuroinflammatory effects of BPA on BV2 microglial cells.

(A) Percentage of BV-2 long and round cells when exposed to various concentrations of BPA. (B) BV2 cell morphological changes after treated with media, LPS (1 µg/mL), 0.1 %, v/v ethanol, and BPA (2.5, 5, and 10 µM) observed under DIC microscope (10×). All data are shown as the mean ± SEM of triplicate values. Statistical significance was analyzed by one-way ANOVA, Dunnett's test. \*  $P < 0.05$  versus the media control.

Moreover, the expression of pro-inflammatory cytokines was evaluated at both mRNA and protein levels by RT-qPCR and ELISA, respectively. As shown in **Figure 22A-22C**, BPA-exposed BV2 cells exhibited increased levels of TNF- $\alpha$ , IL-1 $\beta$ , and IL-6 mRNA expression after 24 h of treatment, particularly at 5  $\mu$ M BPA showed the highest mRNA expression levels.

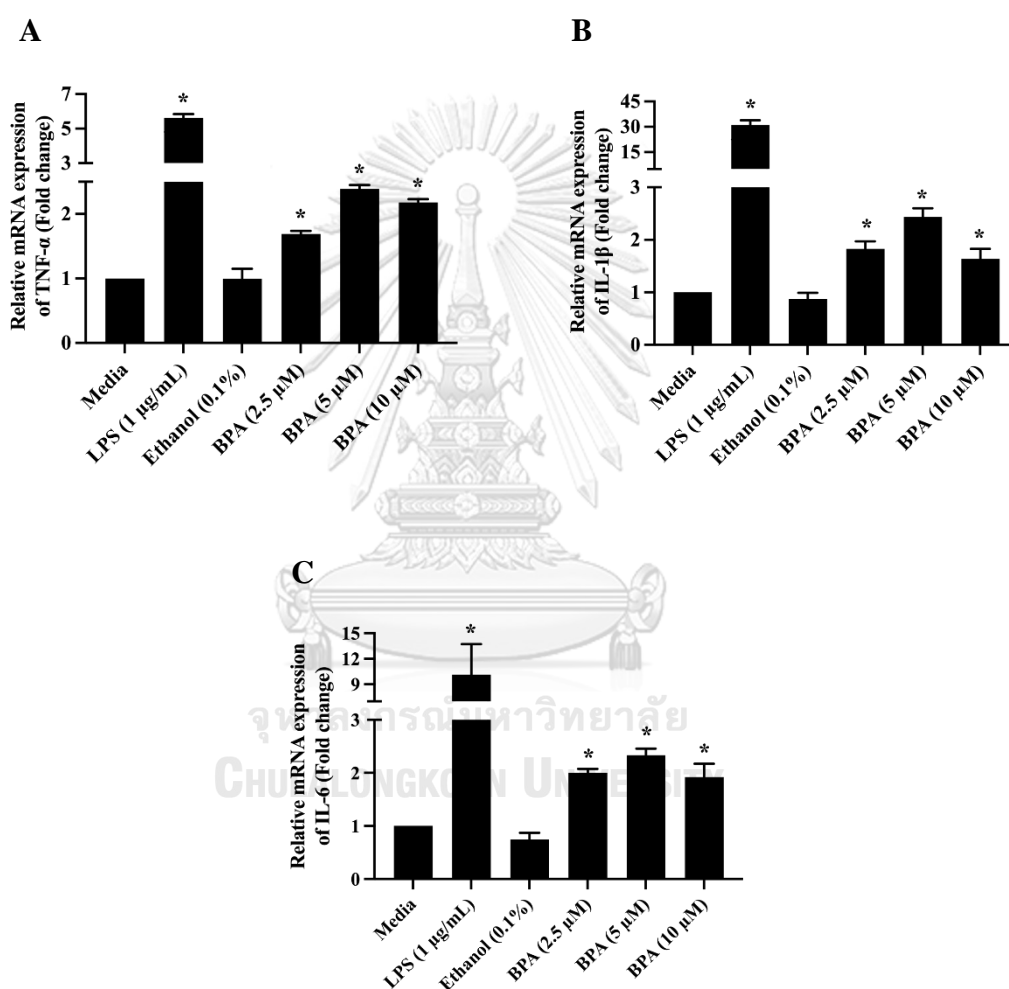


**Figure 22** The mRNA expressions of pro-inflammatory cytokines: (A) TNF- $\alpha$ , (B) IL-1 $\beta$ , and (C) IL-6 in BPA-induced BV2 cells after 24 h of treatment.

All data are shown as the mean  $\pm$  SEM of triplicate values. Statistical significance was analyzed by one-way ANOVA, Dunnett's test. \*  $P < 0.05$  versus the media control.

In addition, the levels of TNF- $\alpha$ , IL-1 $\beta$ , and IL-6 in the cell culture medium were measured. The results showed that BPA (2.5–10  $\mu$ M) significantly increased the secreted TNF- $\alpha$  levels compared to the media control (**Figure 23A**). Similarly, 2.5 and 5  $\mu$ M BPA exhibited significantly higher levels of IL-1 $\beta$ . However, at a high concentration of BPA (10  $\mu$ M), the increase in the production of IL-1 $\beta$  was not significant (**Figure 23B**). Moreover, BPA elevated IL-6 secretion in a dose-dependent manner (**Figure 23C**). Therefore, these results suggest that BPA increased the secretion of pro-inflammatory cytokines in microglial cells. This indicates that BPA could induce neuroinflammation.

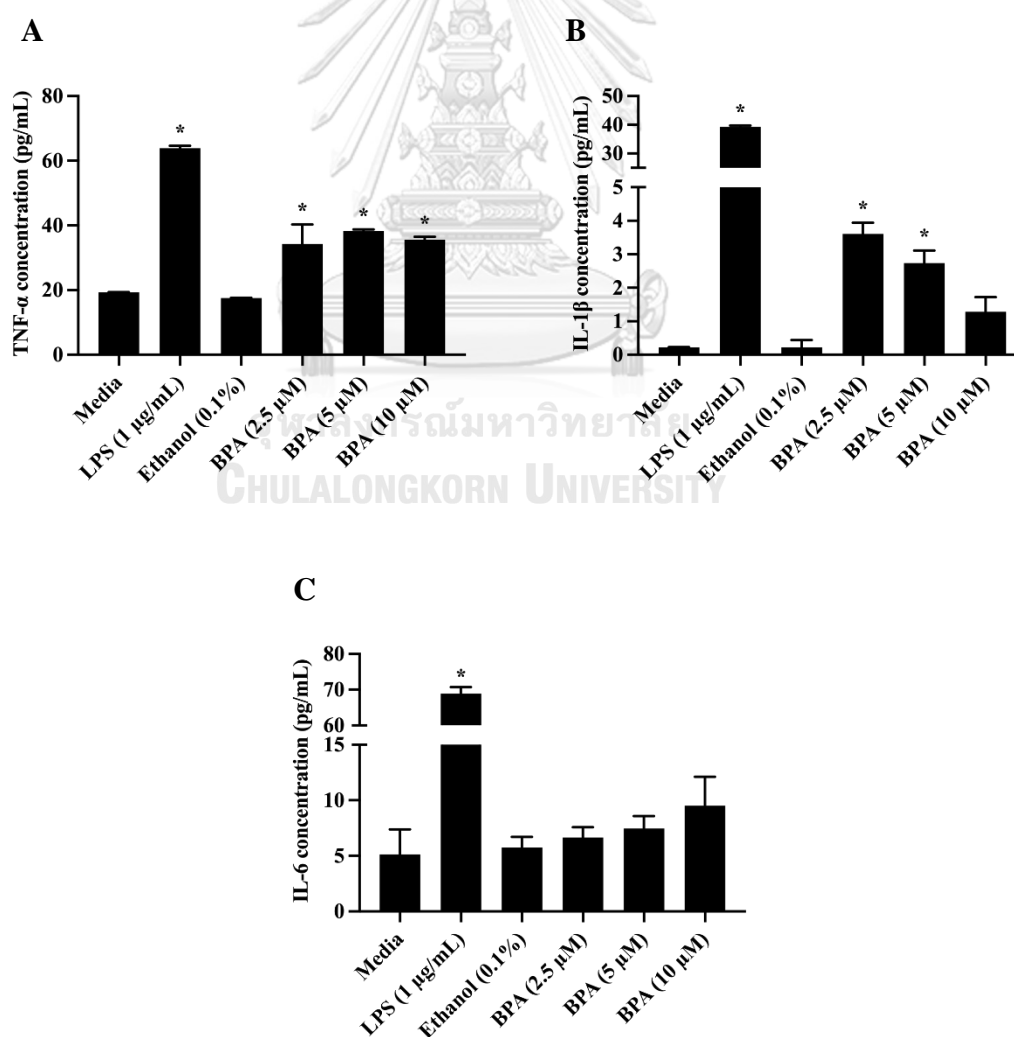
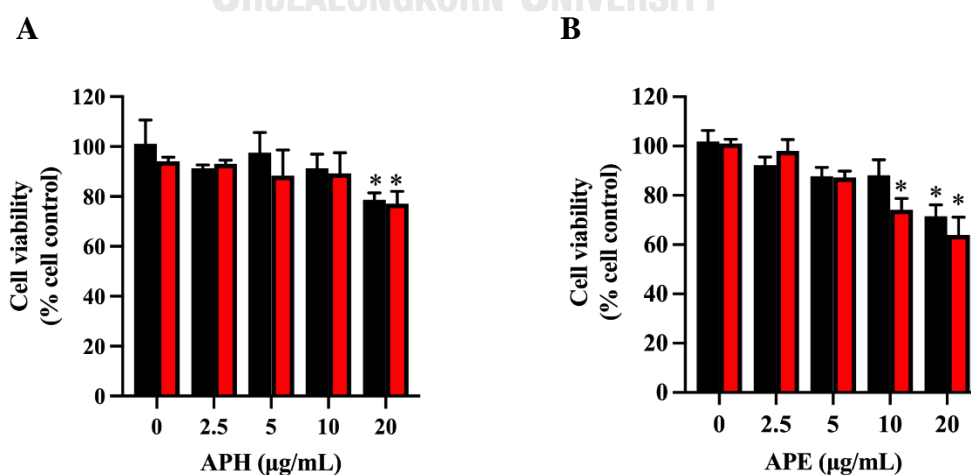


**Figure 23** The levels of pro-inflammatory cytokines: (A) TNF- $\alpha$ , (B) IL-1 $\beta$ , and (C) IL-6 in BV2 cell culture media after the induction of BPA for 48 h.

All data are shown as the mean  $\pm$  SEM of triplicate values. Statistical significance was analyzed by one-way ANOVA, Dunnett's test. \*  $P < 0.05$  versus the media control.

#### 4. Cytotoxicity of AP extracts against BV2 microglial cells

To evaluate the cytotoxicity of AP extracts on BV2 cells, an MTT assay was performed. BV2 cells were treated with various concentrations of APH, APE, and APW for 24 and 48 h. As shown in **Figure 24A-24C**, all extracts showed toxicity to the cells when the concentration was increased. APH (20  $\mu\text{g/mL}$ ) significantly decreased the viability of BV2 cells. In addition, 10 and 20  $\mu\text{g/mL}$  of APE and APW exhibited significant cytotoxicity against BV2 cells. Therefore, concentrations (APH, 5 and 10  $\mu\text{g/mL}$ ; APE, 2.5 and 5  $\mu\text{g/mL}$ ; APW, 2.5 and 5  $\mu\text{g/mL}$ ) that did not significantly suppress BV2 cell viability were selected to determine the anti-neuroinflammatory effects in further experiments.



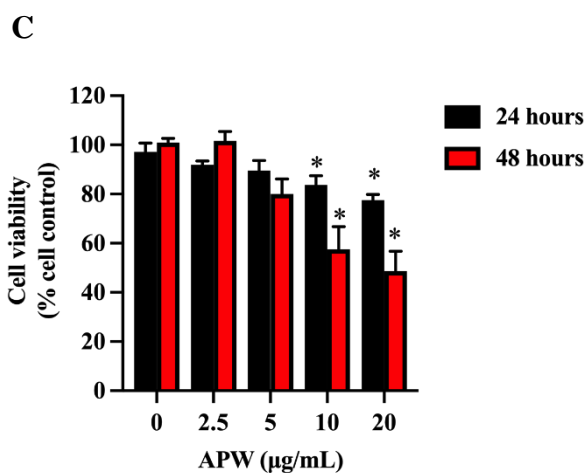


**Figure 24** Cytotoxicity of (A) APH, (B) APE, and (C) APW against BV2 microglial cells at 24 and 48 h.

All data are shown as the mean  $\pm$  SEM of triplicate values. Statistical significance was analyzed by one-way ANOVA, Dunnett's test. \*  $P < 0.05$  versus the media control.

### 5. Anti-neuroinflammatory effects of AP extracts on BPA-induced BV2 microglial cell activation

BV2 cells were co-treated with AP extracts and BPA for 24 h. Cell morphological observation showed that APH (10  $\mu\text{g/mL}$ ) and APE (2.5 and 5  $\mu\text{g/mL}$ ) significantly reduced the number of activated microglia (elongated cells) compared to BPA control. Similarly, 0.8  $\mu\text{M}$  of quercetin, a known natural anti-inflammatory control, significantly reduced BPA-induced BV2 cell activation. In contrast, APW (2.5 and 5  $\mu\text{g/mL}$ ) did not show any protective effect against BPA-induced BV2 cell activation (**Figure 25A and 25B**).

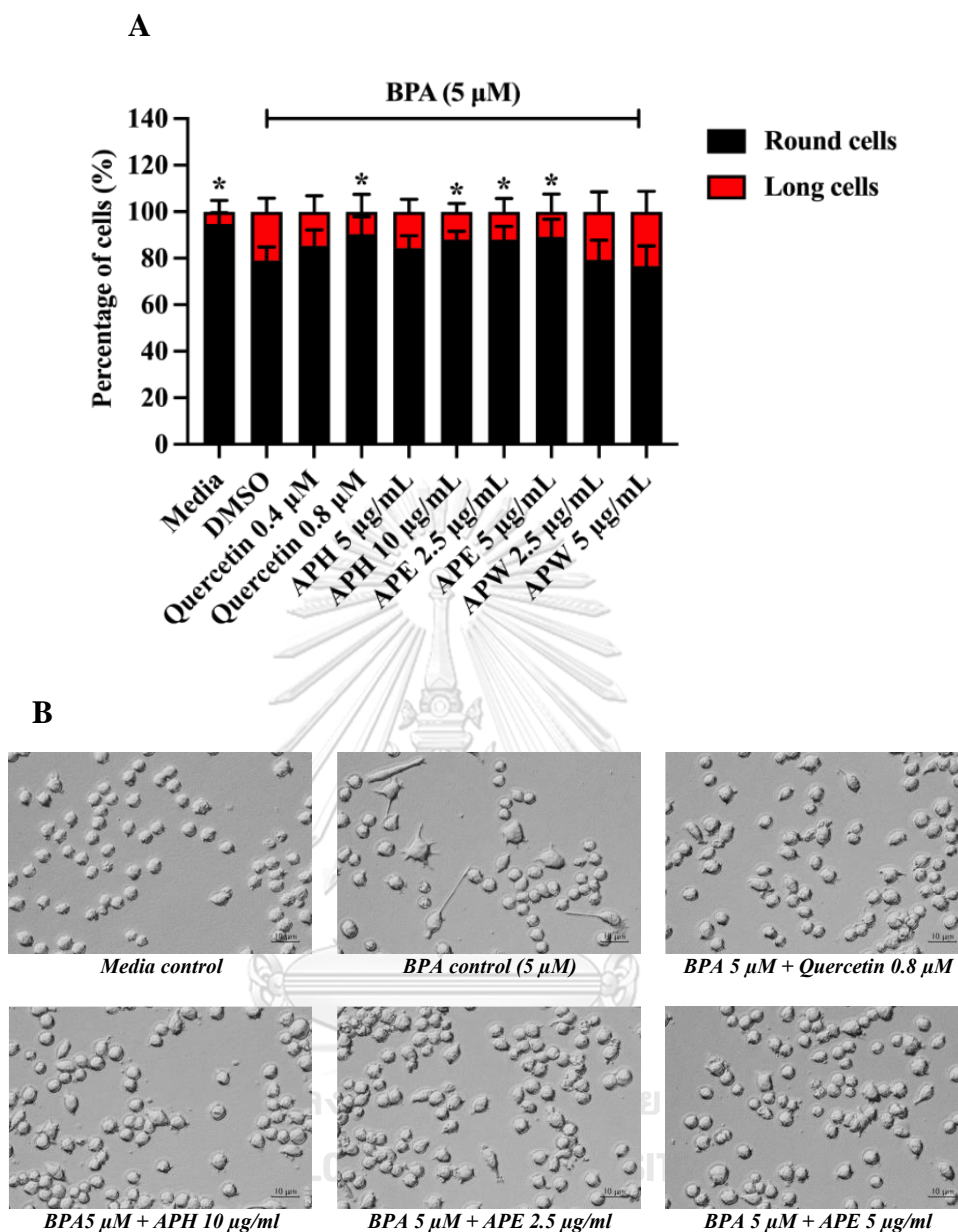
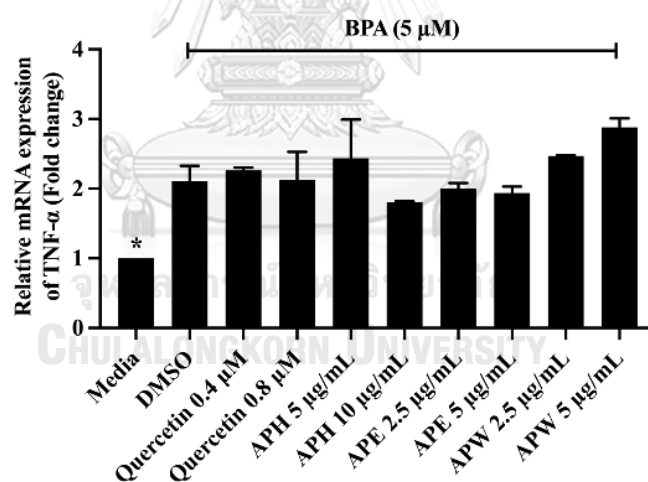


**Figure 25** Anti-neuroinflammatory effects of AP extracts on BPA-induced BV2 microglial cell activation.

(A) Percentage of BV-2 long and round cells after co-treated with BPA and AP extracts for 24 h. (B) BV2 cell morphological changes of media, BPA control and treatments: quercetin (0.8  $\mu\text{M}$ ), APH (10  $\mu\text{g/mL}$ ), and APE (2.5 and 5  $\mu\text{g/mL}$ ) observed under DIC microscope (10 $\times$ ). All data are shown as the mean  $\pm$  SEM of triplicate values. Statistical significance was analyzed by one-way ANOVA, Dunnett's test. \*  $P < 0.05$  versus the media control.

Furthermore, mRNA expression of the pro-inflammatory cytokines TNF- $\alpha$ , IL-1 $\beta$ , and IL-6 in BPA-induced BV2 cells was determined by RT-qPCR. Co-treatment with BPA and AP extracts for 24 h did not significantly affect the mRNA expression of TNF- $\alpha$  compared to the BPA control, as shown in **Figure 26A**. Additionally, APH (10  $\mu$ g/mL), APE (2.5 and 5  $\mu$ g/mL), and APW (2.5  $\mu$ g/mL) significantly reduced mRNA expression of IL-1 $\beta$  in BPA-induced BV2 cells compared to the BPA control (**Figure 26B**). The mRNA expression of IL-6, APH (5 and 10  $\mu$ g/mL), and APE (2.5  $\mu$ g/mL) significantly downregulated this expression (**Figure 26C**). Therefore, co-treatment with BPA and APW increased the mRNA levels of these pro-inflammatory cytokines.

A



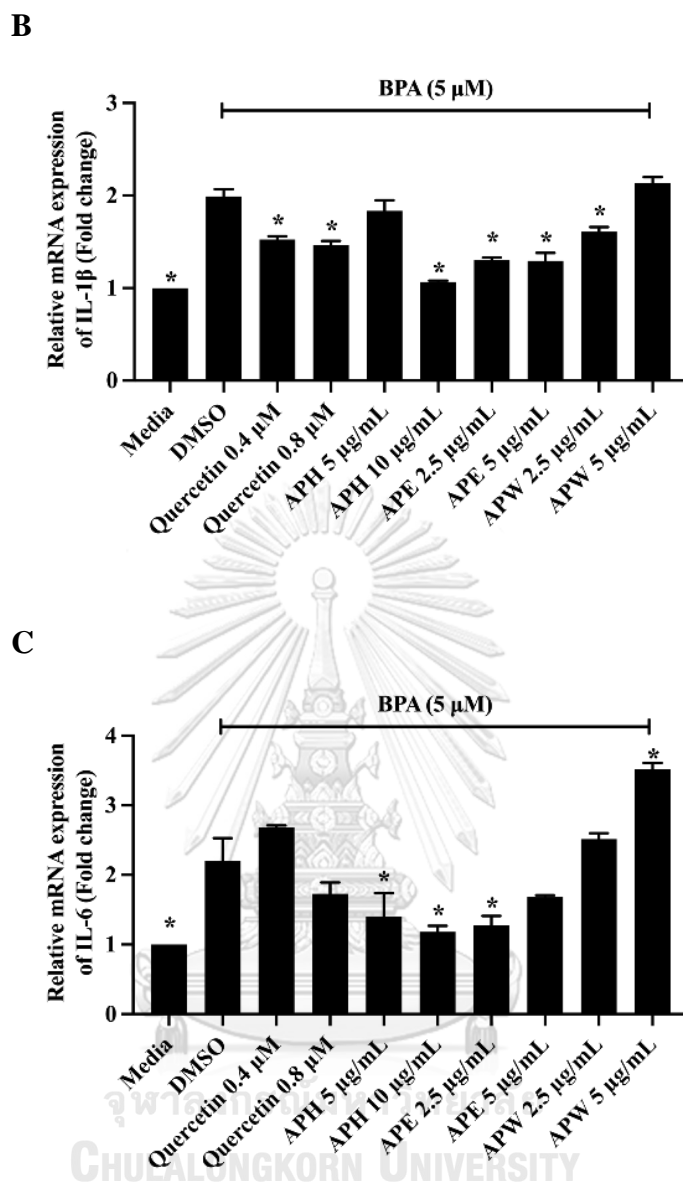


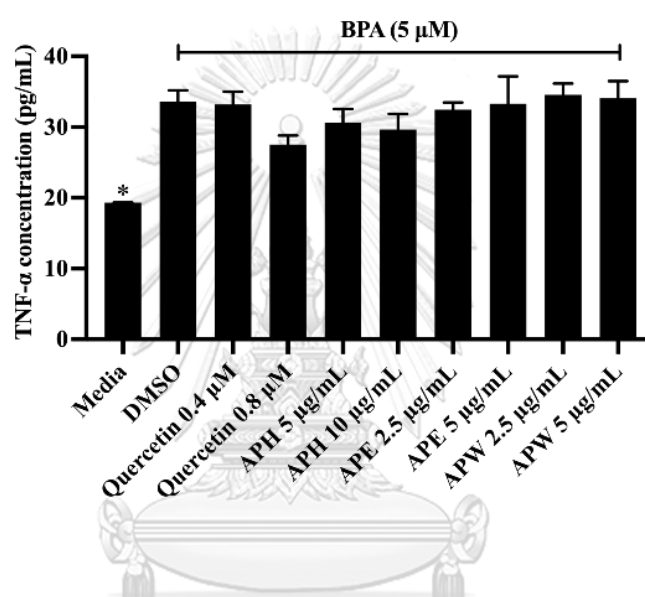
**Figure 26** The mRNA expressions of pro-inflammatory cytokines: (A) TNF- $\alpha$ , (B) IL-1 $\beta$ , and (C) IL-6 in co-treatment of BPA and AP extracts on BV-2 cells for 24 h. All data are shown as the mean  $\pm$  SEM of triplicate values. Statistical significance was analyzed by one-way ANOVA, Dunnett's test. \*  $P < 0.05$  versus the media control.

Besides, the determination of secreted pro-inflammatory cytokines levels showed that APH and APE significantly suppressed the production of IL-6 in BPA-

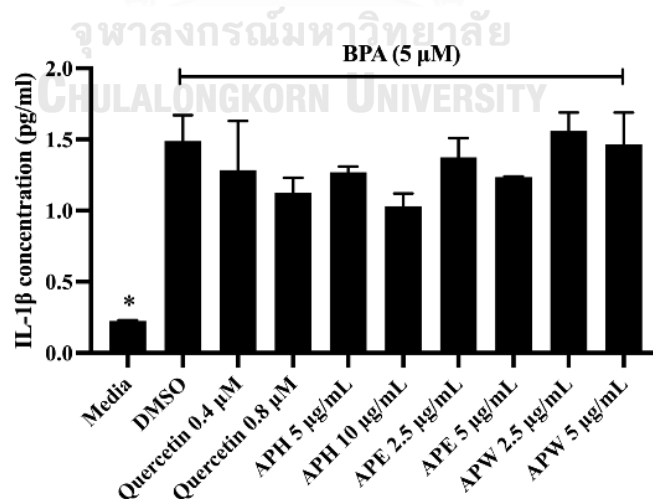


induced BV2 microglial cells, compared to BPA treatment alone. The secretion of TNF- $\alpha$  and IL-1 $\beta$  cytokines slightly decreased when BPA was co-treated with APH or APE. However, their levels were not statistically significant compared to the BPA control (Figure 27A-27C). These data indicate that APH and APE could suppress neuroinflammation stimulated by BPA induction.

A



B



C

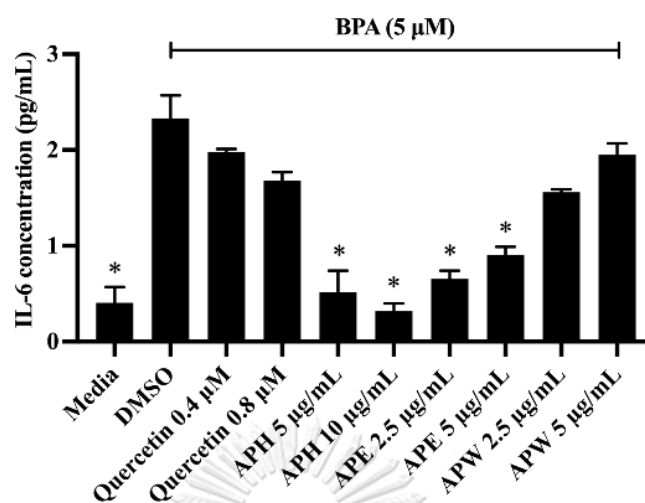


**Figure 27** The levels of pro-inflammatory cytokines: (A) TNF- $\alpha$ , (B) IL-1 $\beta$ , and (C) IL-6 in BV2 cell culture media after co-treatment of BPA and AP extracts for 48 h. All data are shown as the mean  $\pm$  SEM of triplicate values. Statistical significance was analyzed by one-way ANOVA, Dunnett's test. \*  $P < 0.05$  versus the BPA control.

## 6. The effects of AP extracts on NF- $\kappa$ B signaling pathway against BPA-induced BV2 microglial cell activation

To understand the molecular mechanism regulating the neuroinflammation induced by BPA activation, we further examined NF- $\kappa$ B signaling. As shown in **Figure 28A**, BPA activated NF- $\kappa$ B signaling by increasing the expression of p-I $\kappa$ B $\alpha$ /I $\kappa$ B $\alpha$  ratio. In the presence of APE (2.5 and 5  $\mu$ g/mL), the level of p-I $\kappa$ B $\alpha$ /I $\kappa$ B $\alpha$  was significantly decreased when compared to the vehicle (DMSO) control. Similar results were observed in the NF- $\kappa$ B-dependent luciferase activity assay (**Figure 28B**).

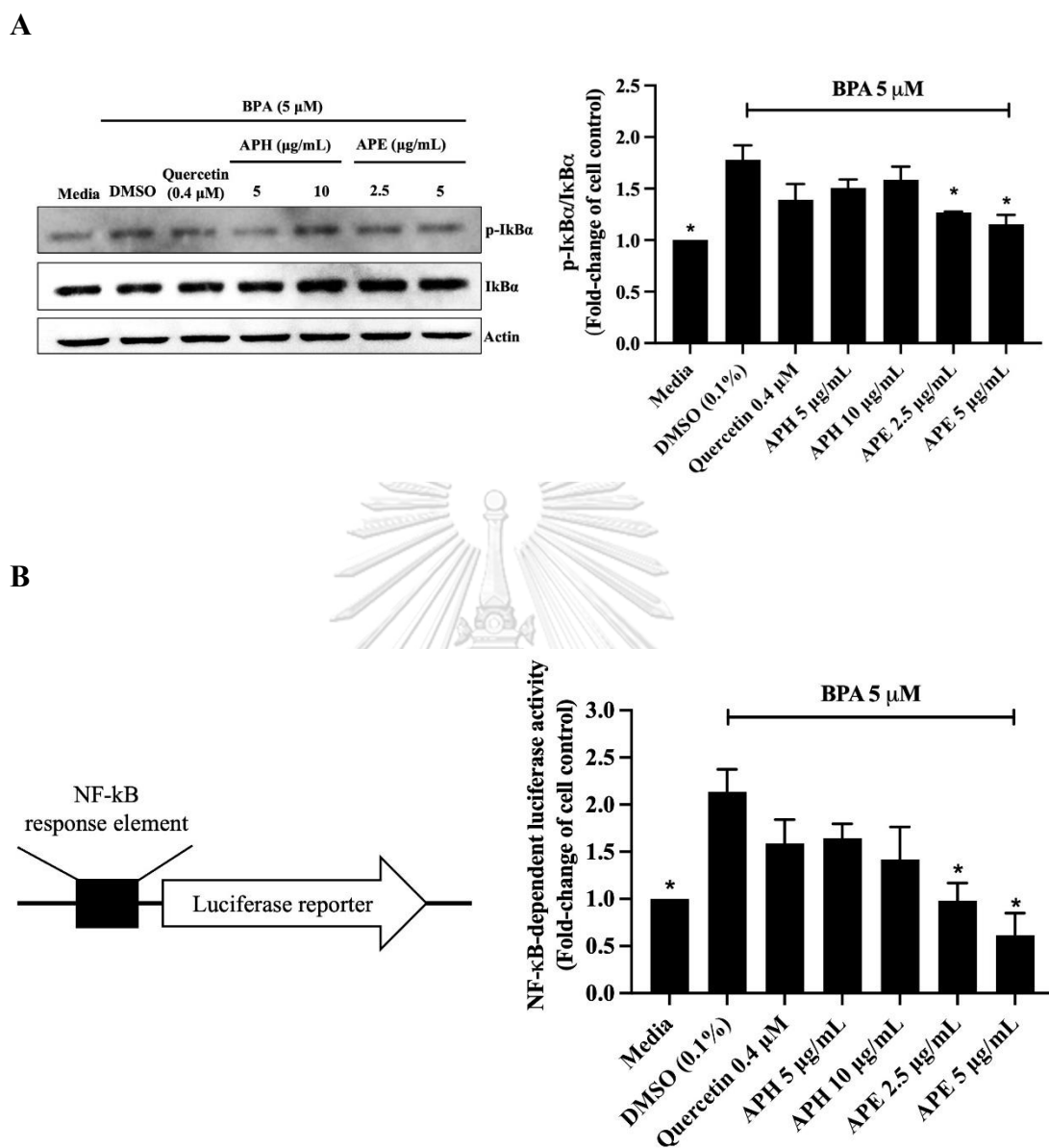


**Figure 28** The effects of AP extracts on NF-κB signaling pathway against BPA-induced BV2 microglial cell activation.

(A) The protein level of p-IκBα/IκBα ratio and (B) the expression of NF-κB-dependent luciferase activity in BV2 cells treated with BPA in the presence or absence of AP extracts for 6 h. All data are shown as the mean ± SEM of triplicate values. Statistical significance was analyzed by one-way ANOVA, Dunnett's test. \*  $P < 0.05$  versus the BPA control.

Moreover, nuclear translocation of NF- $\kappa$ B p65 was determined by immunofluorescence staining. BV2 microglial cells treated with BPA showed an increase in NF- $\kappa$ B p65 accumulation in the nucleus compared to that in the cell control. In contrast, 5  $\mu$ g/mL of APE blocked the NF- $\kappa$ B p65 nuclear translocation induced by BPA stimulation, shown in **Figure 29A**. Quantitative analysis demonstrated that co-treatment with APE and BPA significantly decreased the nuclear/cytoplasmic fluorescence intensity compared to BPA treatment alone (**Figure 29B**). These data suggest that APE could attenuate neuroinflammation activated by BPA induction through the suppression of the NF- $\kappa$ B signaling pathway.

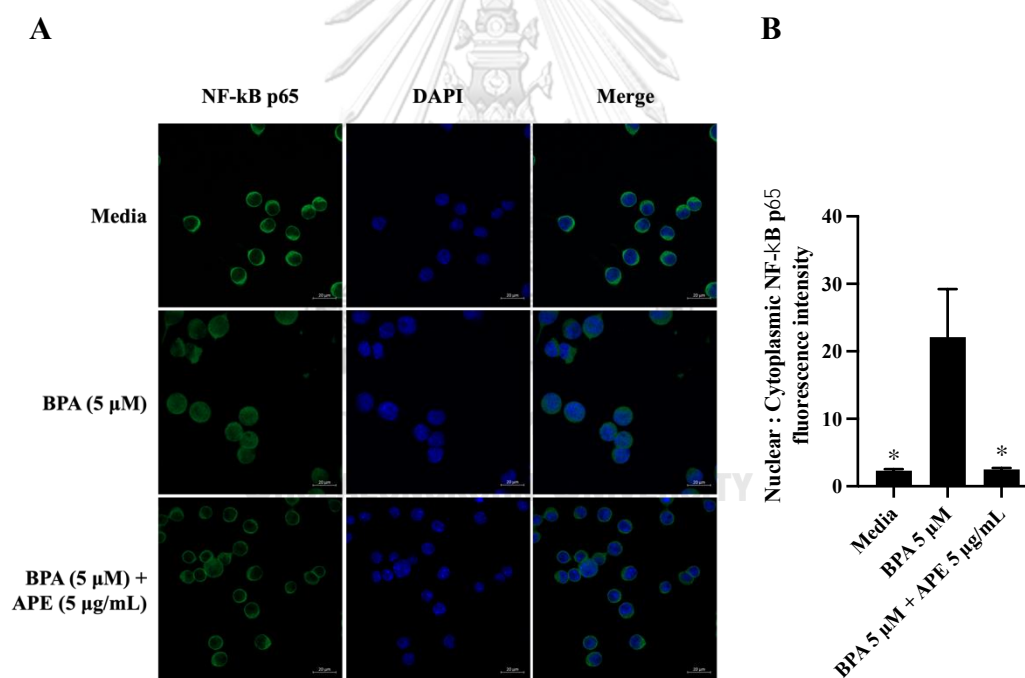


**Figure 29** Effects of AP extracts on NF- $\kappa$ B p65 nuclear translocation in BPA-induced BV2 microglial cell activation.

(A) Representative images of NF- $\kappa$ B p65 immunofluorescence staining and (B) quantitative analysis of nuclear/ cytoplasmic NF- $\kappa$ B p65 fluorescence intensity of cell control, BPA (5  $\mu$ M) control, and co-treatment of BPA (5  $\mu$ M) and APE (5  $\mu$ g/mL) on BV2 microglial cells after 6 hours of exposure. The cells were observed under a

confocal microscope with 40× magnification. scale bar indicates 20 μm. All data are shown as the mean ± SEM of triplicate values. Statistical significance was analyzed by one-way ANOVA, Dunnett's test. \*  $P < 0.05$  versus the BPA control.

Inducible nitric oxide synthase (iNOS) and cyclooxygenase-2 (COX-2) play an important role in the inflammatory response (91), as well as downstream proteins of the NF-κB signaling (92). The inhibition of NF-κB signaling by AP extracts was confirmed by the expression of iNOS and COX-2 levels. **Figure 30A and 30B** show that 5 μM BPA dramatically increased iNOS expression. Treatment with APH (5 and 10 μg/mL) and APE (2.5 and 5 μg/mL) significantly restored the expression of iNOS induced by BPA stimulation. Unfortunately, BPA did not show significant changes in COX-2 levels when treated with BPA or AP extracts (**Figure 30A and 30C**). However, these results suggest that APH and APE may attenuate BPA-induced neuroinflammation.

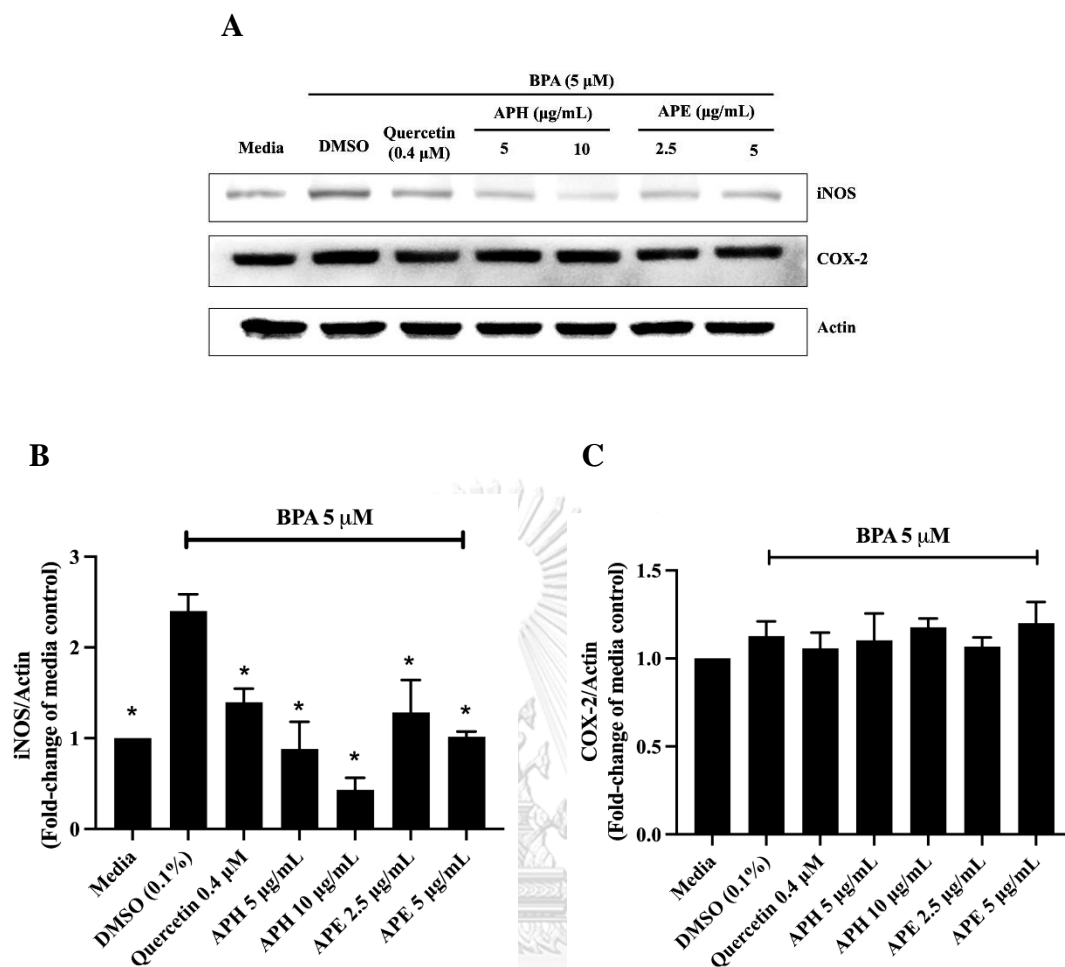


**Figure 30** The protein expressions of iNOS and COX-2 in BV2 cells treated with BPA in the presence or absence of AP extracts for 24 h.

(A) Representative immunoblots and relative fold-change expressions of (B) iNOS and (C) COX-2. All data are shown as the mean  $\pm$  SEM of triplicate values. Statistical significance was analyzed by one-way ANOVA, Dunnett's test. \*  $P < 0.05$  versus the BPA control.

## 7. Antioxidative and neuroprotective effects of AP extracts on BV2 cells

Activated microglial cells produce pro-inflammatory cytokines and cytotoxic factors, including ROS (33, 93). We, therefore, determined the effect of AP extracts on oxidative stress response by measuring the level of superoxide dismutase type 1

(SOD-1), an antioxidant enzyme, and the ability of the extracts to inhibit intracellular ROS clearance. Interestingly, AP extracts increased the expression of SOD-1 (**Figure 31A**). Moreover, these extracts potentially reduced ROS accumulation in BPA-induced BV2 cells to the baseline level (**Figure 31B**). The images representing the ROS level in BV2 cells are shown in **Figure 31C**, where BPA-treated BV2 cells exhibited high fluorescence intensity. Co-treatment with BPA and APH (10  $\mu\text{g}/\text{mL}$ ) or APE (5  $\mu\text{g}/\text{mL}$ ) reduced intracellular ROS signaling.

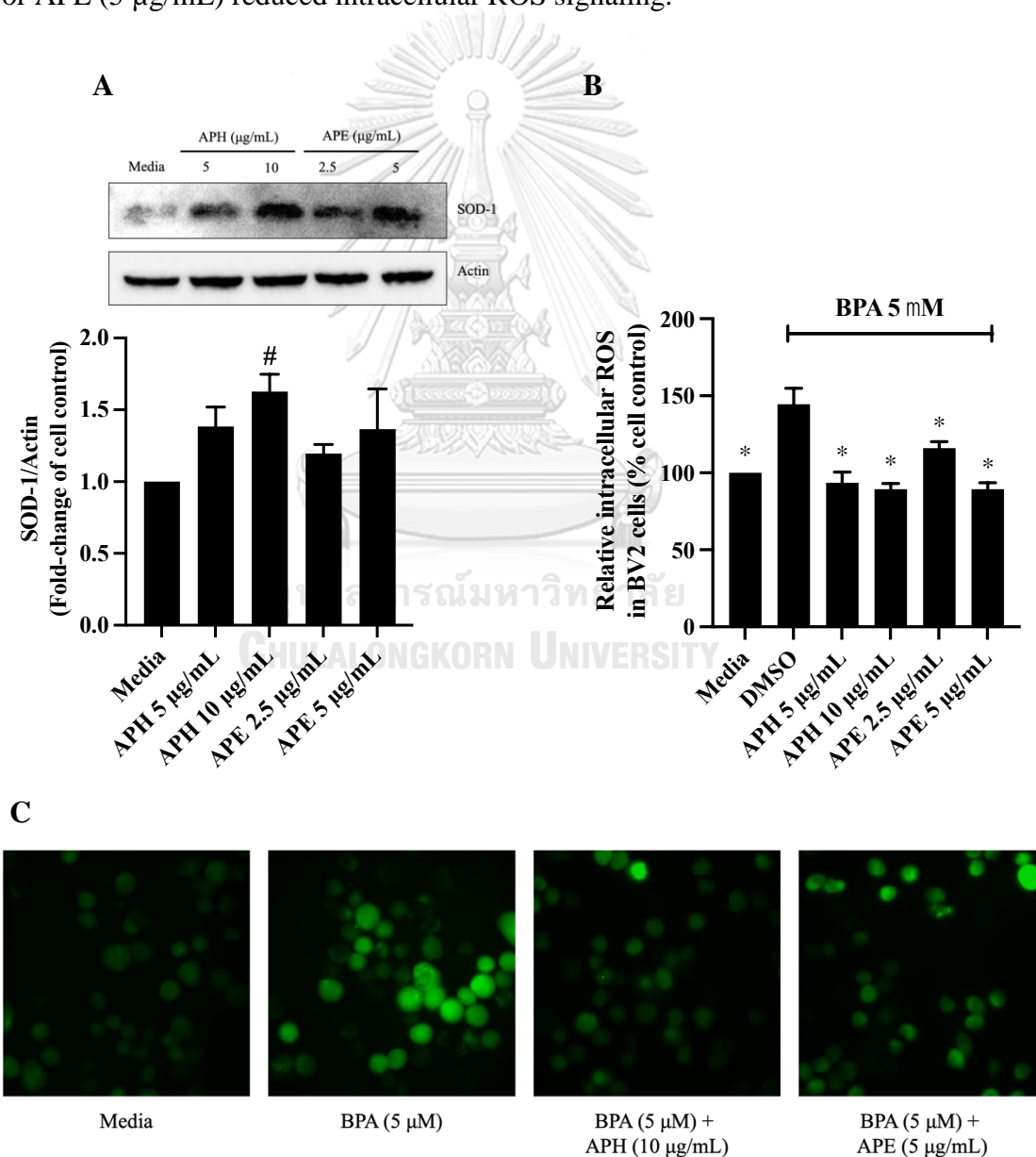


**Figure 31** Antioxidative and neuroprotective effects of AP extracts on BV2 cells.

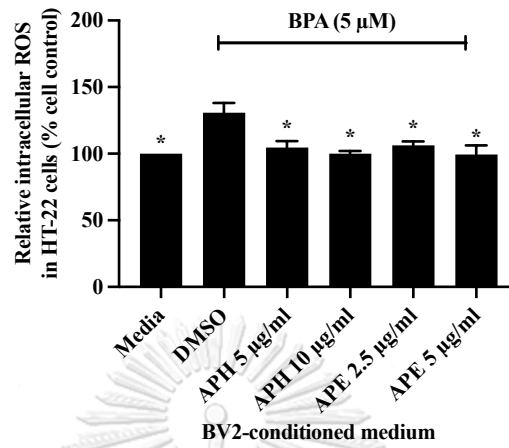
(A) The SOD-1 expression of BV2 cells after treated with APH (5 and 10  $\mu\text{g/mL}$ ) or APE (2.5 and 5  $\mu\text{g/mL}$ ) for 18 h. (B) The effect of APH and APE on ROS production and (C) representative micrographs (40 $\times$  of magnification) of ROS accumulation in BPA-induced BV2 cells. All data are shown as the mean  $\pm$  SEM of triplicate values. Statistical significance was analyzed by one-way ANOVA, Dunnett's test. #  $P < 0.05$  versus the cell control. \*  $P < 0.05$  versus the BPA control.

### **8. Neuroprotective effects of AP extracts against BV2-conditioned medium-exposed HT-22 hippocampal cell damage**

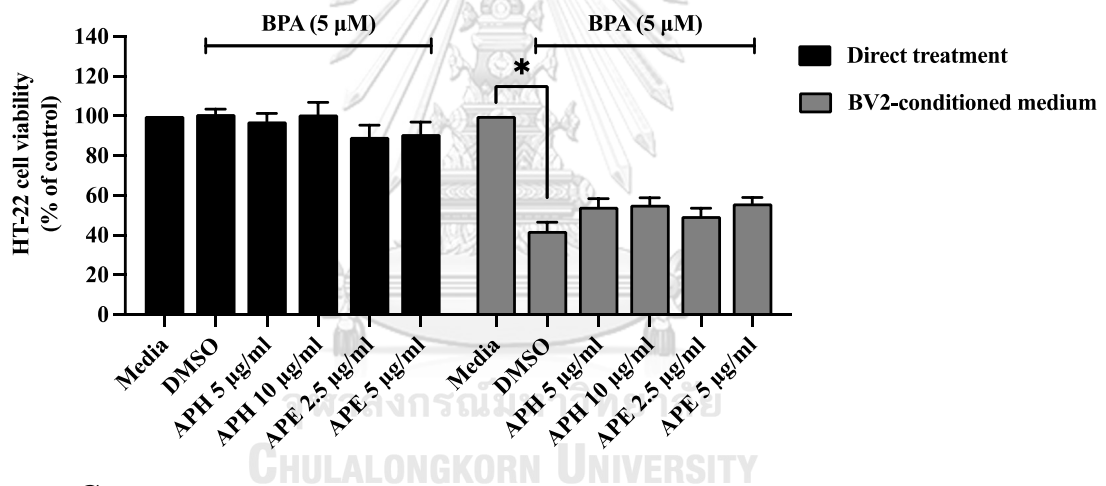
Pro-inflammatory cytokines act as neurotoxic substances that lead to neuronal death (32) (33). In this study, we collected the conditioned medium from BV2 cell culture (BV2-CM), which contained inflammatory and cytotoxic molecules. Then, HT-22 cells were treated with the BV2-CM and the neuronal damage was observed. The results showed that BV2-CM treated with BPA increased the level of intracellular ROS accumulation in HT-22 cells compared to the media control. In contrast, the BV2-CM collected from the AP extract treatments significantly reduced ROS accumulation in HT-22 cells compared to BPA control (**Figure 32A**). Unfortunately, the treatments of APH or APE on BPA-induced BV2 microglia cells did not significantly protect HT-22 hippocampal death in both BV2-CM treatment (**Figure 32B**) and transwell co-culture system (**Figure 32C**).



A



B



C

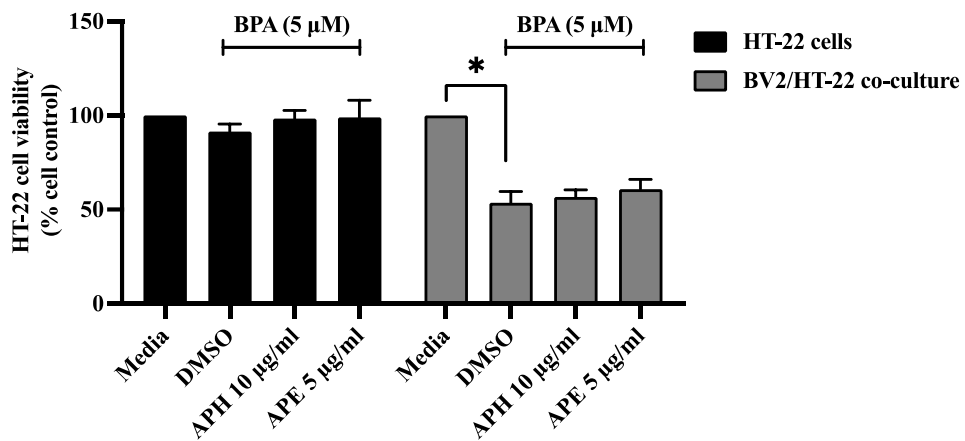


**Figure 32** Neuroprotective effects of AP extracts against BV2 conditioned media-exposed HT-22 hippocampal cell damage.

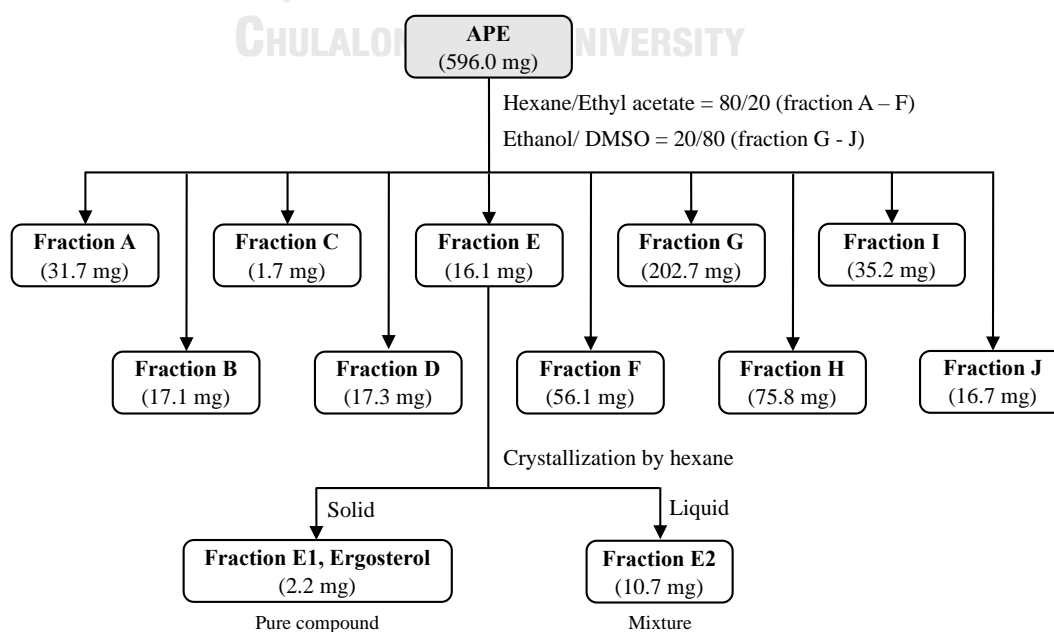
(A) Intracellular ROS accumulation in HT-22 cells after treated with BV2-conditioned medium. (B) HT-22 cell viability after treated with BV2-conditioned medium for 24 h. (C) HT-22 cell viability after treated with BPA and AP extracts for 24 h in the transwell co-culture system with BV2 cells. All data are shown as the mean  $\pm$  SEM of triplicate values. Statistical significance was analyzed by one-way ANOVA, Dunnett's test. \*  $P < 0.05$  versus the BPA control.

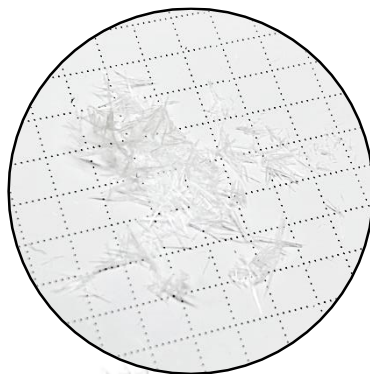
## 9. Chemical compound isolation and identification

### 9.1. Column chromatography and crystallization

APE exhibited the most potential in suppressing NF- $\kappa$ B signaling among all AP extracts. Thus, we further fractionated the chemical constituents of APE by column chromatography, as illustrated in **Figure 33A**. Then, fraction E was crystallized by absolute hexane at room temperature to get fraction E1 (APE-E1) as a white needle (**Figure 33B**).

A



**B**

**Figure 33** The isolation of chemical constituents from APE crude extracts.

(A) Schematic of APE chemical isolation by column chromatography. (B) Characteristic of APE-E1 (ergosterol) crystal.

### 9.2. Thin layer chromatography (TLC)

The TLC was performed using silica gel 60 F254 aluminum sheet and developed in hexane/ethyl acetate (80/20). The isolated spots were visualized under UV light (254 and 365 nm) and iodine vapor staining. The results exhibited that the  $R_f$  value of the band obtained from APE-E1 was compared to that of the APH extract, whose complete chemical composition was previously determined (17). The  $R_f$  value of APE-E1 was 0.42, while reference ergosterol showed an  $R_f$  value of 0.46 (**Figure 34**).

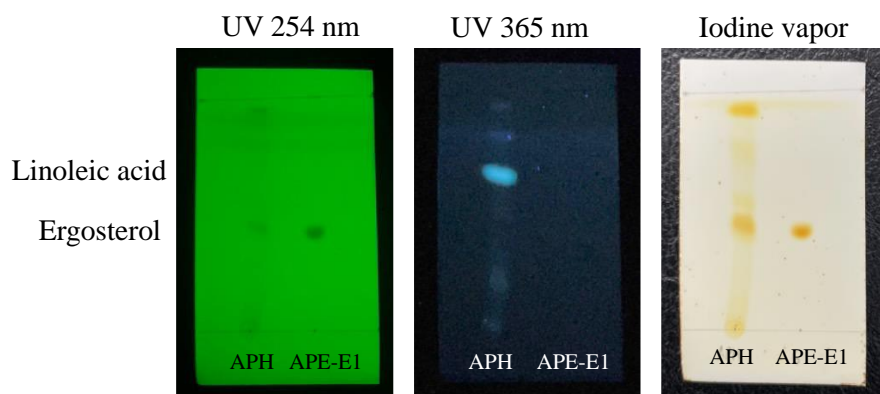


**Figure 34** Thin layer chromatography analysis of APH and APE-E1 developed in hexane/ ethyl acetate (80/ 20), visualizing under UV light at 254 and 365 nm, and iodine vapor staining.

### 9.3. Nuclear magnetic resonance (NMR)

From the  $^1\text{H}$  NMR data, the spectrum of APE-E1 matched the published spectrum of ergosterol (94) (**Figure 35**). These results suggest that the compound present in APE was ergosterol.

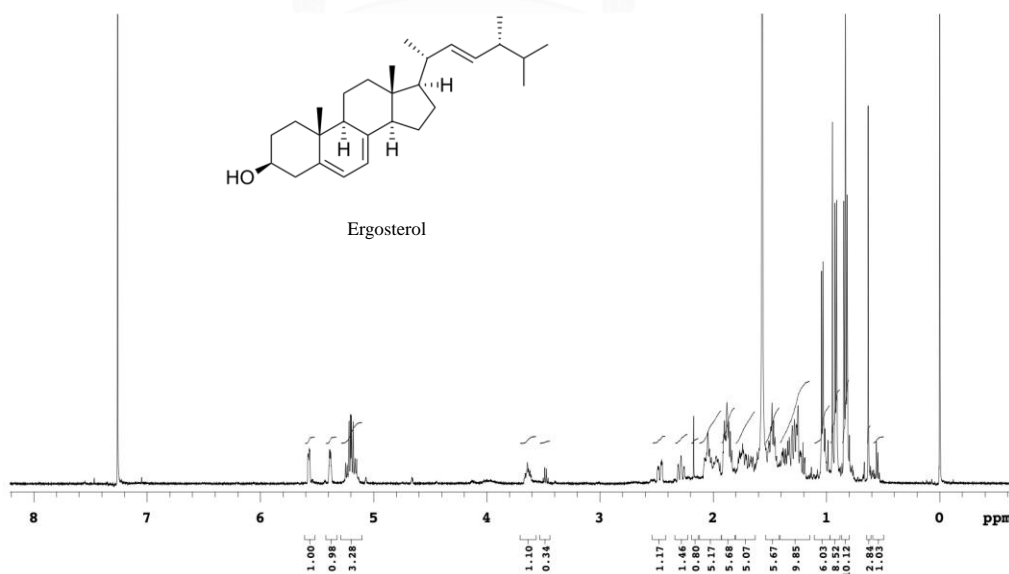


**Figure 35** The  $^1\text{H}$  NMR spectrum of APE-E1 and ergosterol structure.

### 10. The effects of ergosterol against BPA-induced BV2 microglial cell activation

To determine the effects of ergosterol on BPA-induced microglial cell activation, the cytotoxicity of ergosterol on BV2 microglial cells was initially studied. More than 100 nM of ergosterol concentration significantly reduced the viability of BV2 cells (**Figure 36**). Thus, ergosterol concentrations lower than 100 nM were selected to test the anti-inflammatory effects in the current study.

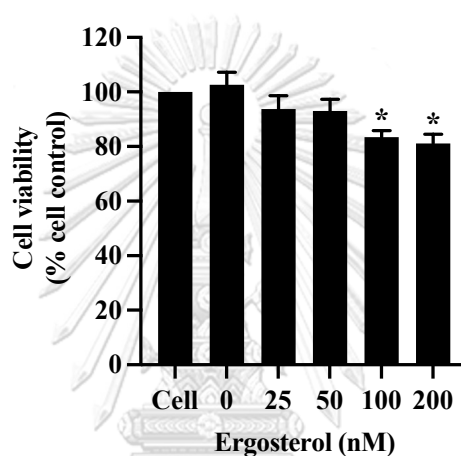


**Figure 36** Cytotoxicity of ergosterol against BV2 cells after exposure for 24 h.

All data are shown as the mean  $\pm$  SEM of triplicate values. Statistical significance was analyzed by one-way ANOVA, Dunnett's test. \*  $P < 0.05$  versus the cell control.

Next, different concentrations of ergosterol (25 and 50 nM) were co-treated with BPA and NF- $\kappa$ B signaling-associated molecules were determined. The results showed that ergosterol reduced the expression of p-I $\kappa$ B $\alpha$ /I $\kappa$ B $\alpha$  ratio, as well as iNOS levels (**Figure 37A and 37B**).

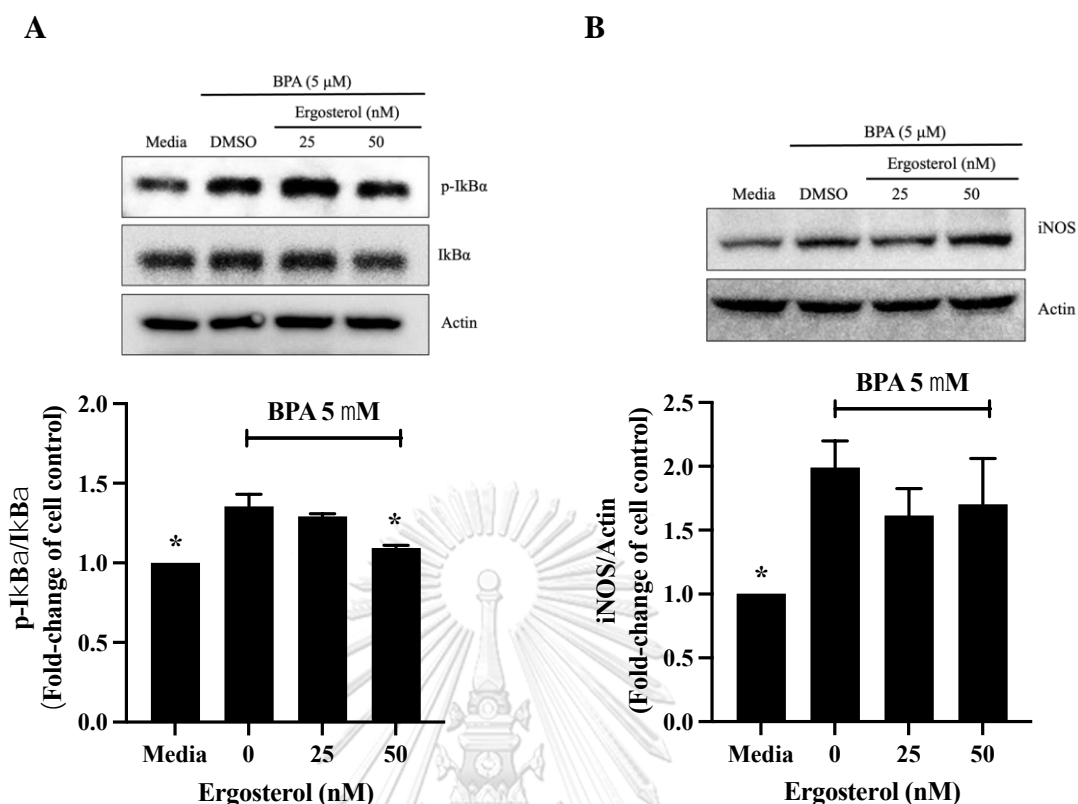


**Figure 37** The effects of ergosterol against BPA-induced BV2 cell activation.

Anti-neuroinflammatory effect of ergosterol on BPA-induced BV2 cells via suppressing of (A) p-IκBα/IκBα and (B) iNOS expressions after 6 and 24 h of treatments, respectively. All data are shown as the mean ± SEM of triplicate values. Statistical significance was analyzed by one-way ANOVA, Dunnett's test. \*  $P < 0.05$  versus the BPA control.

## 11. Neuroprotective effect of ergosterol against the TNF-α-induced HT-22 cell death

The cytotoxicity of TNF-α on HT-22 cells was determined by MTS assays. TNF-α, at concentrations of 1, 10, and 100 ng/mL, significantly suppressed the HT-22 cell viability by approximately 60% after the cells were treated with TNF-α for 24 h (Figure 38A). Thus, 1 ng/mL of TNF-α was used for the induction of neuronal death

in subsequent experiments. Then, the ergosterol toxicity in HT-22 cells was assessed by an MTS assay, leading to the conclusion that ergosterol does not affect the viability of these cells in concentrations of up to 1  $\mu\text{M}$  (**Figure 38B**).

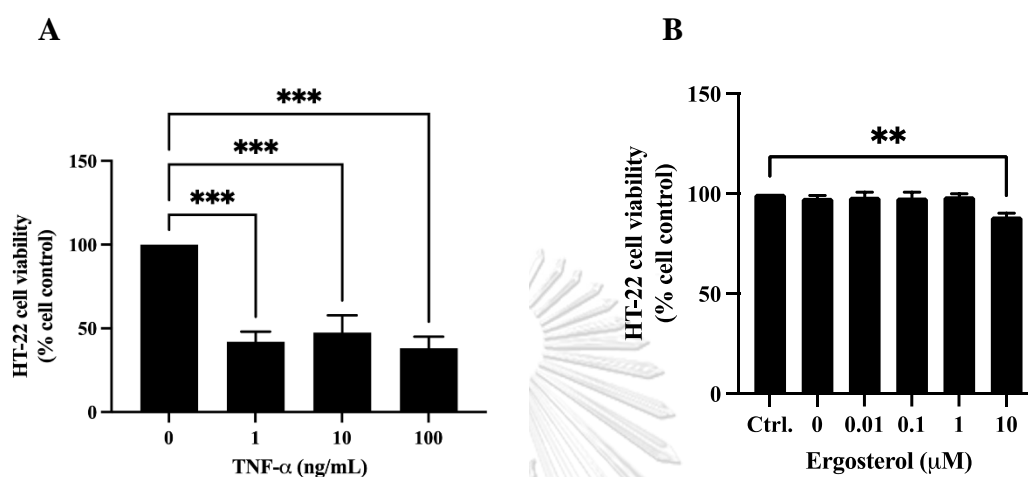


**Figure 38** Cytotoxicity of (A) TNF- $\alpha$  and (B) ergosterol on HT-22 cells at 24 h. All data are shown as the mean  $\pm$  SEM of experiments conducted in triplicate. Statistical significance was analyzed by a one-way ANOVA and a Dunnett's test. \*\*  $P < 0.01$  and \*\*\*  $P < 0.001$ .

Furthermore, we found that 100 nM of ergosterol was able to significantly protect against TNF- $\alpha$ -induced neuronal death (**Figure 39A**). Finally, the cell morphology of the HT-22 cells after exposure to TNF- $\alpha$  and ergosterol is presented in **Figure 39B**.

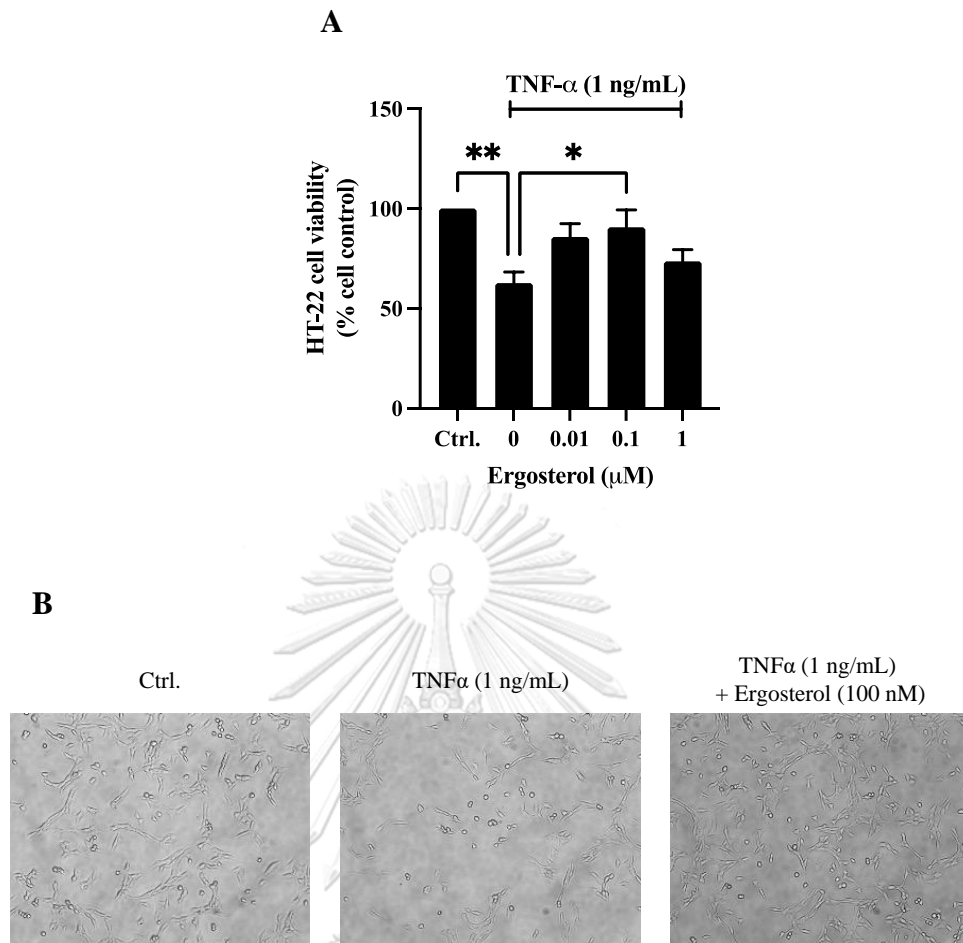


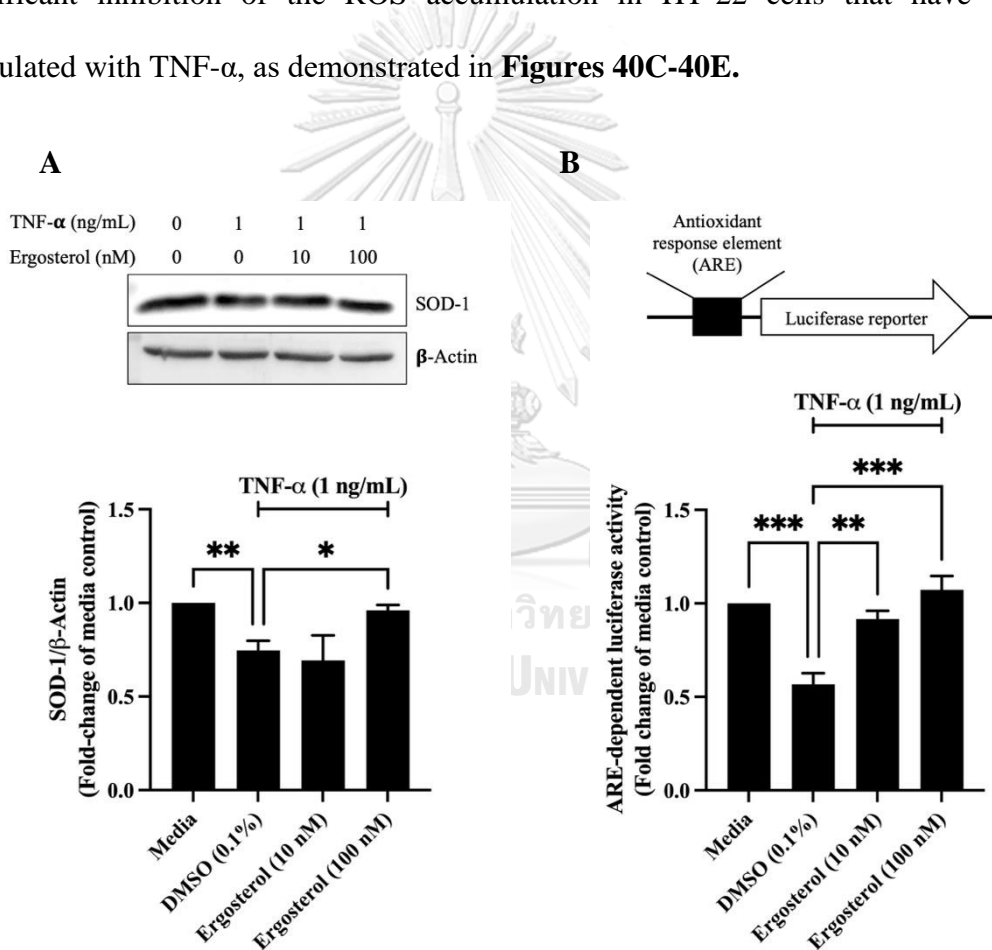
**Figure 39** Neuroprotective effect of ergosterol against TNF- $\alpha$ -induced HT-22 hippocampal cell death.

(A) Cell viability of the HT-22 cells when treated with ergosterol in the presence of TNF- $\alpha$ , for 24 h. All data are shown as the mean  $\pm$  SEM of experiments conducted in triplicate. Statistical significance was analyzed by a one-way ANOVA and a Dunnett's test. \*  $P < 0.05$  and \*\*  $P < 0.01$ . (B) Representative images of the HT-22 cells under the light microscope (10 $\times$  magnification) when treated with media (Ctrl.), TNF- $\alpha$ , or TNF- $\alpha$  + ergosterol, for 24 h.



## 12. Antioxidant activity of ergosterol on TNF- $\alpha$ -induced HT-22 cell injury

Ergosterol was administered to TNF- $\alpha$ -HT-22 cells, and the SOD-1 expression in these cells was examined. As shown in **Figure 40A**, 100 nM of ergosterol was able to increase the SOD-1 expression. Moreover, ergosterol (at concentrations of 10 and 100 nM) was able to significantly restore the ARE-dependent luciferase activity in TNF- $\alpha$ -treated HT-22 cells (**Figure 40B**). Besides, 100 nM of ergosterol resulted in significant inhibition of the ROS accumulation in HT-22 cells that have been stimulated with TNF- $\alpha$ , as demonstrated in **Figures 40C-40E**.



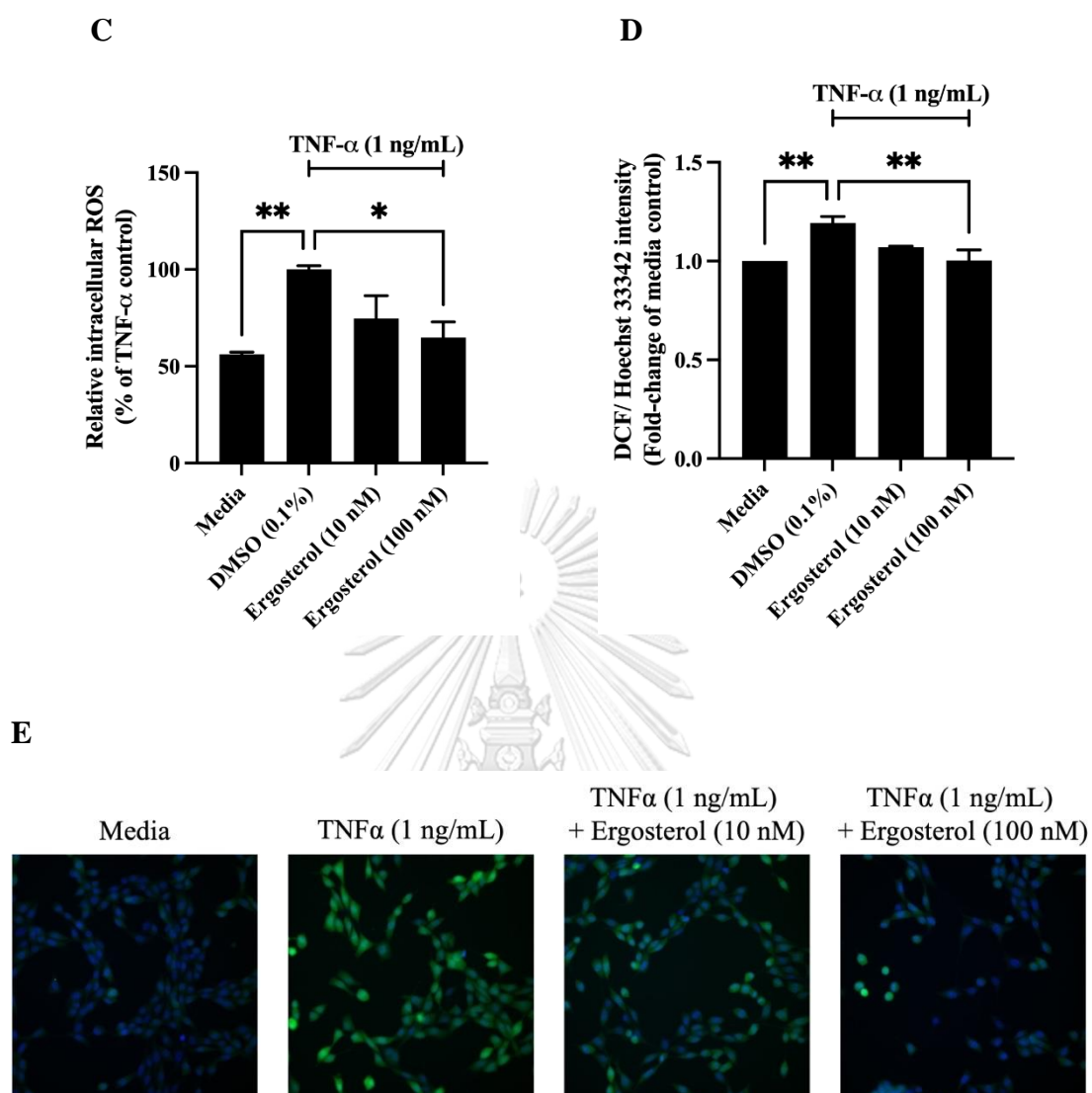


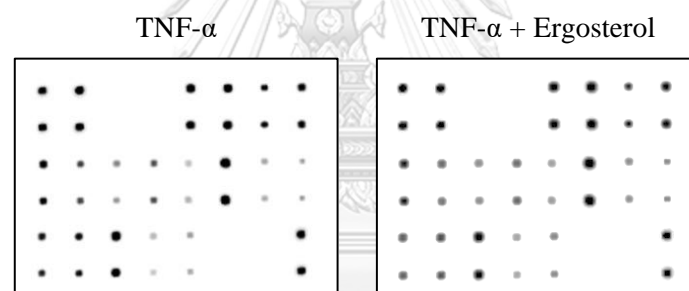
**Figure 40** Antioxidant activity of ergosterol in the TNF- $\alpha$ -induced HT-22 hippocampal cell damage.

(A) Western blotting analysis of the SOD-1 expression in the TNF- $\alpha$ -induced HT-22 cells treated with ergosterol. (B) ARE-dependent luciferase activity of ergosterol in the TNF- $\alpha$ -induced HT-22 cell damage. (C) Intracellular ROS accumulation in TNF- $\alpha$ -induced HT-22 cells, in the presence or absence of ergosterol, as determined by a microplate assay. (D) The relative intensity of DCF/Hoechst 33342, and (E) the representative images of ROS accumulation in TNF- $\alpha$ -induced HT-22 cells, in the presence or absence of ergosterol, were observed by a CellInsight CX7 high-content screening (20 $\times$  magnification). All data are shown as the mean  $\pm$  SEM of experiments

conducted in triplicate. Statistical significance was analyzed by a one-way ANOVA and a Dunnett's test. \*  $P < 0.05$ , \*\*  $P < 0.01$ , and \*\*\*  $P < 0.001$ .

### 13. The molecular mechanism of ergosterol against TNF- $\alpha$ -induced HT-22 cell death

Signaling pathways involved in the ergosterol effect on TNF- $\alpha$ -induced HT-22 cell death were screened by using a mouse apoptosis signaling pathway antibody array. As demonstrated in **Figure 41**, several molecules were affected when the TNF- $\alpha$ -induced HT-22 cells were treated with 100 nM of ergosterol, for 24 h. Among those molecules, one could identify elements of the Akt signaling pathway; a pathway that has been linked to neurodegenerative disorders (95, 96).



Array map

	A	B	C	D	E	F	G	H
1	POS	POS	NEG	NEG	Akt (S473)	ATM (S1981)	BAD (S112)	Cas3 (D175)
2								
3	Casp7 (D198)	CHK (S296)	eIF2a (S51)	Erk1/2 (T202)	Hsp27 (S82)	Ikb $\alpha$ (S32)	JNK (T183)	NFkB (S536)
4								
5	p27 (T198)	p38 (T180/ Y182)	P53 (S15)	SMAD2 (S245)	TAK1 (S412)	NEG	NEG	POS
6								

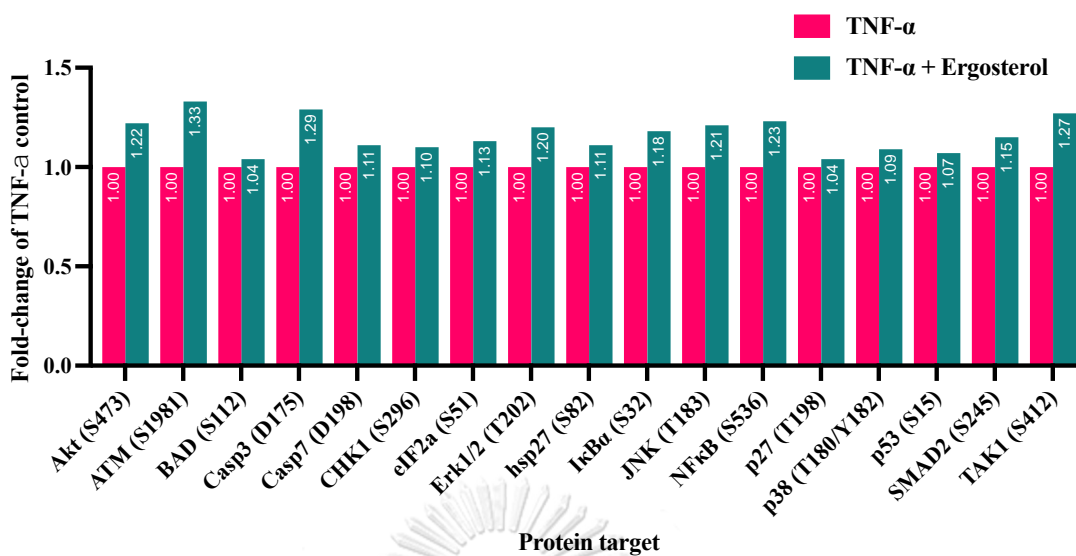


**Figure 41** Apoptosis-associated protein antibody array results after a 24-h treatment with TNF- $\alpha$ , in the presence or absence of ergosterol, in HT-22 cells.

We further confirmed the antibody array results by determining the pAkt (S473)/Akt protein expression. The Western blotting results demonstrated that ergosterol can significantly increase the expression of pAkt (S473)/Akt in the TNF- $\alpha$ -exposed HT-22 cells, as shown in **Figure 42A**. We further determined the expression of pAkt (S473)/Akt on HT-22 cells after the latter were treated with TNF- $\alpha$  in the presence or absence of ergosterol for 1, 6, and 12 h. The results exhibited that TNF- $\alpha$  can significantly decrease the expression of pAkt (S473)/Akt after 6 h of treatment, as compared to the media control. In contrast, ergosterol was able to significantly upregulate the pAkt (S473)/Akt levels in the TNF- $\alpha$ -treated HT-22 cells after a 6-h treatment (**Figure 42B**).

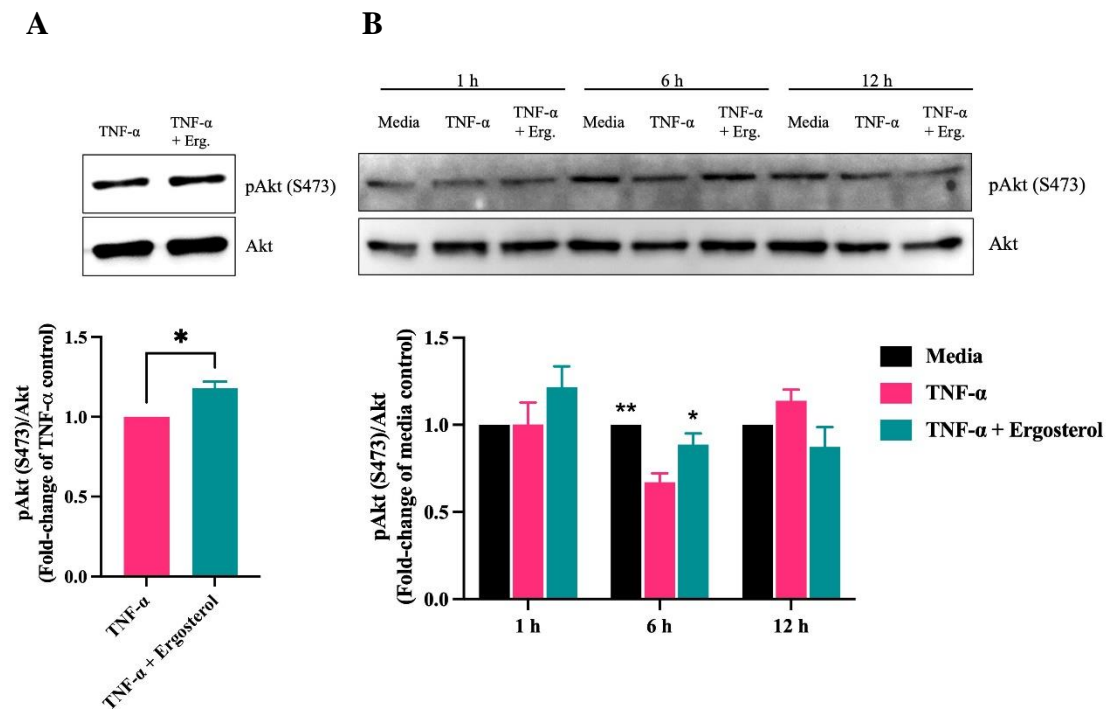


**Figure 42** The effect of ergosterol on the phosphorylation of Akt at Ser473 in TNF- $\alpha$ -treated HT-22 hippocampal cells.

(A) Western blotting analysis of the pAkt (S473) expression in TNF- $\alpha$ -treated HT-22 cells in the presence or absence of ergosterol, after 24 h. (B) The effect of ergosterol on the pAkt (S473) expression in TNF- $\alpha$ -treated HT-22 cells at different time points: 1, 6, and 12 h. All data are shown as the mean  $\pm$  SEM of experiments conducted in triplicate. Statistical significance was analyzed by a one-way ANOVA and a Dunnett's test. \*  $P < 0.05$  and \*\*  $P < 0.01$ .

In addition, rapamycin-insensitive companion of mammalian target of rapamycin (RICTOR), an upstream target that controls the Akt Ser473 phosphorylation (97, 98) was investigated. At 1 ng/mL of TNF- $\alpha$  significantly down-regulated the expression of RICTOR in HT-22 cells, while in the presence of TNF- $\alpha$  and 100 nM ergosterol showed inverted RICTOR expression, as shown in **Figures 43A and 43B**. Furthermore, the downstream molecules of the Akt signaling pathway

were evaluated by GSK-3 $\beta$  modulation. TNF- $\alpha$  (at 1 ng/mL) was able to significantly decrease the pGSK-3 $\beta$  (S9) levels, as compared to those of the untreated HT-22 cells. Ergosterol (at a concentration of 100 nM) was able to significantly upregulate the levels of pGSK-3 $\beta$  (S9) in the presence of TNF- $\alpha$ , as compared to those of the TNF- $\alpha$  treatment alone (**Figure 43A and 43C**). We also measured the expression of NAG-1; a neuroprotective protein (99). Unfortunately, the expression of NAG-1 showed unnoticeable changes in the media, the TNF- $\alpha$ , and the TNF- $\alpha$  + ergosterol treatments (**Figure 43A and 43D**).

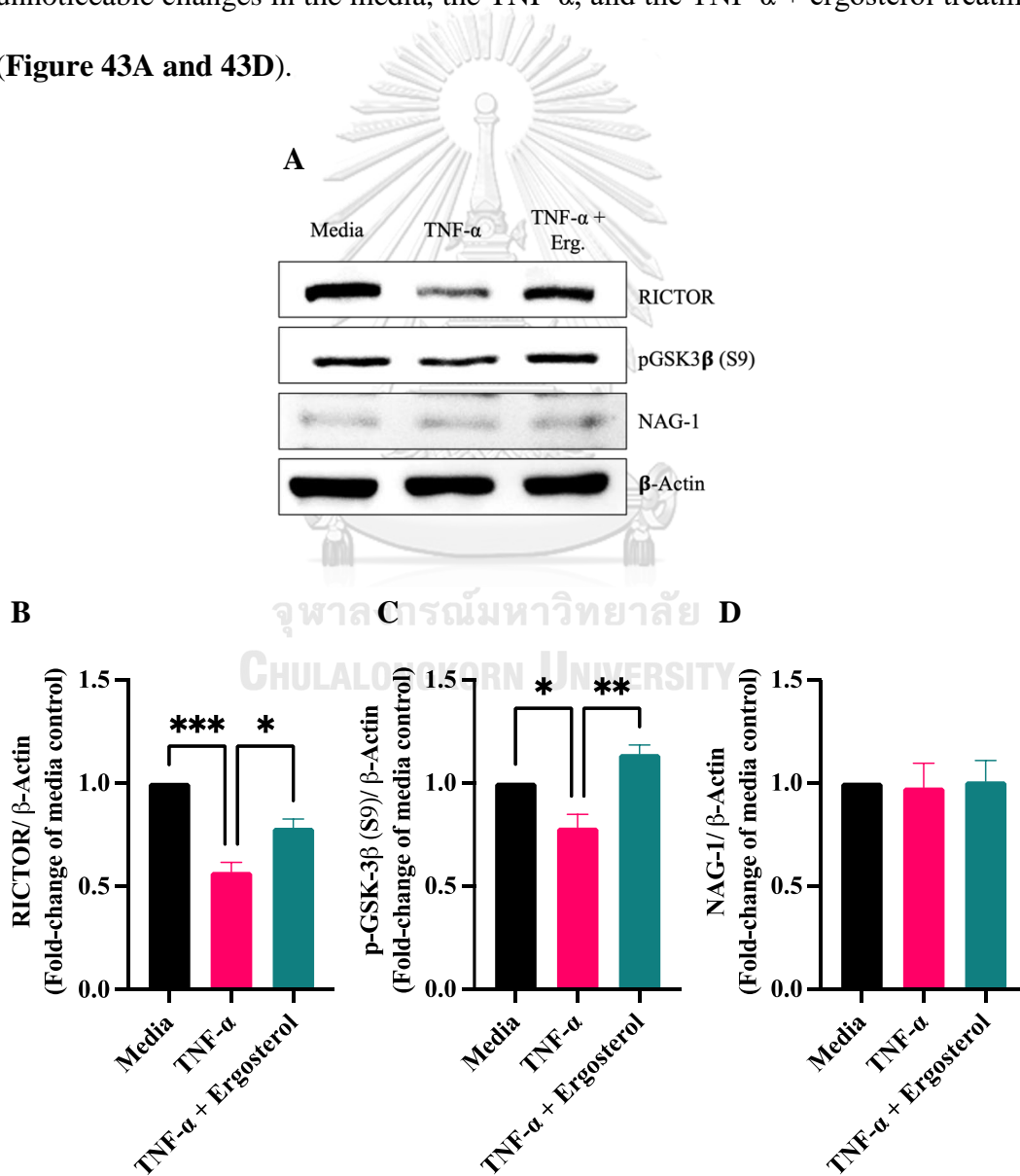


**Figure 43** The molecular mechanism of ergosterol associated with programmed cell death in TNF- $\alpha$ -treated HT-22 hippocampal cells.

(A) Representative immunoblots and relative fold-change expressions of (B) RICTOR, (C) GSK-3 $\beta$  (S9), and (D) NAG-1 in TNF- $\alpha$ -treated HT-22 cells in the presence or absence of ergosterol, after 24 h. All data are shown as the mean  $\pm$  SEM of experiments conducted in triplicate. Statistical significance was analyzed by a one-way ANOVA and a Dunnett's test. \*  $P < 0.05$ , \*\*  $P < 0.01$  and \*\*\*  $P < 0.001$ .

#### **14. The effect of ergosterol on NMDA receptors in TNF- $\alpha$ -induced HT-22 cell death**

TNF- $\alpha$  can stimulate the surface expression of glutamate receptors, including AMPA and NMDA receptors (6, 100). Based on the characterization of the cell model, the HT-22 cells do not express the AMPA receptors. In this study, we, therefore, investigated the expression of NMDA receptors associated with the treatment of TNF- $\alpha$  and ergosterol. The transcriptional expressions of the glutamate ionotropic receptor NMDA type subunit 2A (*Grin2a*) and 2B (*Grin2b*) were determined by RT-PCR. As shown in **Figure 44**, TNF- $\alpha$  was able to dramatically elevate the mRNA expression of both *Grin2a* and *Grin2b*. On the other hand, the co-exposure of the HT-22 cells to ergosterol and TNF- $\alpha$  led to a significant downregulation of the expression of both *Grin2a* and *Grin2b*.

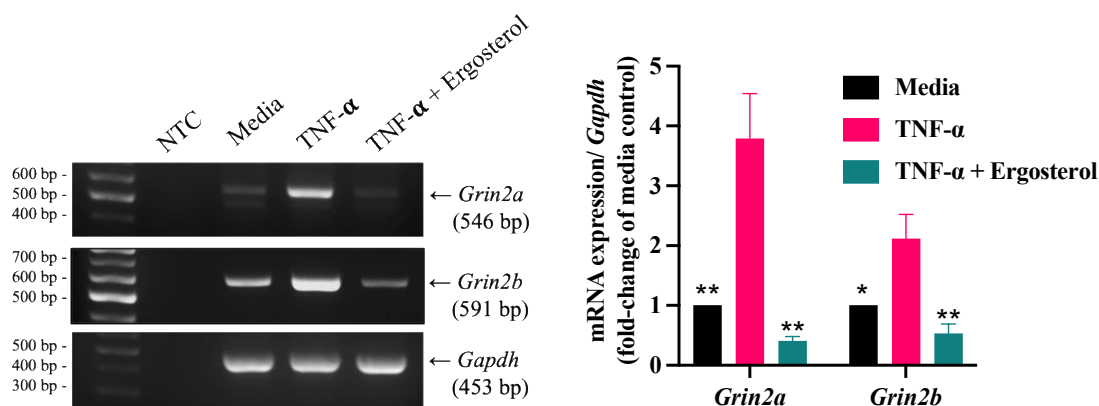


**Figure 44** The mRNA expressions of the glutamate ionotropic receptor NMDA type subunit 2A (*Grin2a*) and 2B (*Grin2b*) in TNF- $\alpha$ -treated HT-22 cells, in the presence or absence of ergosterol, after 24 h.

All data are shown as the mean  $\pm$  SEM of experiments conducted in triplicate. Statistical significance was analyzed by a one-way ANOVA and a Dunnett's test. \*  $P < 0.05$  and \*\*  $P < 0.01$

It has been reported that the transcriptional expression of NMDA receptors is regulated by several transcription factors, including EGR proteins (44). Thus, we further determined the expression of EGR-1 through Western blotting. The results showed that TNF- $\alpha$  was able to significantly upregulate the expression of EGR-1, as compared to the vehicle-treated cells. In contrast, ergosterol potentially inverted the expression of EGR-1 in the TNF- $\alpha$ -treated HT-22 cells (**Figure 45A**). Moreover, we examined the EGR-1 activity by using a luciferase construct containing an EGR-1 binding site (EBS). As expected, TNF- $\alpha$  significantly induced the EBS-luciferase activity in HT-22 cells (as compared to the media control); however, the EBS-luciferase activity was significantly decreased (as compared to the TNF- $\alpha$  control) in the presence of ergosterol (**Figure 45B**).



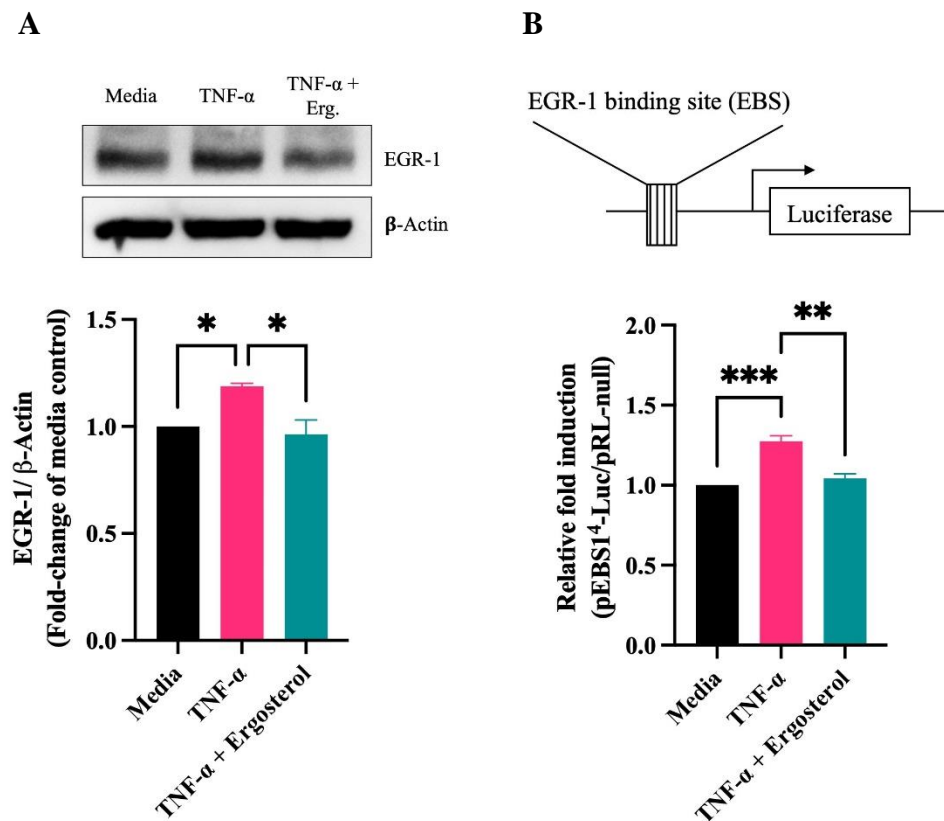


**Figure 45** The effects of ergosterol on EGR-1 signaling in TNF- $\alpha$ -induced HT-22 hippocampal cells.

(A) The protein expression of EGR-1 in TNF- $\alpha$ -treated HT-22 cells, in the presence or absence of ergosterol, after 24 h. (B) Luciferase activity of EGR-1 binding site (EBS) of TNF- $\alpha$ -induced HT-22 cells, in the presence or absence of ergosterol, after 24 h. All data are shown as the mean  $\pm$  SEM of experiments conducted in triplicate. Statistical significance was analyzed by a one-way ANOVA and a Dunnett's test. \*  $P < 0.05$ , \*\*  $P < 0.01$ , and \*\*\*  $P < 0.001$ .

To examine whether the EGR-1 can regulate the *Grin2a* and *Grin2b* gene expressions in HT-22 cells, EGR-1-overexpressing HT-22 cells were constructed, and the expressions of *Grin2a* and *Grin2b* were determined. As shown in **Figure 46A**, the EGR-1-overexpressing HT-22 cells exhibited an increase in both the protein and the

mRNA EGR-1 expression levels, as compared to those of the negative control (LacZ). Interestingly, the EGR-1-overexpressing HT-22 cells upregulated the transcriptional levels of *Grin2b* (as compared to those of the LacZ control), whereas the mRNA expression of *Grin2a* was not affected (**Figure 46B**). These results suggest that the EGR-1 is involved in the regulation of *Grin2b* transcription in the HT-22 cells.

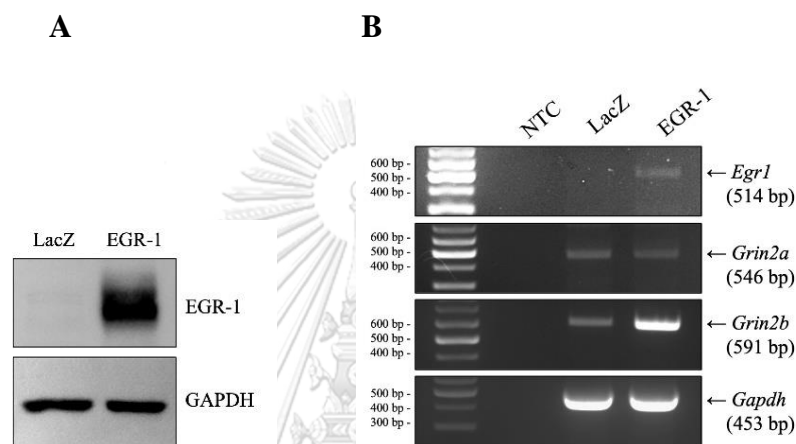


**Figure 46** The effects of EGR-1 on NMDA receptors in HT-22 hippocampal cells. (A) The EGR-1 protein expression of EGR-1-overexpressing HT-22 cells, as compared to the negative control (LacZ-transfected HT-22 cells). (B) The transcriptional expressions of *Grin2a* and *Grin2b* in the EGR-1-transfected HT-22 cells.

Next, the protein expression of NMDA receptor subunit 2B (NR2B) was further examined by Western blot and immunofluorescence imaging assays. As shown in **Figure 47A**, TNF- $\alpha$  significantly increased NR2B protein expression compared to the media control. Ergosterol exhibited significant down-regulation of NR2B in TNF- $\alpha$ -exposed HT-22 cells. Moreover, the immunofluorescence staining resulted in the same trend as the Western blot analysis (**Figure 47B**).

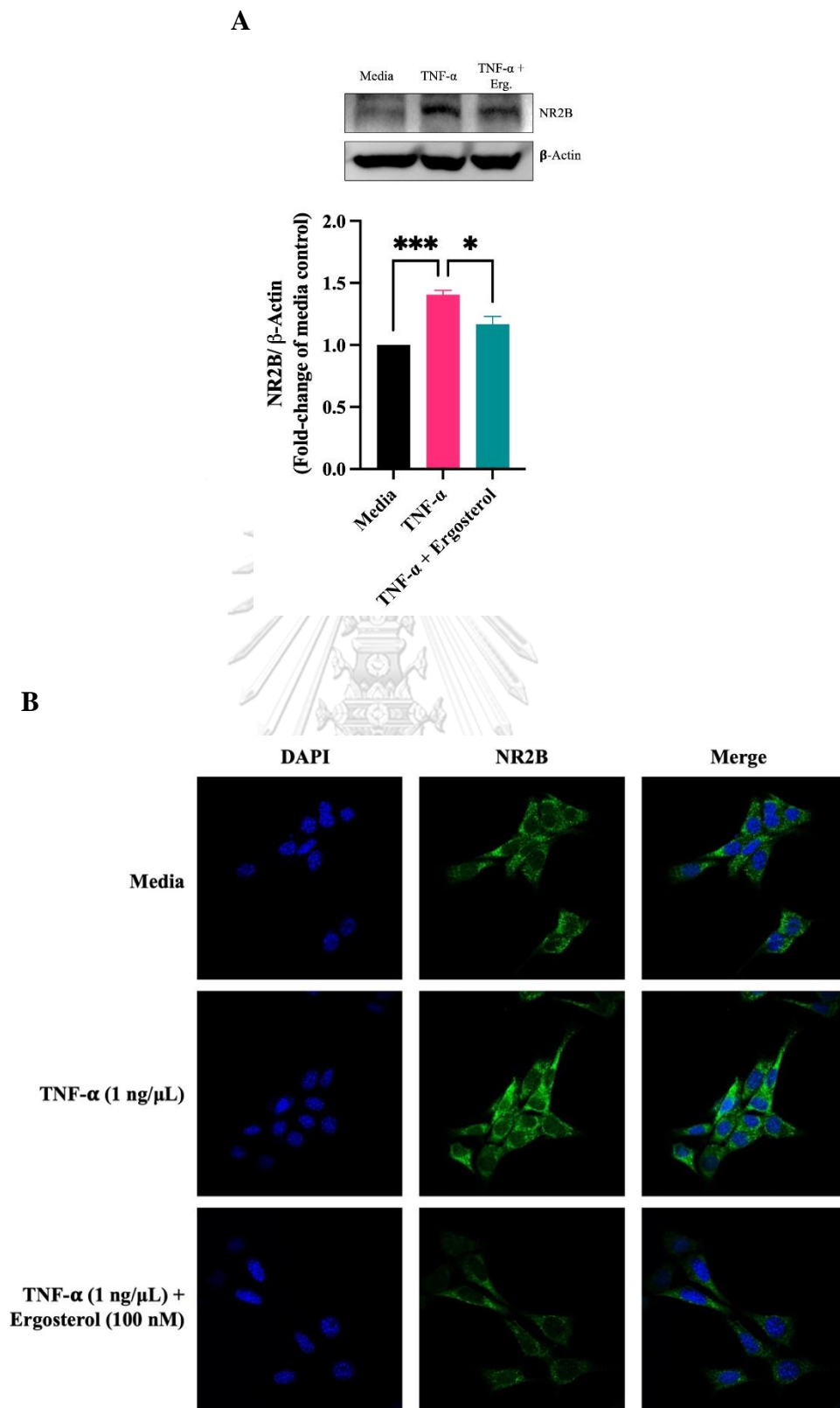


**Figure 47** The effect of ergosterol on NMDA receptor expression in TNF- $\alpha$ -induced HT-22 hippocampal cells.

(A) The protein expression of NMDA receptor subunit 2B (NR2B) in TNF- $\alpha$ -treated HT-22 cells, in the presence or absence of ergosterol, after 24 h. All data are shown as the mean  $\pm$  SEM of experiments conducted in triplicate. Statistical significance was analyzed by a one-way ANOVA and a Dunnett's test. \*  $P < 0.05$  and \*\*\*  $P < 0.001$ .

(B) Representative images of NR2B immunofluorescence staining in TNF- $\alpha$ -treated HT-22 cells, in the presence or absence of ergosterol, after 24 h. The cells were observed under a confocal microscope with 40 $\times$  magnification.



## CHAPTER V

### DISCUSSION

Brain inflammation is a pathological hallmark of AD and is characterized by an increased number of activated microglial cells, which are the resident macrophages in the central nervous system. Activated cells produce inflammatory substances such as pro-inflammatory cytokines (TNF- $\alpha$ , IL-1 $\beta$ , IL-6, and IFN- $\gamma$ ), chemokines, prostaglandins, ROS, nitric oxide (NO), complement factors, and C-reactive protein (30). Accumulating data suggest that inflammatory mediators could increase A $\beta$  production in neuronal cells, and that A $\beta$  could activate glial cell inflammation in a vicious circle (31). A previous study showed that pro-inflammatory cytokines released from microglia act as neurotoxins that cause neuronal injury and lead to AD (32). Furthermore, pro-inflammatory cytokines contribute to neurodegeneration by inducing apoptosis, excitotoxicity, immune activation, and cytotoxicity in neurons (33). Therefore, inhibition of microglial cytokine production may be a potential target for treating neurodegenerative diseases, including AD.

BPA-derived plastics have applications in day-to-day activities (1). Previous studies have reported that free BPA was detected in the urine and serum of pregnant women, umbilical cord serum, and breast milk (2). The U.S. Food and Drug Administration and the European Food Safety Authority have determined that the safety levels of BPA exposure are lower than 50–4  $\mu\text{g}/\text{kg}$  body weight/day in animals and lower than 10  $\mu\text{M}$  in cell lines (34). Our current study found that exposure of

BV2 microglial cells to BPA exhibited acute toxicity at a concentration of 10  $\mu\text{M}$ . In contrast, doses lower than or equal to 10  $\mu\text{M}$  BPA were safe for BV2 cells when treated for up to 48 h (**Figure 20**). Moreover, micromolar BPA concentrations ( $\leq 10$   $\mu\text{M}$ ) could induce microglial cell activation by changing both cell morphology and gene expression. mRNA expression of pro-inflammatory cytokines (TNF- $\alpha$ , IL-1 $\beta$ , and IL-6) in BV2 cells was upregulated after exposure to BPA (2.5–10  $\mu\text{M}$ ) for 24 h (**Figure 22 and 23**). Cell imaging showed that BPA could induce microglial cell activation by increasing the population of cells with elongated morphology, indicating active BV2 microglial cells (81) (**Figure 21**). These findings are consistent with a previous report by Zhu *et al.* (2015), who reported that BPA could activate microglial inflammation by inducing morphological changes and increased TNF- $\alpha$  and IL-1 $\beta$  inflammatory cytokines production (4).

AP, an edible mushroom, has been used as a medicinal food (46). Previous studies have demonstrated that AP has several medicinal properties, including antioxidant (13), anti-tumor (14, 15), anti-hypercholesterolemic (16), anti-human immunodeficiency virus type-1 (17), and anti-inflammatory (18) activities. Chiu *et al.* reported that aqueous extracts of AP could protect nonalcoholic fatty liver disease by attenuating the inflammatory response in rats (18). Herein, we studied the anti-neuroinflammatory activity of AP extracts derived from three extraction solvents, including hexane, ethanol, and water, in BPA-induced BV2 microglial cells. We found that APH (10  $\mu\text{g/mL}$ ) and APE (2.5, 5  $\mu\text{g/mL}$ ) could ameliorate BPA-induced BV2 inflammation by suppressing mRNA expression and production of TNF- $\alpha$ , IL-1 $\beta$ , and IL-6, as well as the number of activated microglial cells (**Figure 25-27**). Previous study reported that APE displayed the highest anti-inflammatory activity

among all the AP extracts by suppressing NO production and increasing lipid accumulation in RAW264.7 macrophages (19).

However, in this study, we observed that APW could not attenuate BPA-induced BV2 inflammation; moreover, it increased pro-inflammatory cytokines at both the mRNA and protein levels (**Figure 26 and 27**). Previous studies have reported that the aqueous extract of mushrooms is rich in polysaccharides, including  $\beta$ -glucans, which have immunomodulatory activity (101, 102). Yan J *et al.* found that polysaccharides isolated from *Amillariella mellea* could promote macrophage phagocytosis and production of inflammatory substances including NO, ROS, TNF- $\alpha$ , IL-6, and IL-1 $\beta$  *via* NF- $\kappa$ B/ MAPK signaling pathways in RAW264.7 mouse macrophages cell line (103). Thus, the increase in inflammatory markers in BPA/APW-treated BV2 cells could be due to the presence of bioactive polysaccharides in APW.

The activation of c-Jun N-terminal protein kinase (JNK), extracellular signal-regulated kinase (ERK), mitogen-activated protein kinase (MAPK), and nuclear factor kappa-light-chain-enhancer of activated B cells (NF- $\kappa$ B) has been observed in BPA-induced microglial cells (4). Sukjamnong *et al.* reported that BPA-exposed maternal rats significantly increased the risk of AD pathological development in offspring by downregulation of genes associated with AD neuropathology and inflammation; moreover, they observed that the expression of NF- $\kappa$ B protein significantly increased in the offspring hippocampus of BPA-exposed maternal rats (37). The current study also demonstrated that BV2 microglial cells exposed to 5  $\mu$ M BPA upregulated NF- $\kappa$ B signaling by increasing p-I $\kappa$ B $\alpha$ /I $\kappa$ B $\alpha$  expression and NF- $\kappa$ B p65 nuclear

translocation and transcription *via* the NF- $\kappa$ B-response element (**Figure 28 and 29**). Furthermore, BPA elevated the expression of iNOS, an inflammatory marker, in the NF- $\kappa$ B signaling pathway (104). Interestingly, co-treatment with BPA and APE attenuated these inflammatory responses in BV2 cells *via* the NF- $\kappa$ B pathway. However, COX-2, an inflammatory mediator regulated by NF- $\kappa$ B signaling, slightly increased when BV2 cells were exposed to BPA at 5  $\mu$ M (**Figure 30A and 30C**). The previous report of Huang FM *et al.* demonstrated that a high concentration of BPA (10  $\mu$ M) significantly upregulated the expression of COX-2 in RAW264.7 macrophages (104). To the best of our knowledge, this is the first study to report COX-2 expression induced by BPA in BV2 cells. These results suggest that APE may be a valuable source of natural compounds which exhibit neuroinflammatory activity and protect against neurodegenerative diseases caused by BPA toxicity.

According to a previous report, BPA induces neurodegeneration *via* ROS induction (93). Moreover, excess ROS causes inflammation through the activation of NF- $\kappa$ B signaling (105-107). Thus, we have determined the ability of AP extracts to suppress oxidative stress. APH and APE increased the production of the antioxidant enzyme SOD-1 in BV2 cells; moreover, these extracts restored ROS levels in BPA-induced BV2 cells (**Figure 31**).

The chemical composition of APE was further analyzed based on the potential anti-inflammatory effects of APE. In this study, ergosterol was isolated from APE and its biological activity against BPA induction of inflammation was examined. Recent findings demonstrated that ergosterol significantly suppressed NF- $\kappa$ B signaling in BPA-induced BV2 cells by inhibiting the phosphorylation of I $\kappa$ B $\alpha$  and expression of



iNOS (**Figure 37**). Based on the GC/MS analysis, APH and APE were composed of ergosterol approximately 25.75 (17) and 19.14% (**Appendix, Figure A6-A7 and Table A1-A2**), respectively. In comparison, APH is a rich source of ergosterol than APE. Based on the anti-neuroinflammatory effects, APE (5  $\mu\text{g/mL}$ , calculated ergosterol content = 0.96  $\mu\text{g/mL}$ ) suppressed the NF- $\kappa\text{B}$  signaling stronger than that of APH (10  $\mu\text{g/mL}$ , calculated ergosterol content = 2.58  $\mu\text{g/mL}$ ). However, the overall activity of APE may also be contributed by other polar compounds in APE. A previous study reported AP ethanol crude extract composed of phenolic compounds such as gallic acid and vanillic acid (48). We also found that APE contained higher phenolic and flavonoid content than that found in APH. Sangphech N *et al.* demonstrated that the ethanolic extract of AP was composed of 15-deoxy- $\Delta^{12,14}$ -prostaglandin J2-2-glycerol ester, which suppressed inflammation in RAW264.7 macrophages through inhibition of the peroxisome proliferator-activated receptor gamma (PPAR $\gamma$ ) and induction of lipid accumulation (19).

Moreover, APH showed better activity on iNOS inhibition than APE (**Figure 30A and 30B**). This effect is correlated to the amount of ergosterol contained in the extracts. Nallathamby *et al.* observed that ergosterol could attenuate LPS-induced BV2 cell inflammation by reducing the production of NO, which was generated by iNOS (21). Ergosterol is classified as a phytosterol or plant-derived sterol (108). Furthermore, phytosterols have been suggested to have potential therapeutic applications for neurodegenerative diseases, primarily targeting neuroinflammation and neurodegeneration (109). Previous studies reported that ergosterol showed anti-inflammatory activity through NF- $\kappa\text{B}$  signaling in several cells, such as human bronchial epidermal cells (16HBE) (69), mouse macrophages (RAW264.7) (70), and

mouse lungs (69, 71). These findings suggest that ergosterol might be an active component of APE and responsible for its anti-inflammatory effects in BPA-induced BV2 cells.

The cytotoxicity of AP extract-treated BV2-conditioned medium against HT-22 cells showed that the conditioned medium collected from BPA-induced BV2 cells significantly reduced HT-22 cell viability. However, the conditioned medium collected from the co-treatment of BPA and AP extracts on BV2 cells did not significantly exhibit a neuroprotective effect (**Figure 32B**). These results were supported by using the co-culture system between BV2 microglial and HT-22 hippocampal cells (**Figure 32C**). This effect may be caused by other cytotoxic factors presented in the conditioned medium such as interferon- $\gamma$ , glutamic acid, and histamine (33). Moreover, APH and APE did not suppress the level of TNF- $\alpha$  production in the BPA-induced BV2 cells (**Figure 26A and 27A**), this TNF- $\alpha$  might still cause neurotoxic in the HT-22 cells. Therefore, we further investigated the direct neuroprotective effect of AP isolated compound, ergosterol against TNF- $\alpha$ -induced neuronal death.

Neuroinflammation is characterized by an elevation of the levels of inflammatory mediators in the CNS. TNF- $\alpha$  is one of the inflammatory mediators that is found to increase brain inflammation. The excess levels of TNF- $\alpha$  lead to synaptic dysfunction and neuronal death, which can be a cause of the development of neurodegenerative disorders. Herein, we focused on the neuroprotective effects of ergosterol against TNF- $\alpha$ -induced hippocampal cell injury. We found that 100 nM of ergosterol was able to significantly increase the number of viable cells in the TNF- $\alpha$ -

treated HT-22 cells (**Figure 39**). Ergosterol is a natural sterol commonly found in mushroom species such as *Agaricus blazei* (54), *Ganoderma lucidum* (55), and *Hericium novae-zealandiae* (110). Several medicinal properties of ergosterol have been reported: antioxidant (73), anti-inflammatory (21), antiviral (17), and anti-cancer (111). However, the neuroprotective effects of ergosterol have not been elucidated in detail. In this study, we found that ergosterol can increase the expression of SOD-1, and protect against TNF- $\alpha$ -induced neuronal death by increasing the ARE and the ROS scavenging activities (**Figure 40**). Sun *et al.* have evaluated the antioxidant activity of ergosterol against cigarette smoke extract-induced chronic obstructive pulmonary disease, and have found that ergosterol could increase the levels of certain antioxidant enzymes (such as SOD and catalase), and suppress the levels of malondialdehyde (a highly reactive compound) not only in human bronchial epithelial cells (16HBE cells), but also in BALB/c mice (69). Thus, ergosterol might be a good candidate to consider as a basis for the development of an antioxidant compound.

Furthermore, molecules that regulate programmed cell death were screened by using an apoptosis antibody array, after a 24-h treatment with TNF- $\alpha$  in the presence and absence of ergosterol. Among seventeen molecules, the top five proteins that showed different expressions between TNF- $\alpha$  and TNF- $\alpha$  + ergosterol treatments were considered. Ergosterol tended to upregulate these candidate molecules: ATM (S1981), Casp3 (D175), TAK1 (S412), I $\kappa$ B $\alpha$  (S32), and Akt (S473), compared to TNF- $\alpha$  control (**Figure 41**). According to the literature, three out of five molecules have been reported to promote neuronal survival, such as pATM (S1981), I $\kappa$ B $\alpha$  (S32), and pAkt (S473). We have, herein, focused on the activation of the Akt signaling, which is a well-known signaling pathway that is capable of potentiating neuroprotection.

Western blotting results confirmed the antibody array screening findings in that ergosterol was able to induce the phosphorylation of Akt (S473), as shown in **Figure 42A**. According to the previous study, Akt Ser473 phosphorylation is induced by growth factors through mammalian target of rapamycin complex 2 (mTORC2), a serine/threonine protein kinase (97, 98). The mTORC2 is composed of four core subunits, including mTOR, rapamycin-insensitive companion of mTOR (RICTOR), mammalian stress-activated Map kinase-interacting 1 (mSIN1), and mammalian lethal with SEC13 protein 8 (mLST8) (112). A previous study demonstrated that silencing of RICTOR expression in 3T3-L1 adipocytes inhibited Ser473 phosphorylation of Akt (113). Herein, we found that ergosterol increased the expression of RICTOR in the TNF- $\alpha$ -induced HT-22 cells (**Figure 43A and 43B**). An active Akt can in turn activate the phosphorylation of GSK-3 $\beta$  and promote neural development (114). The current study has demonstrated that TNF- $\alpha$  can suppress pGSK-3 $\beta$  (S9) expression, while the presence of ergosterol could invert the expression of pGSK-3 $\beta$  (S9) (**Figure 43A and 43C**). These results suggest that ergosterol could protect against neuronal death, through the activation of the Akt/GSK-3 $\beta$  signaling pathway. The upregulating of the Akt/GSK-3 $\beta$  signaling could inhibit the accumulation of amyloid- $\beta$  and tau phosphorylation, which are the hallmarks of Alzheimer's disease (95, 96). Thus, ergosterol could affect the Akt/GSK-3 $\beta$  signaling pathway, thereby exerting a neuroprotective effect against amyloid- $\beta$ -induced primary hippocampal cell apoptosis (115).

The ataxia-telangiectasia mutated (ATM) signaling is another interesting target of ergosterol for the promotion of its neuroprotective effects. ATM plays a crucial role in the DNA repair process (116); therefore, an upregulation of the ATM

expression may attenuate the cellular damage caused by TNF- $\alpha$  toxicity. According to a previous report, ATM phosphorylation was able to potentiate the myocyte enhancer factor 2D activation, thereby resulting in an enhancement of neuronal survival after an exposure to a DNA-damaging agent (117). Moreover, ATM plays a fundamental role in neuronal homeostasis, by participating in chromatin remodeling, in the DNA repair response, and in the differentiation of immortalized human neural stem cells (118-120). Besides, I $\kappa$ B $\alpha$  is an inhibitory subunit of the NF- $\kappa$ B protein complex, which is an inactive form residing in the cytoplasm. Phosphorylation of I $\kappa$ B $\alpha$  by the I $\kappa$ B kinase complex (IKK) subsequently induces I $\kappa$ B $\alpha$  degradation and releases the active NF- $\kappa$ B. This active NF- $\kappa$ B translocates into the nucleus and regulates several gene expressions (121). Gene targets of NF- $\kappa$ B that have been shown to promote neuronal survival such as brain-derived neurotrophic factor (BDNF), B-cell lymphoma 2 (Bcl-2), B-cell lymphoma-extra-large (Bcl-xL), superoxide dismutase 2 (SOD-2), and inhibitor of apoptosis proteins (IAP) (122, 123). Moreover, NF- $\kappa$ B plays role in synaptic plasticity and long-term memory (124). Thus, these proteins: pATM (S1981) and I $\kappa$ B $\alpha$  (S32) might elucidate the underlying mechanism for the neuroprotective effect of ergosterol against TNF- $\alpha$ -induced hippocampal cell injury.

NAG-1, or growth/differentiation factor-15 (GDF-15) is widely distributed in the CNS and plays a role in neuronal homeostasis (125, 126). According to a report by Liu *et al.*, GDF-15 overexpression was able to protect against neuronal death through the promotion of the mitochondrial function in oligomycin-treated HT-22 cells (99). Moreover, based on a transcriptional analysis, they proposed that GDF-15 might regulate these effects *via* the PI3K/Akt signaling pathway (99). However, we have found that the translational level of NAG-1 did not significantly change in either

the TNF- $\alpha$ -treated or the TNF- $\alpha$ - and ergosterol-treated HT-22 cells (**Figure 43A and 43D**). This finding suggests that TNF- $\alpha$  does not affect neuronal proliferation *via* the NAG-1 signaling pathway.

The dysregulation of neuroplasticity is a common cause of brain disorders (127, 128). The activation of the NMDA receptor can cause synaptic dysfunction, leading to the development of Alzheimer's disease (39). An excessive level of inflammatory mediators (including TNF- $\alpha$ ) in the CNS can activate the translocation of NMDA receptors to the membrane; this event causes a calcium influx into the neuronal cells, thereby causing neuronal death (6, 100). A recent study has demonstrated that TNF- $\alpha$  can stimulate the transcriptional expression of *Grin2a* and *Grin2b*; the glutamate ionotropic NMDA receptor encoding genes. Interestingly, the presence of ergosterol was able to downregulate the expressions of these genes (**Figure 44**). The transcriptional expression of the NMDA receptors is regulated by several transcription factors, including those belonging to the NF- $\kappa$ B family, the Jun and Fos families, and the EGR family (44). We, herein, demonstrate that an upregulation of the *Grin2b* levels was at least regulated by an increase in the levels of the EGR-1 transcription factor, occurring through the binding of the EGR-1 response element (**Figure 45–47**). However, EGR-1 was not involved in the transcriptional regulation of *Grin2a*, as shown in **Figure 45B**.

Ergosterol could protect the TNF- $\alpha$ -induced HT-22 hippocampal cell injury through antioxidant, cell survival, and NMDA receptor signaling pathways. In the normal condition, an absence of the TNF- $\alpha$  activation, ergosterol trend to increase the expression on SOD-1, an antioxidant enzyme in HT-22 cells in a dose-dependent

manner (**Appendix, Figure A8A**). Besides, ergosterol (10 and 100 nM)-treated HT-22 cells did not show significant alterations on RICTOR, Akt, GSK3 $\beta$ , EGR-1, and NR2B levels (**Appendix, Figure A8B-A8G**). These results indicate that ergosterol protects TNF- $\alpha$ -induced HT-22 cells without altering molecular signalings of inactivated HT-22 cells.



## CHAPTER VI

### CONCLUSION

#### 1. Conclusion

The current study revealed that BPA could induce inflammation in BV2 microglial cells by upregulating the secretion of pro-inflammatory mediators *via* NF- $\kappa$ B signaling. This subsequently caused HT-22 hippocampal cell damage by increasing ROS accumulation in the neurons. AP extracts prepared from an edible mushroom exhibited anti-inflammatory and neuroprotective effects in BPA-induced BV2 cells. APE displayed the most significant potential against BPA-induced inflammation in BV2 cells by suppressing ROS production and NF- $\kappa$ B signaling, leading to the reduction of the expression of pro-inflammatory mediators. Accordingly, it could protect against BPA-induced neuronal damage, which is a cause of neurodegeneration. Furthermore, ergosterol was isolated from APE, and its biological activities against BPA-induced BV2 cells were evaluated. Ergosterol increased SOD-1 expression and suppressed NF- $\kappa$ B signaling, suggesting that ergosterol might be an active component of APE that plays a role in the anti-inflammatory effect *via* the NF- $\kappa$ B pathway in BPA-induced BV2 cell activation (Figure 48).



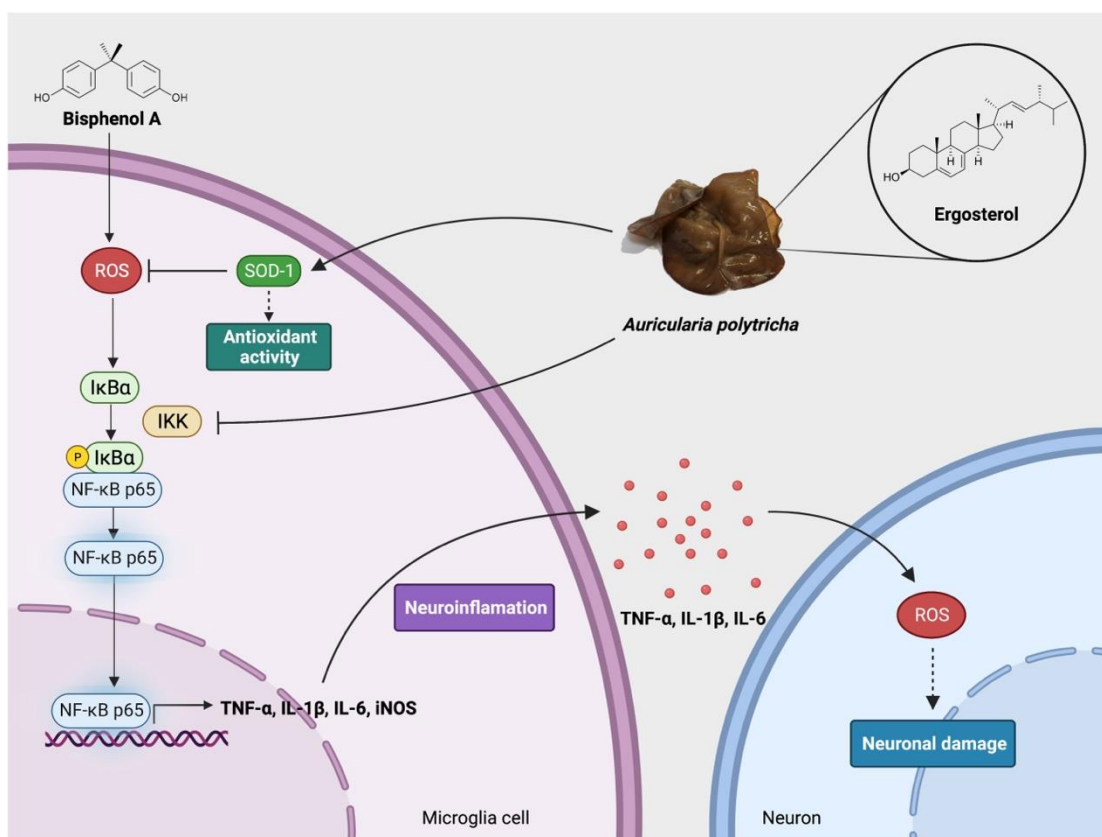


**Figure 48** Schematic diagram showing the proposed mechanisms underlying anti-neuroinflammatory effects of *A. polytricha* extracts and ergosterol against BPA-induced microglial cell activation.

Moreover, this study has demonstrated that ergosterol can attenuate the TNF- $\alpha$ -induced neuronal toxicity in HT-22 cells. This neuroprotective activity is regulated by the antioxidant, cell survival, and NMDA receptor pathways. Ergosterol was able to increase the expression of SOD-1, RICTOR, pAkt, and pGSK3 $\beta$  and to suppress the *Grin2b* transcription via an EGR-1 regulation (**Figure 49**). These findings demonstrate novel therapeutic activities of AP extracts and ergosterol in anti-neuroinflammation and neuroprotection that might be of benefit for patients with neurodegenerative diseases.

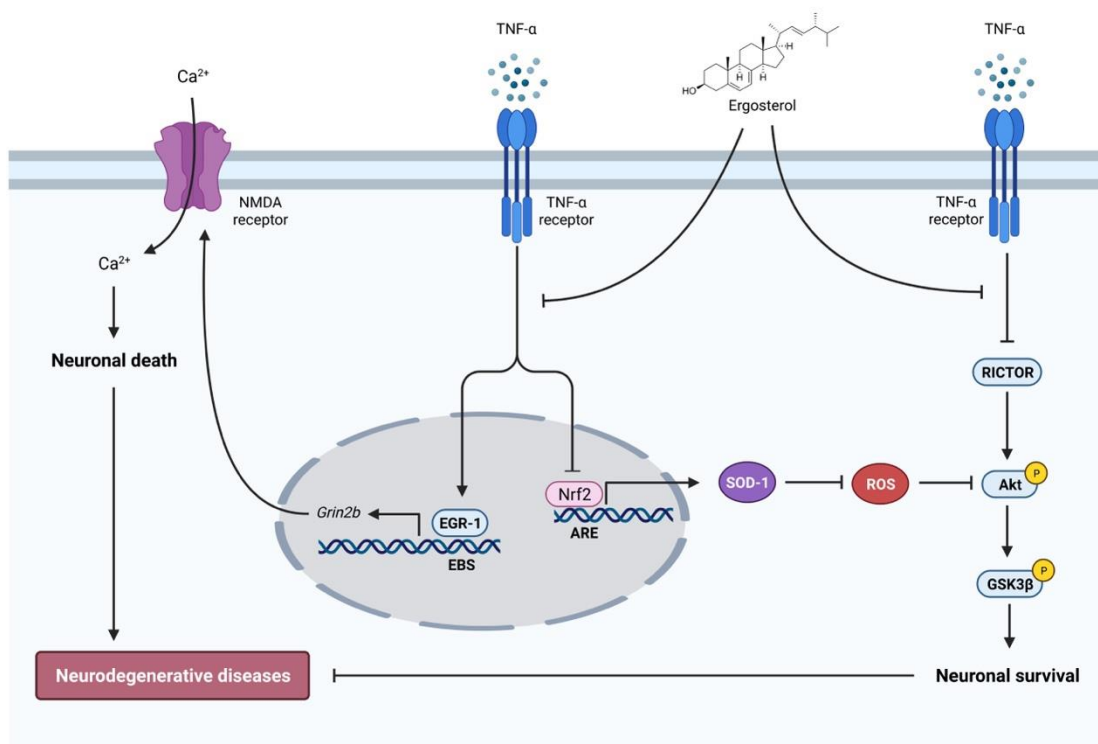


**Figure 49** Schematic diagram showing the proposed mechanisms underlying neuroprotective effects of ergosterol against TNF- $\alpha$ -induced hippocampal cell damage.

## 2. Limitation of the study

The present study determined the *in vitro* anti-neuroinflammatory and neuroprotective effects of AP extracts and chemical constituent, ergosterol using BV2 microglial and HT-22 hippocampal cell lines. However, this work is an initial step in the development of drugs or supplementary substances. The *in vivo* models and clinical trials should be further investigated to prove these findings.

## REFERENCES



จุฬาลงกรณ์มหาวิทยาลัย  
**CHULALONGKORN UNIVERSITY**

1. Chapin RE, Adams J, Boekelheide K, Gray Jr LE, Hayward SW, Lees PS, et al. NTP-CERHR expert panel report on the reproductive and developmental toxicity of bisphenol A. *Birth Defects Research Part B: Developmental and Reproductive Toxicology*. 2008;83(3):157-395.
2. Murata M, Kang J-H. Bisphenol A (BPA) and cell signaling pathways. *Biotechnology advances*. 2018;36(1):311-327.
3. Wang T, Xie C, Yu P, Fang F, Zhu J, Cheng J, et al. Involvement of insulin signaling disturbances in bisphenol a-induced alzheimer's disease-like neurotoxicity. *Scientific reports*. 2017;7(1):1-12.
4. Zhu J, Jiang L, Liu Y, Qian W, Liu J, Zhou J, et al. MAPK and NF- $\kappa$ B pathways are involved in bisphenol A-induced TNF- $\alpha$  and IL-6 production in BV2 microglial cells. *Inflammation*. 2015;38(2):637-648.
5. Thongkorn S, Kanlayaprasit S, Jindatip D, Tencomnao T, Hu VW, Sarachana T. Sex differences in the effects of prenatal bisphenol A exposure on genes associated with autism spectrum disorder in the hippocampus. *Scientific reports*. 2019;9(1):1-14.
6. Olmos G, Lladó J. Tumor necrosis factor alpha: a link between neuroinflammation and excitotoxicity. *Mediat Inflamm*. 2014;2014:1-12.
7. Xiao J, Yao R, Xu B, Wen H, Zhong J, Li D, et al. Inhibition of PDE4 attenuates TNF- $\alpha$ -triggered cell death through suppressing NF- $\kappa$ B and JNK activation in HT-22 neuronal cells. *Cell Mol Neurobiol*. 2020;40(3):421-435.
8. Yang L, Lindholm K, Konishi Y, Li R, Shen Y. Target depletion of distinct tumor necrosis factor receptor subtypes reveals hippocampal neuron death and

- survival through different signal transduction pathways. *J Neurosci.* 2002;22(8):3025-3032.
9. Krönke M. Involvement of sphingomyelinases in TNF signaling pathways. *Chem Phys Lipids.* 1999;102(1-2):157-166.
  10. Liu S, Wang X, Li Y, Xu L, Yu X, Ge L, et al. Necroptosis mediates TNF-induced toxicity of hippocampal neurons. *BioMed research international.* 2014;2014:1-11.
  11. Wang L, Deng B, Yan P, Wu H, Li C, Zhu H, et al. Neuroprotective effect of ketamine against TNF- $\alpha$ -induced necroptosis in hippocampal neurons. *Journal of cellular and molecular medicine.* 2021;25(7):3449-3459.
  12. Wheeler D, Knapp E, Bandaru VV, Wang Y, Knorr D, Poirier C, et al. Tumor necrosis factor- $\alpha$ -induced neutral sphingomyelinase-2 modulates synaptic plasticity by controlling the membrane insertion of NMDA receptors. *J Neurochem.* 2009;109(5):1237-1249.
  13. Chen Y, Xue Y. Purification, chemical characterization and antioxidant activities of a novel polysaccharide from *Auricularia polytricha*. *International journal of biological macromolecules.* 2018;120:1087-1092.
  14. Yu J, Sun R, Zhao Z, Wang Y. *Auricularia polytricha* polysaccharides induce cell cycle arrest and apoptosis in human lung cancer A549 cells. *International Journal of Biological Macromolecules.* 2014;68:67-71.
  15. Song G, Du Q. Isolation of a polysaccharide with anticancer activity from *Auricularia polytricha* using high-speed countercurrent chromatography with an aqueous two-phase system. *Journal of Chromatography A.* 2010;1217(38):5930-5934.

16. Zhao S, Rong C, Liu Y, Xu F, Wang S, Duan C, et al. Extraction of a soluble polysaccharide from *Auricularia polytricha* and evaluation of its anti-hypercholesterolemic effect in rats. *Carbohydrate polymers*. 2015;122:39-45.
17. Sillapachaiyaporn C, Nilkhet S, Ung AT, Chuchawankul S. Anti-HIV-1 protease activity of the crude extracts and isolated compounds from *Auricularia polytricha*. *BMC Complementary and Alternative Medicine*. 2019;19(1):1-10.
18. Chiu WC, Yang HH, Chiang SC, Chou YX, Yang HT. *Auricularia polytricha* aqueous extract supplementation decreases hepatic lipid accumulation and improves antioxidative status in animal model of nonalcoholic fatty liver. *BioMedicine*. 2014;4(2):29-38.
19. Sangphech N, Sillapachaiyaporn C, Nilkhet S, Chuchawankul S. *Auricularia polytricha* ethanol crude extract from sequential maceration induces lipid accumulation and inflammatory suppression in RAW264. 7 macrophages. *Food & Function*. 2021;12(21):10563-10570.
20. Bennett L, Sheean P, Zabarar D, Head R. Heat-stable components of wood ear mushroom, *Auricularia polytricha* (higher Basidiomycetes), inhibit in vitro activity of beta secretase (BACE1). *International journal of medicinal mushrooms*. 2013;15(3):233-249.
21. Nallathamby N, Guan-Serm L, Vidyadaran S, Malek SNA, Raman J, Sabaratnam V. Ergosterol of *Cordyceps militaris* attenuates LPS induced inflammation in BV2 microglia cells. *Natural product communications*. 2015;10(6):885-886.
22. Shankar GM, Walsh DM. Alzheimer's disease: synaptic dysfunction and A $\beta$ . *Molecular neurodegeneration*. 2009;4(1):1-13.

23. Chen Y, Deng Y, Zhang B, Gong C-X. Deregulation of brain insulin signaling in Alzheimer's disease. *Neuroscience bulletin*. 2014;30(2):282-294.
24. Polidori M, Griffiths H, Mariani E, Mecocci P. Hallmarks of protein oxidative damage in neurodegenerative diseases: focus on Alzheimer's disease. *Amino acids*. 2007;32(4):553-559.
25. Congdon EE, Sigurdsson EM. Tau-targeting therapies for Alzheimer disease. *Nature Reviews Neurology*. 2018;14(7):399-415.
26. Drolle E, Hane F, Lee B, Leonenko Z. Atomic force microscopy to study molecular mechanisms of amyloid fibril formation and toxicity in Alzheimer's disease. *Drug metabolism reviews*. 2014;46(2):207-223.
27. Bitan G, Kirkitadze MD, Lomakin A, Vollers SS, Benedek GB, Teplow DB. Amyloid beta -protein (A $\beta$ ) assembly: A $\beta$  40 and A $\beta$  42 oligomerize through distinct pathways. *Proceedings of the National Academy of Sciences of the United States of America*. 2003;100(1):331-335.
28. Raskin J, Cummings J, Hardy J, Schuh K, A Dean R. Neurobiology of Alzheimer's disease: integrated molecular, physiological, anatomical, biomarker, and cognitive dimensions. *Current Alzheimer Research*. 2015;12(8):712-722.
29. Glass CK, Saijo K, Winner B, Marchetto MC, Gage FH. Mechanisms underlying inflammation in neurodegeneration. *Cell*. 2010;140(6):918-934.
30. Tuppo EE, Arias HR. The role of inflammation in Alzheimer's disease. *The international journal of biochemistry & cell biology*. 2005;37(2):289-305.

31. Rubio-Perez JM, Morillas-Ruiz JM. A review: inflammatory process in Alzheimer's disease, role of cytokines. *The Scientific World Journal*. 2012;2012:1-15.
32. Jian M, Kwan JS-C, Bunting M, Ng RC-L, Chan KH. Adiponectin suppresses amyloid- $\beta$  oligomer (A $\beta$ O)-induced inflammatory response of microglia via AdipoR1-AMPK-NF- $\kappa$ B signaling pathway. *Journal of neuroinflammation*. 2019;16(1):1-19.
33. Smith JA, Das A, Ray SK, Banik NL. Role of pro-inflammatory cytokines released from microglia in neurodegenerative diseases. *Brain research bulletin*. 2012;87(1):10-20.
34. Acconcia F, Pallottini V, Marino M. Molecular Mechanisms of Action of BPA. Dose Response. 2015;13(4):1-9.
35. Tabb MM, Blumberg B. New modes of action for endocrine-disrupting chemicals. *Molecular endocrinology*. 2006;20(3):475-482.
36. Kurosawa T, Hiroi H, Tsutsumi O, Ishikawa T, Osuga Y, Fujiwara T, et al. The activity of bisphenol A depends on both the estrogen receptor subtype and the cell type. *Endocrine Journal*. 2002;49(4):465-471.
37. Sukjamnong S, Thongkorn S, Kanlayaprasit S, Saeliw T, Hussem K, Warayanon W, et al. Prenatal exposure to bisphenol A alters the transcriptome-interactome profiles of genes associated with Alzheimer's disease in the offspring hippocampus. *Scientific Reports*. 2020;10(1):1-15.
38. Montgomery SL, Bowers WJ. Tumor necrosis factor-alpha and the roles it plays in homeostatic and degenerative processes within the central nervous system. *Journal of neuroimmune pharmacology*. 2012;7(1):42-59.



39. Liu J, Chang L, Song Y, Li H, Wu Y. The role of NMDA receptors in Alzheimer's disease. *Front Neurosci.* 2019;1-22.
40. Krzystanek M, Pałasz A. NMDA receptor model of antipsychotic drug-induced hypofrontality. *International Journal of Molecular Sciences.* 2019;20(6):1-17.
41. Paoletti P. Molecular basis of NMDA receptor functional diversity. *European Journal of Neuroscience.* 2011;33(8):1351-1365.
42. Parameshwaran K, Dhanasekaran M, Suppiramaniam V. Amyloid beta peptides and glutamatergic synaptic dysregulation. *Experimental neurology.* 2008;210(1):7-13.
43. Wang R, Reddy PH. Role of glutamate and NMDA receptors in Alzheimer's disease. *Journal of Alzheimer's Disease.* 2017;57(4):1041-1048.
44. Bai G, Hoffman PW. Transcriptional regulation of NMDA receptor expression. In: AM VD, editor. *Biology of the NMDA Receptor.* 5: CRC Press/Taylor & Francis; 2009.
45. Zhang WJ, Wang HH, Lv YD, Liu CC, Sun WY, Tian LJ. Downregulation of Egr-1 expression level via GluN2B underlies the antidepressant effects of ketamine in a chronic unpredictable stress animal model of depression. *Neuroscience.* 2018;372:38-45.
46. Teke N, Kinge T, Bechem E, Nji T, Ndam L, Mih A. Ethnomycological study in the kilum-ijim mountain forest, northwest region, cameroon. *Journal of ethnobiology and ethnomedicine.* 2018;14(1):1-12.
47. Ng ZX, Rosman NF. In vitro digestion and domestic cooking improved the total antioxidant activity and carbohydrate-digestive enzymes inhibitory potential of

- selected edible mushrooms. *Journal of food science and technology*. 2019;56(2):865-877.
48. Hossen M, Billah Prince M, Tanvir E, Chowdhury M, Rahman M, Alam F, et al. *Ganoderma lucidum* and *Auricularia polytricha* mushrooms protect against Carbofuran-induced toxicity in rats. *Evidence-Based Complementary and Alternative Medicine*. 2018;2018:1-13.
49. Koyama K, Akiba M, Imaizumi T, Kinoshita K, Takahashi K, Suzuki A, et al. Antinociceptive constituents of *Auricularia polytricha*. *Planta medica*. 2002;68(03):284-285.
50. Dupont S, Lemetais G, Ferreira T, Cayot P, Gervais P, Beney L. Ergosterol biosynthesis: a fungal pathway for life on land? *Evolution: International Journal of Organic Evolution*. 2012;66(9):2961-2968.
51. Rodrigues ML. The multifunctional fungal ergosterol. *MBio*. 2018;9(5):1-5.
52. Shao S, Hernandez M, Kramer JK, Rinker DL, Tsao R. Ergosterol profiles, fatty acid composition, and antioxidant activities of button mushrooms as affected by tissue part and developmental stage. *Journal of agricultural and food chemistry*. 2010;58(22):11616-11625.
53. Poniedziałek B, Siwulski M, Wiater A, Komaniecka I, Komosa A, Gąsecka M, et al. The Effect of Mushroom Extracts on Human Platelet and Blood Coagulation: In vitro Screening of Eight Edible Species. *Nutrients*. 2019;11(12):1-22.
54. Corrêa RCG, Barros L, Fernandes Â, Sokovic M, Bracht A, Peralta RM, et al. A natural food ingredient based on ergosterol: optimization of the extraction from

- Agaricus blazei*, evaluation of bioactive properties and incorporation in yogurts. *Food & Function*. 2018;9(3):1465-1474.
55. Martínez-Montemayor MM, Ling T, Suárez-Arroyo IJ, Ortiz-Soto G, Santiago-Negrón CL, Lacourt-Ventura MY, et al. Identification of biologically active *Ganoderma lucidum* compounds and synthesis of improved derivatives that confer anti-cancer activities in vitro. *Frontiers in Pharmacology*. 2019;10:1-17.
56. Kawai J, Mori K, Hirasawa N. *Grifola frondosa* extract and ergosterol reduce allergic reactions in an allergy mouse model by suppressing the degranulation of mast cells. *Bioscience, biotechnology, and biochemistry*. 2019;83(12):2280-2287.
57. Kawai J, Higuchi Y, Hirota M, Hirasawa N, Mori K. Ergosterol and its derivatives from *Grifola frondosa* inhibit antigen-induced degranulation of RBL-2H3 cells by suppressing the aggregation of high affinity IgE receptors. *Bioscience, biotechnology, and biochemistry*. 2018;82(10):1803-1811.
58. Ma L, Chen H, Dong P, Lu X. Anti-inflammatory and anticancer activities of extracts and compounds from the mushroom *Inonotus obliquus*. *Food chemistry*. 2013;139(1-4):503-508.
59. Kalogeropoulos N, Yanni AE, Koutrotsios G, Aloupi M. Bioactive microconstituents and antioxidant properties of wild edible mushrooms from the island of Lesbos, Greece. *Food and chemical toxicology : an international journal published for the British Industrial Biological Research Association*. 2013;55:378-385.
60. Morales D, Tejedor-Calvo E, Jurado-Chivato N, Polo G, Taberero MD, Ruíz-Rodríguez A, et al. In vitro and in vivo testing of the hypocholesterolemic

- activity of ergosterol- and  $\beta$ -glucan-enriched extracts obtained from shiitake mushrooms (*Lentinula edodes*). *Food & Function*. 2019;10(11):7325-7332.
61. Yongxia Z, Jian X, Suyuan H, Aixin N, Lihong Z. Isolation and characterization of ergosterol from *Monascus anka* for anti-lipid peroxidation properties. *Journal de mycologie medicale*. 2020;30(4):1-11.
  62. Quintero-Cabello KP, Palafox-Rivera P, Lugo-Flores MA, Gaitán-Hernández R, González-Aguilar GA, Silva-Espinoza BA, et al. Contribution of Bioactive Compounds to the Antioxidant Capacity of the Edible Mushroom *Neolentinus lepideus*. *Chemistry & biodiversity*. 2021;18(7):1-11.
  63. Hu SH, Liang ZC, Chia YC, Lien JL, Chen KS, Lee MY, et al. Antihyperlipidemic and antioxidant effects of extracts from *Pleurotus citrinopileatus*. *Journal of Agricultural and Food Chemistry*. 2006;54(6):2103-2110.
  64. Milovanovic I, Zengin G, Maksimovic S, Tadic V. Supercritical and ultrasound-assisted extracts from *Pleurotus pulmonarius* mushroom: chemical profiles, antioxidative, and enzyme-inhibitory properties. *Journal of the science of food and agriculture*. 2021;101(6):2284-2293.
  65. Abidin MH, Abdullah N, Abidin NZ. Protective Effect of Antioxidant Extracts from Grey Oyster Mushroom, *Pleurotus pulmonarius* (Agaricomycetes), Against Human Low-Density Lipoprotein Oxidation and Aortic Endothelial Cell Damage. *International Journal of Medicinal Mushrooms*. 2016;18(2):109-121.
  66. Kim JH, Sim HA, Jung DY, Lim EY, Kim YT, Kim BJ, et al. *Poria cocos* Wolf Extract Ameliorates Hepatic Steatosis through Regulation of Lipid Metabolism,

- Inhibition of ER Stress, and Activation of Autophagy via AMPK Activation. *International Journal of Medicinal Mushrooms*. 2019;20(19):1-17.
67. Tel-Çayan G, Muhammad A, Duru ME, Öztürk M, Adhikari A, Türkoğlu A. A new fatty acid ester from an edible mushroom *Rhizopogon luteolus*. *Natural Product Research*. 2016;30(20):2258-2264.
68. Sułkowska-Ziaja K, Muszyńska B, Szewczyk A. Antioxidant components of selected indigenous edible mushrooms of the obsolete order Aphyllophorales. *Revista iberoamericana de micologia*. 2015;32(2):99-102.
69. Sun X, Feng X, Zheng D, Li A, Li C, Li S, et al. Ergosterol attenuates cigarette smoke extract-induced COPD by modulating inflammation, oxidative stress and apoptosis in vitro and in vivo. *Clinical Science*. 2019;133(13):1523-1536.
70. Kobori M, Yoshida M, Ohnishi-Kameyama M, Shinmoto H. Ergosterol peroxide from an edible mushroom suppresses inflammatory responses in RAW264. 7 macrophages and growth of HT29 colon adenocarcinoma cells. *British journal of pharmacology*. 2007;150(2):209-219.
71. Zhang SY, Xu LT, Li AX, Wang SM. Effects of ergosterol, isolated from *Scleroderma polyrhizum* Pers., on lipopolysaccharide-induced inflammatory responses in acute lung injury. *Inflammation*. 2015;38(5):1979-1985.
72. Liu C, Zhao S, Zhu C, Gao Q, Bai J, Si J, et al. Ergosterol ameliorates renal inflammatory responses in mice model of diabetic nephropathy. *Biomedicine & pharmacotherapy*. 2020;128:1-7.
73. Dupont S, Fleurat-Lessard P, Cruz RG, Lafarge C, Grangeteau C, Yahou F, et al. Antioxidant Properties of Ergosterol and Its Role in Yeast Resistance to Oxidation. *Antioxidants*. 2021;10(7):1-21.

74. Xu J, Lin C, Wang T, Zhang P, Liu Z, Lu C. Ergosterol attenuates LPS-induced myocardial injury by modulating oxidative stress and apoptosis in rats. *Cellular Physiology and Biochemistry*. 2018;48(2):583-592.
75. Xie Q, Li S, Gao Y, Jin L, Dai C, Song J. Ergosterol attenuates isoproterenol-induced myocardial cardiotoxicity. *Cardiovascular Toxicology*. 2020;20(5):500-506.
76. Pires DE, Blundell TL, Ascher DB. pkCSM: predicting small-molecule pharmacokinetic and toxicity properties using graph-based signatures. *Journal of medicinal chemistry*. 2015;58(9):4066-4072.
77. Lipinski CA, Lombardo F, Dominy BW, Feeney PJ. Experimental and computational approaches to estimate solubility and permeability in drug discovery and development settings. *Advanced drug delivery reviews*. 2001;46(1-3):3-26.
78. Clark DE, Pickett SD. Computational methods for the prediction of 'drug-likeness'. *Drug discovery today*. 2000;5(2):49-58.
79. Henn A, Lund S, Hedtjörn M, Schrattenholz A, Pörzgen P, Leist M. The suitability of BV2 cells as alternative model system for primary microglia cultures or for animal experiments examining brain inflammation. *ALTEX-Alternatives to animal experimentation*. 2009;26(2):83-94.
80. Wu WY, Wu YY, Huang H, He C, Li WZ, Wang HL, et al. Biochanin A attenuates LPS-induced pro-inflammatory responses and inhibits the activation of the MAPK pathway in BV2 microglial cells. *International journal of molecular medicine*. 2015;35(2):391-398.

81. Cai Q, Li Y, Pei G. Polysaccharides from *Ganoderma lucidum* attenuate microglia-mediated neuroinflammation and modulate microglial phagocytosis and behavioural response. *Journal of neuroinflammation*. 2017;14(1):1-13.
82. Morimoto BH, Koshland Jr DE. Induction and expression of long-and short-term neurosecretory potentiation in a neural cell line. *Neuron*. 1990;5(6):875-880.
83. Prasansuklab A, Meemon K, Sobhon P, Tencomnao T. Ethanolic extract of *Streblus asper* leaves protects against glutamate-induced toxicity in HT22 hippocampal neuronal cells and extends lifespan of *Caenorhabditis elegans*. *BMC complementary and alternative medicine*. 2017;17(1):1-14.
84. Sukprasansap M, Chanvorachote P, Tencomnao T. Cyanidin-3-glucoside activates Nrf2-antioxidant response element and protects against glutamate-induced oxidative and endoplasmic reticulum stress in HT22 hippocampal neuronal cells. *BMC Complementary Medicine and Therapies*. 2020;20(1):1-12.
85. Pang Q, Li Y, Meng L, Li G, Luo Z, Fan R. Neurotoxicity of BPA, BPS, and BPB for the hippocampal cell line (HT-22): An implication for the replacement of BPA in plastics. *Chemosphere*. 2019;226:545-552.
86. Brimson JM, Brimson SJ, Brimson CA, Rakkhitawatthana V, Tencomnao T. *Rhinacanthus nasutus* extracts prevent glutamate and amyloid- $\beta$  neurotoxicity in HT-22 mouse hippocampal cells: possible active compounds include lupeol, stigmasterol and  $\beta$ -sitosterol. *International journal of molecular sciences*. 2012;13(4):5074-5097.

87. Zhang MY, Li Y, Yin SY, Kong L, Liu XL, Yin XX, et al. Sarsasapogenin suppresses A $\beta$  overproduction induced by high glucose in HT-22 cells. *Naunyn-Schmiedeberg's archives of pharmacology*. 2018;391(2):159-168.
88. Zhao Z, Lu R, Zhang B, Shen J, Yang L, Xiao S, et al. Differentiation of HT22 neurons induces expression of NMDA receptor that mediates homocysteine cytotoxicity. *Neurological Research*. 2012;34(1):38-43.
89. Martin AM, Kuhlmann C, Trossbach S, Jaeger S, Waldron E, Roebroek A, et al. The functional role of the second NPXY motif of the LRP1  $\beta$ -chain in tissue-type plasminogen activator-mediated activation of N-methyl-D-aspartate receptors. *Journal of Biological Chemistry*. 2008;283(18):12004-12013.
90. Kelley JB, Paschal BM. Fluorescence-based quantification of nucleocytoplasmic transport. *Methods*. 2019;157:106-114.
91. Kim BW, More SV, Yun YS, Ko HM, Kwak JH, Lee H, et al. A novel synthetic compound MCAP suppresses LPS-induced murine microglial activation in vitro via inhibiting NF-kB and p38 MAPK pathways. *Acta Pharmacologica Sinica*. 2016;37(3):334-343.
92. Jayasooriya RGPT, Lee KT, Lee HJ, Choi YH, Jeong JW, Kim GY. Anti-inflammatory effects of  $\beta$ -hydroxyisovalerylshikonin in BV2 microglia are mediated through suppression of the PI3K/Akt/NF-kB pathway and activation of the Nrf2/HO-1 pathway. *Food and Chemical Toxicology*. 2014;65:82-89.
93. Wang H, Zhao P, Huang Q, Chi Y, Dong S, Fan J. Bisphenol-A induces neurodegeneration through disturbance of intracellular calcium homeostasis in human embryonic stem cells-derived cortical neurons. *Chemosphere*. 2019;229:618-630.



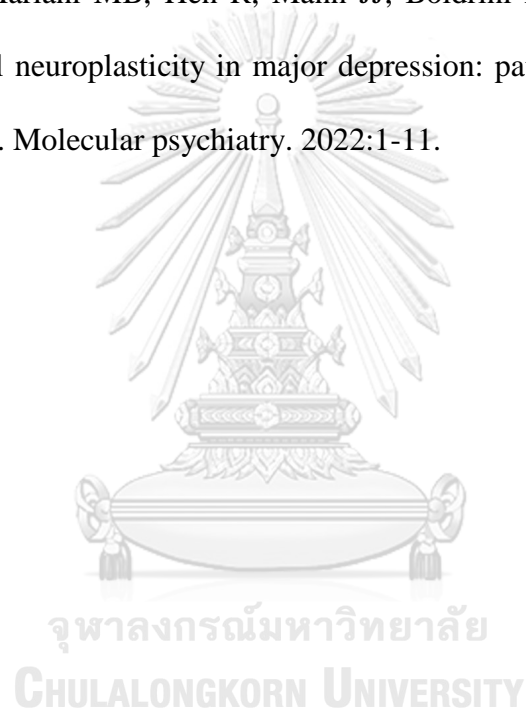
94. Tao R, Wang CZ, Kong ZW. Antibacterial/antifungal activity and synergistic interactions between polyprenols and other lipids isolated from Ginkgo biloba L. leaves. *Molecules*. 2013;18(2):2166-2182.
95. Liu Y, Chu JMT, Yan T, Zhang Y, Chen Y, Chang RCC, et al. Short-term resistance exercise inhibits neuroinflammation and attenuates neuropathological changes in 3xTg Alzheimer's disease mice. *Journal of neuroinflammation*. 2020;17(1):1-16.
96. Chu J, Lauretti E, Praticò D. Caspase-3-dependent cleavage of Akt modulates tau phosphorylation via GSK3 $\beta$  kinase: Implications for Alzheimer's disease. *Molecular psychiatry*. 2017;22(7):1002-1008.
97. Rai SN, Dilnashin H, Birla H, Singh SS, Zahra W, Rathore AS, et al. The role of PI3K/Akt and ERK in neurodegenerative disorders. *Neurotoxicity research*. 2019;35(3):775-795.
98. Sarbassov DD, Guertin DA, Ali SM, Sabatini DM. Phosphorylation and regulation of Akt/PKB by the rictor-mTOR complex. *Science*. 2005;307(5712):1098-1101.
99. Liu H, Liu J, Si L, Guo C, Liu W, Liu Y. GDF-15 promotes mitochondrial function and proliferation in neuronal HT22 cells. *Journal of Cellular Biochemistry*. 2019;120(6):10530-10547.
100. Park KM, Bowers WJ. Tumor necrosis factor-alpha mediated signaling in neuronal homeostasis and dysfunction. *Cell Signal*. 2010;22(7):977-983.
101. Qu Y, Zhao X, Guo H, Meng Y, Wang Y, Zhou Y, et al. Structural analysis and macrophage activation of a novel  $\beta$ -glucan isolated from *Cantharellus cibarius*. *International Journal of Molecular Medicine*. 2021;47(4):1-10.

102. van Steenwijk HP, Bast A, de Boer A. Immunomodulating Effects of Fungal Beta-Glucans: From Traditional Use to Medicine. *Nutrients*. 2021;13(4):1-20.
103. Yan J, Han Z, Qu Y, Yao C, Shen D, Tai G, et al. Structure elucidation and immunomodulatory activity of a beta-glucan derived from the fruiting bodies of *Amillariella mellea*. *Food chemistry*. 2018;240:534-543.
104. Huang FM, Chang YC, Lee SS, Yang ML, Kuan YH. Expression of pro-inflammatory cytokines and mediators induced by Bisphenol A via ERK-NF $\kappa$ B and JAK1/2-STAT3 pathways in macrophages. *Environmental toxicology*. 2019;34(4):486-494.
105. Morgan MJ, Liu Z-g. Crosstalk of reactive oxygen species and NF- $\kappa$ B signaling. *Cell research*. 2011;21(1):103-115.
106. Ranneh Y, Ali F, Akim AM, Hamid HA, Khazaai H, Fadel A. Crosstalk between reactive oxygen species and pro-inflammatory markers in developing various chronic diseases: a review. *Applied Biological Chemistry*. 2017;60(3):327-338.
107. Ranneh Y, Akim AM, Ab Hamid H, Khazaai H, Fadel A, Mahmoud AM. Stingless bee honey protects against lipopolysaccharide induced-chronic subclinical systemic inflammation and oxidative stress by modulating Nrf2, NF- $\kappa$ B and p38 MAPK. *Nutrition & metabolism*. 2019;16(1):1-17.
108. Ito M, Ishimaru M, Shibata T, Hatate H, Tanaka R. High-performance liquid chromatography with fluorescence detection for simultaneous analysis of phytosterols (stigmasterol,  $\beta$ -sitosterol, campesterol, ergosterol, and fucosterol) and cholesterol in plant foods. *Food Analytical Methods*. 2017;10(8):2692-2699.

109. Dash R, Mitra S, Ali MC, Oktaviani DF, Hannan M, Choi SM, et al. Phytosterols: targeting neuroinflammation in neurodegeneration. *Current Pharmaceutical Design*. 2021;27(3):383-401.
110. Chen ZG, Bishop KS, Tanambell H, Buchanan P, Smith C, Quek SY. Characterization of the bioactivities of an ethanol extract and some of its constituents from the New Zealand native mushroom *Herichium novae-zealandiae*. *Food & Function*. 2019;10(10):6633-6643.
111. Li X, Wu Q, Xie Y, Ding Y, Du WW, Sdiri M, et al. Ergosterol purified from medicinal mushroom *Amauroderma rude* inhibits cancer growth in vitro and in vivo by up-regulating multiple tumor suppressors. *Oncotarget*. 2015;6(19):17832–17846.
112. Fu W, Hall MN. Regulation of mTORC2 signaling. *Genes*. 2020;11(9):1-19.
113. Hresko RC, Mueckler M. mTOR· RICTOR is the Ser473 kinase for Akt/protein kinase B in 3T3-L1 adipocytes. *Journal of Biological Chemistry*. 2005;280(49):40406-40416.
114. Hur EM, Zhou FQ. GSK3 signalling in neural development. *Nature reviews neuroscience*. 2010;11(8):539-551.
115. Hooshmandi E, Ghasemi R, Iloun P, Moosavi M. The neuroprotective effect of agmatine against amyloid  $\beta$ -induced apoptosis in primary cultured hippocampal cells involving ERK, Akt/GSK-3 $\beta$ , and TNF- $\alpha$ . *Molecular biology reports*. 2019;46(1):489-496.
116. Herrup K, Li J, Chen J. The role of ATM and DNA damage in neurons: upstream and downstream connections. *DNA repair*. 2013;12(8):600-604.

117. Chan SF, Sances S, Brill LM, Okamoto S-i, Zaidi R, McKercher SR, et al. ATM-dependent phosphorylation of MEF2D promotes neuronal survival after DNA damage. *Journal of neuroscience*. 2014;34(13):4640-4653.
118. Carlessi L, De Filippis L, Lecis D, Vescovi A, Delia D. DNA-damage response, survival and differentiation in vitro of a human neural stem cell line in relation to ATM expression. *Cell death & differentiation*. 2009;16(6):795-806.
119. Berger ND, Stanley FK, Moore S, Goodarzi AA. ATM-dependent pathways of chromatin remodelling and oxidative DNA damage responses. *Philosophical transactions of the royal society B*. 2017;372(1731):1-14.
120. Pizzamiglio L, Focchi E, Antonucci F. ATM protein kinase: old and new implications in neuronal pathways and brain circuitry. *Cells*. 2020;9(9):1-24.
121. Napetschnig J, Wu H. Molecular basis of NF- $\kappa$ B signaling. *Annual review of biophysics*. 2013;42:443-468.
122. Mattson M, Meffert M. Roles for NF- $\kappa$ B in nerve cell survival, plasticity, and disease. *Cell Death & Differentiation*. 2006;13(5):852-860.
123. Wooten MW. Function for NF- $\kappa$ B in neuronal survival: Regulation by atypical protein kinase C. *Journal of neuroscience research*. 1999;58(5):607-611.
124. Levenson JM, Pizzi M, Sweatt JD. NF- $\kappa$ B in Neurons. *NF- $\kappa$ B/Rel Transcription Factor Family*: Springer; 2006. p. 147-161.
125. Wang X, Krebbers J, Charalambous P, Machado V, Schober A, Bosse F, et al. Growth/differentiation factor-15 and its role in peripheral nervous system lesion and regeneration. *Cell and tissue research*. 2015;362(2):317-330.

126. Xiong WP, Yao WQ, Wang B, Liu K. BMSCs-exosomes containing GDF-15 alleviated SH-SY5Y cell injury model of Alzheimer's disease via AKT/GSK-3 $\beta$ / $\beta$ -catenin. *Brain research bulletin*. 2021;177:92-102.
127. Weerasinghe-Mudiyanselage PD, Ang MJ, Kang S, Kim J-S, Moon C. Structural Plasticity of the Hippocampus in Neurodegenerative Diseases. *International journal of molecular sciences*. 2022;23(6):1-34.
128. Tartt AN, Mariani MB, Hen R, Mann JJ, Boldrini M. Dysregulation of adult hippocampal neuroplasticity in major depression: pathogenesis and therapeutic implications. *Molecular psychiatry*. 2022:1-11.





**APPENDIX**

จุฬาลงกรณ์มหาวิทยาลัย  
**CHULALONGKORN UNIVERSITY**

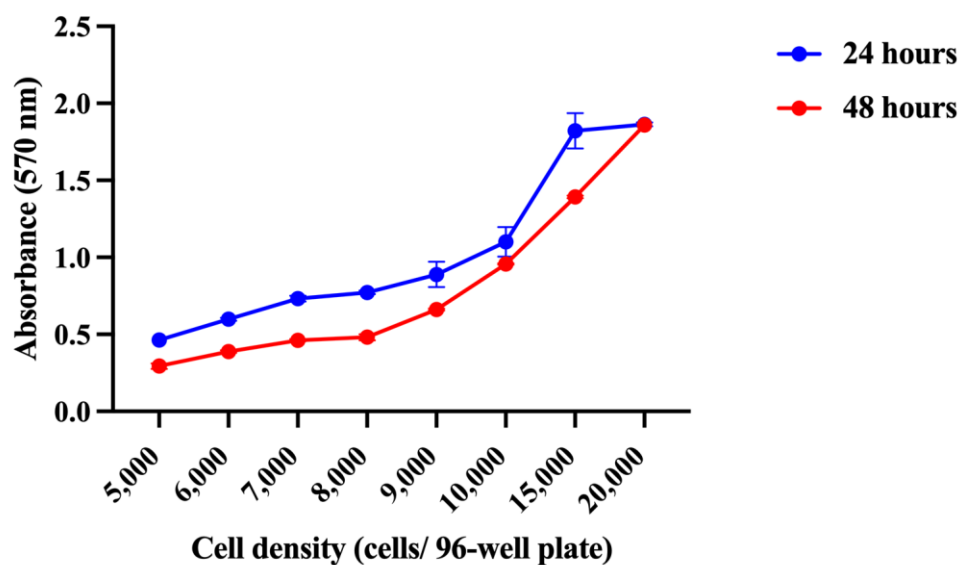


**Figure A 1** The association graph between cell density and absorbance at 570 nm. BV2 cells were incubated in cell culture media for 24 and 48 h, then an MTT assay was performed. All data are shown as the mean  $\pm$  SEM of experiments conducted in triplicate.

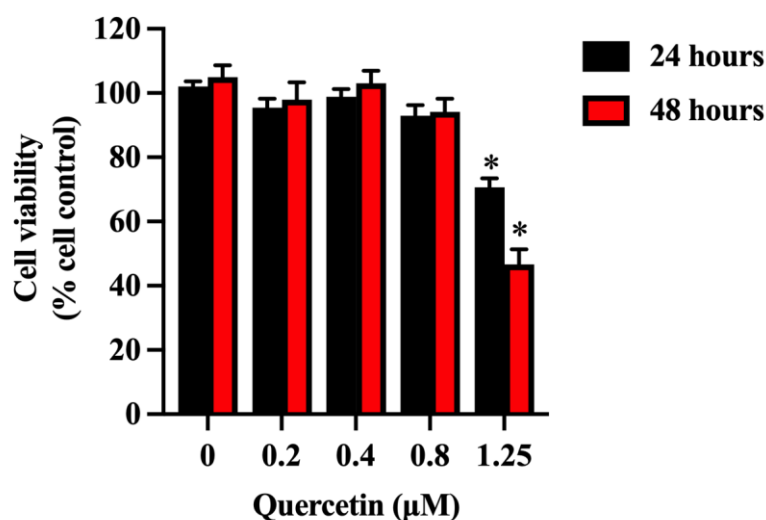


**Figure A 2** Cytotoxicity of quercetin against BV2 microglial cells after 24 and 48 h of exposures. All data are shown as the mean  $\pm$  SEM of experiments conducted in triplicate. Statistical significance was analyzed by a one-way ANOVA and a Dunnett's test. \*  $P < 0.05$  versus cell control.

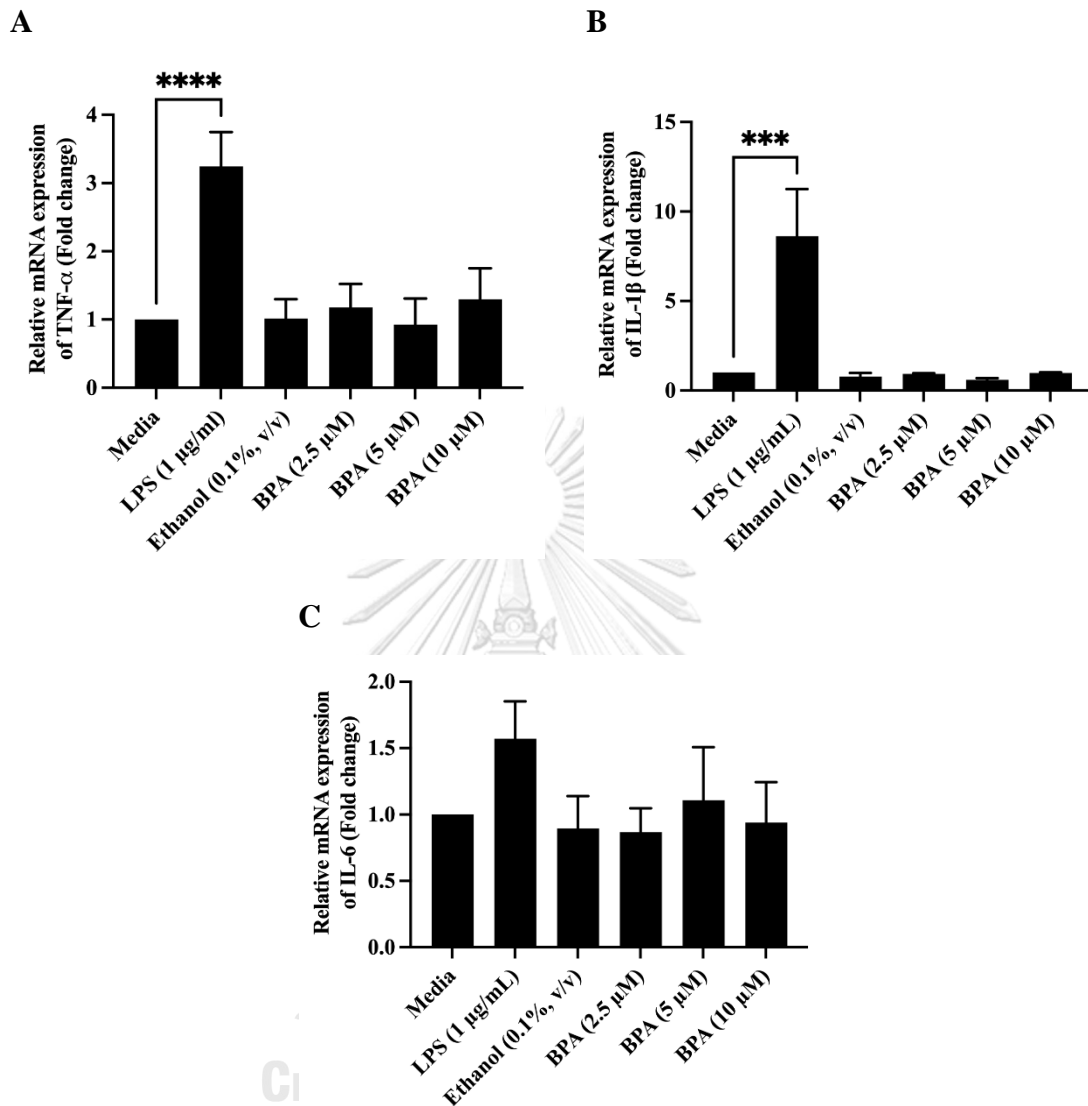


**Figure A 3** The mRNA expressions of pro-inflammatory cytokines: (A) TNF- $\alpha$ , (B) IL-1 $\beta$ , and (C) IL-6 in BPA-induced BV2 cells after 12 h of treatment. All data are shown as the mean  $\pm$  SEM of triplicate values. Statistical significance was analyzed by one-way ANOVA, Dunnett's test. \*\*\*  $P < 0.001$  and \*\*\*\*  $P < 0.0001$ .



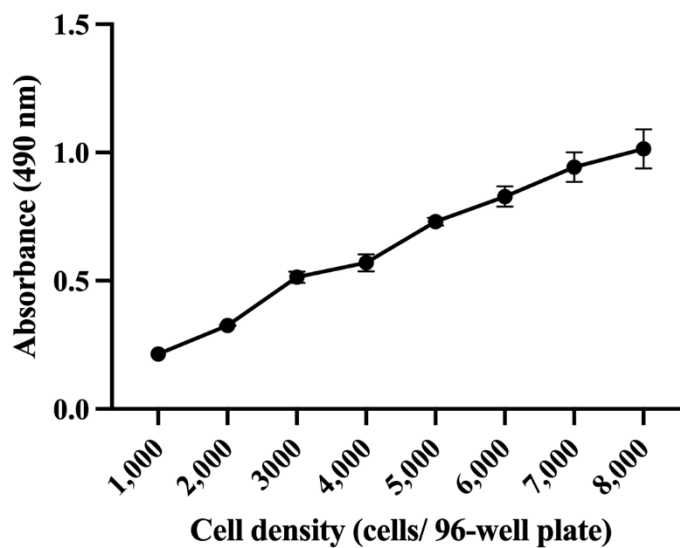


**Figure A 4** The association graph between cell density and absorbance at 490 nm. HT-22 cells were incubated in cell culture media for 24 h, then an MTS assay was performed. All data are shown as the mean  $\pm$  SEM of experiments conducted in triplicate.

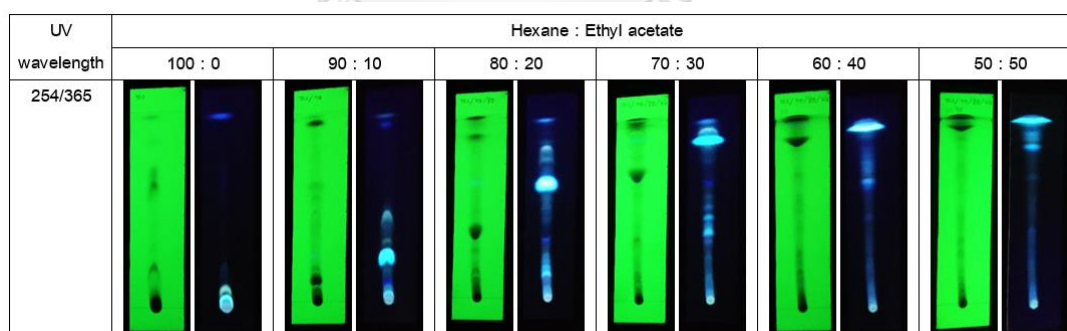


**Figure A 5** The results of TLC analysis in the gradient of hexane/ ethyl acetate system

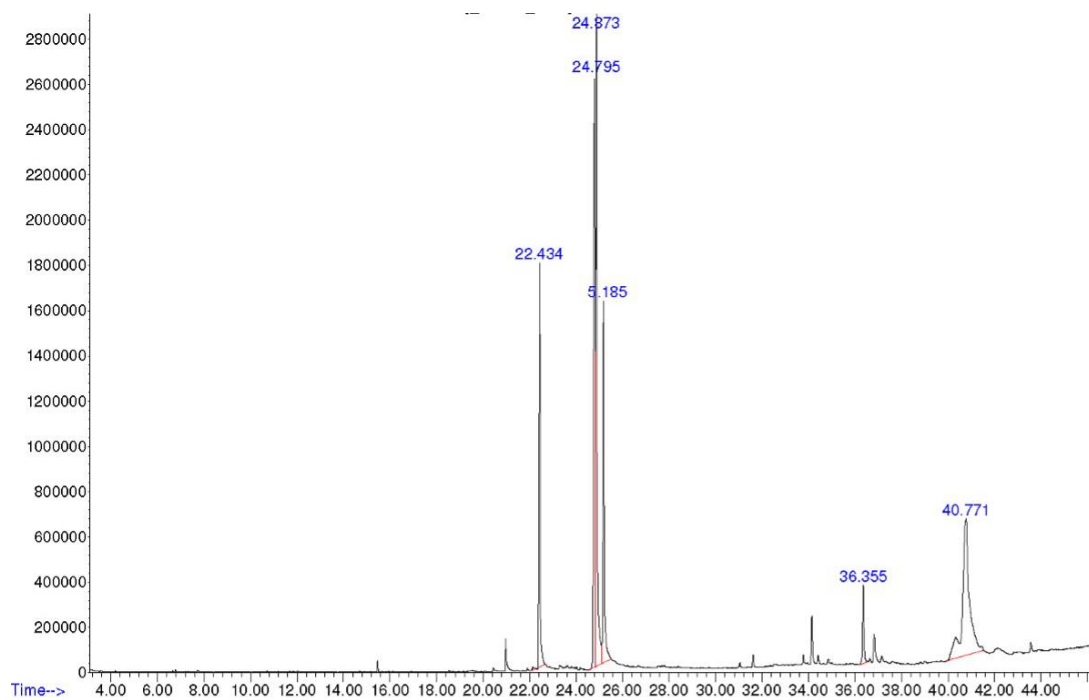


**Figure A 6** Gas chromatogram of APH crude extracts analyzed by GC/MS (17)

**Table A 1** Chemical profile of APH crude extract analyzed by GC/MS (17)

RT (min)	Identified compound	% Area of total
22.434	Palmitic acid	12.02
24.795	Linoleic acid	23.75
24.873	Oleic acid	23.23
25.185	Stearic acid	12.20
36.355	Anthraergostapentene	3.05
40.771	Ergosterol	25.75

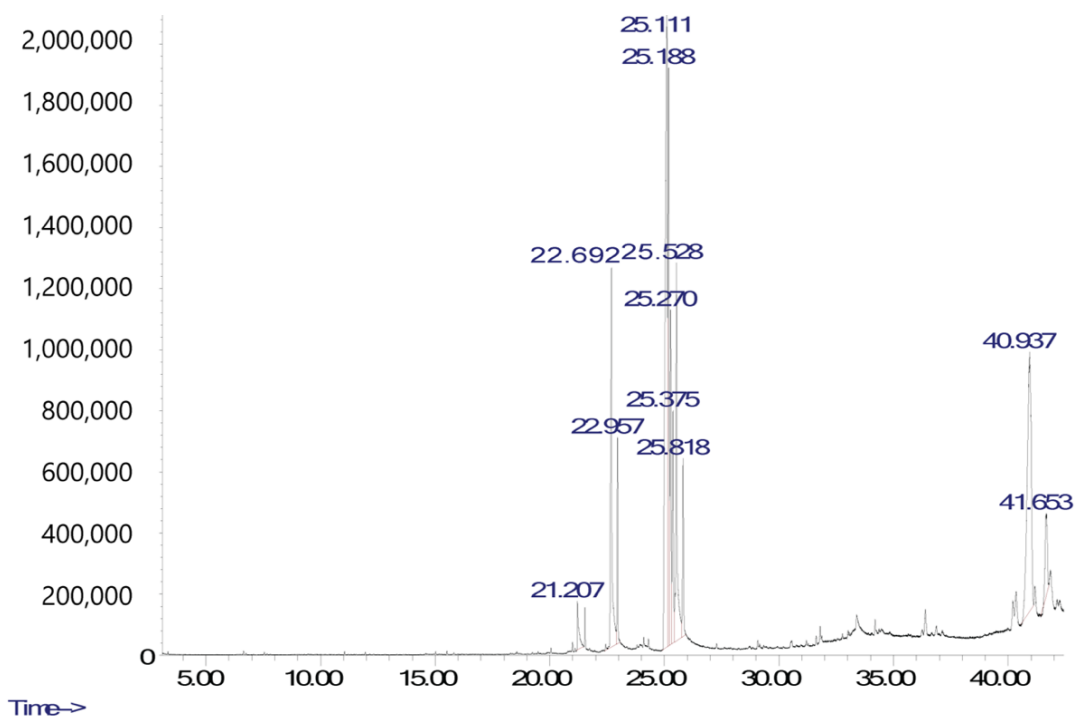


**Figure A 7** Gas chromatogram of APE crude extracts analyzed by GC/MS

**Table A 2** Chemical profile of APE crude extract analyzed by GC/MS

RT (min)	Identified compound	% Area of total
21.206	Pentadecanoic acid	1.47
22.693	Palmitic acid	10.55
22.958	Palmitic acid, ethyl ester	2.87
25.111	Linoleic acid	26.23
25.187	<i>cis</i> -Vaccenic acid	11.67
25.271	Linoleic acid, ethyl ester	6.93
25.375	Oleic acid, ethyl ester	4.63
25.527	Stearic acid	9.84
25.817	Stearic acid, ethyl ester	3.24
40.936	Ergosterol	19.14

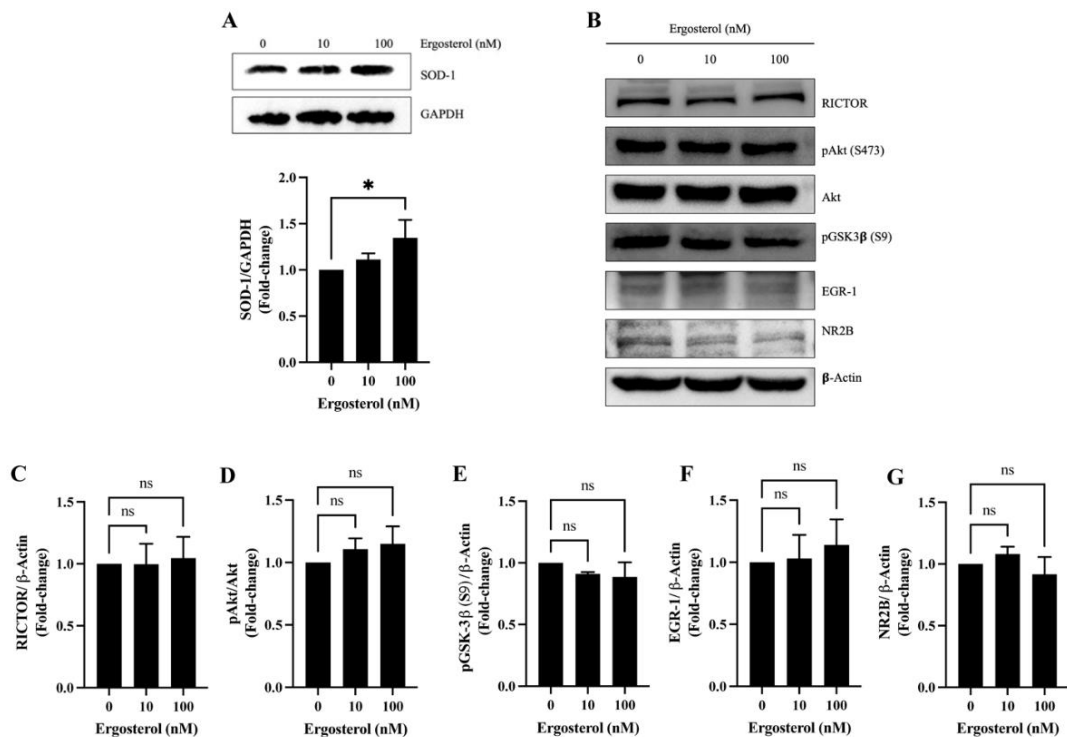


**Figure 8** The effects of ergosterol on antioxidant and anti-cell death signaling pathway. **(A)** The expression of SOD-1 in ergosterol-treated HT-22 cells for 18 h. **(B)** Western blot analysis of the cell death-associated proteins in ergosterol-treated HT-22 cells for 24 h. The quantitative analysis of **(C)** RICTOR, **(D)** pAkt (S473)/Akt, **(E)** pGSK3 $\beta$  (S9), **(F)** EGR-1, and **(G)** NR2B levels in HT-22 cells exposed to ergosterol (10 and 100 nM) for 24 h. All data are shown as the mean  $\pm$  SEM of experiments conducted in triplicate. Statistical significance was analyzed by a one-way ANOVA and a Dunnett's test. \*  $P < 0.05$ , ns = non-significance.

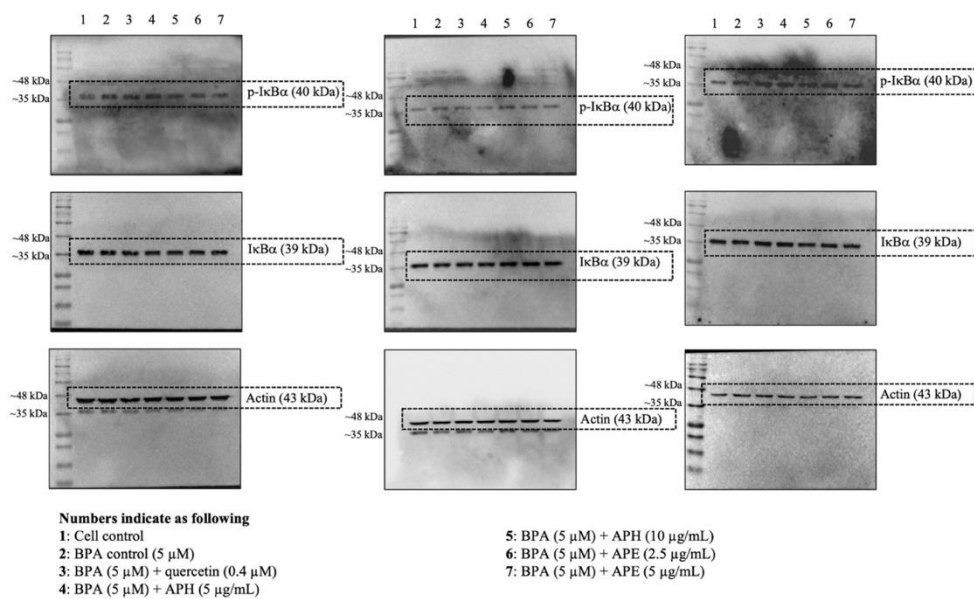


**Figure A 9** The original immunoblots of p-I $\kappa$ B $\alpha$ , I $\kappa$ B $\alpha$ , and actin in BPA-induced BV2 cells treated with APH or APE for 6 h.

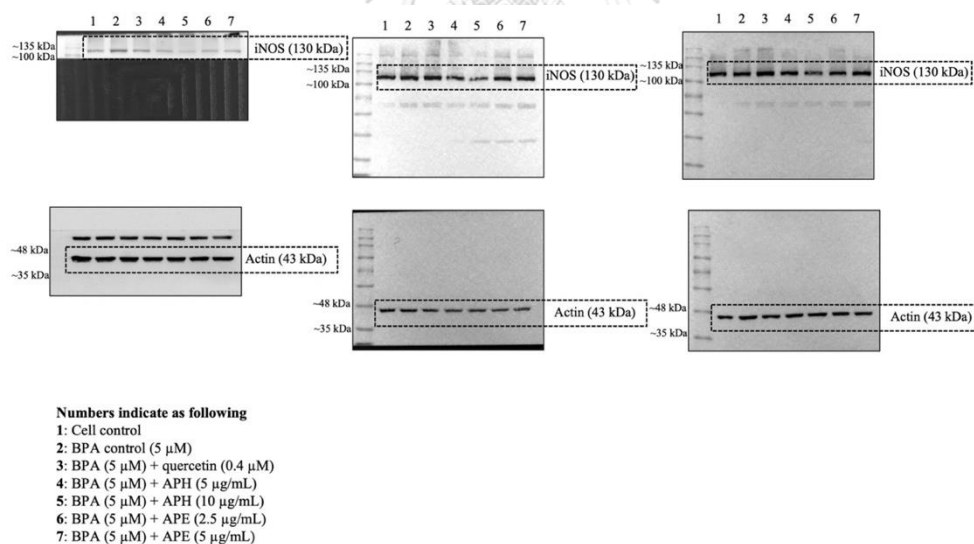


**Figure A 10** The original immunoblots of iNOS and actin in BPA-induced BV2 cells treated with APH or APE for 24 h.

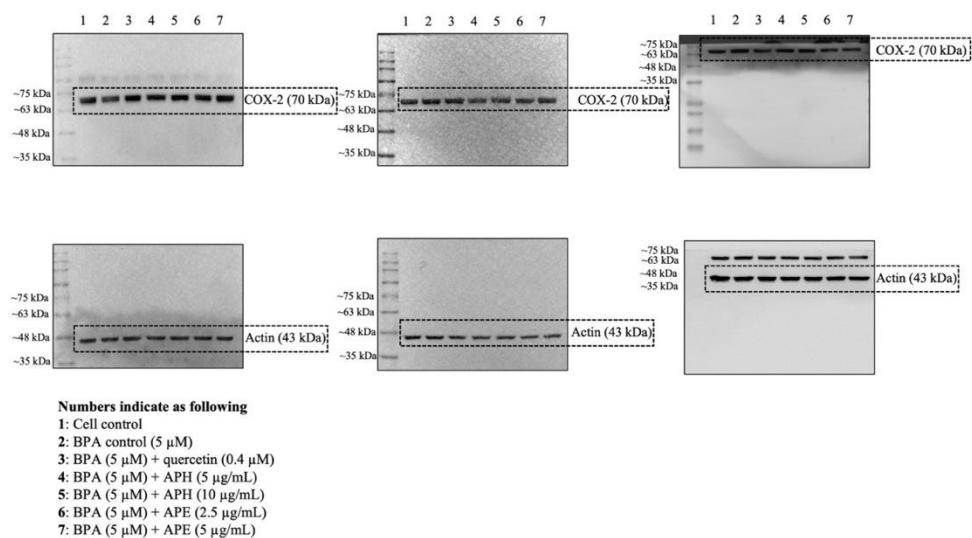


**Figure A 11** The original immunoblots of COX-2 and actin in BPA-induced BV2 cells treated with APH or APE for 24 h.

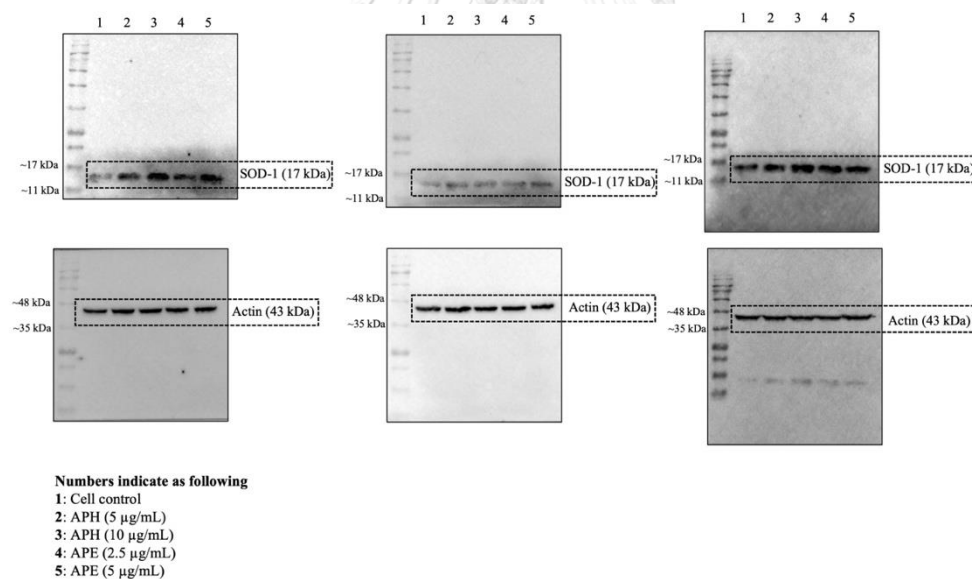


**Figure A 12** The original immunoblots of SOD-1 and actin in BPA-induced BV2 cells treated with APH or APE for 18 h.

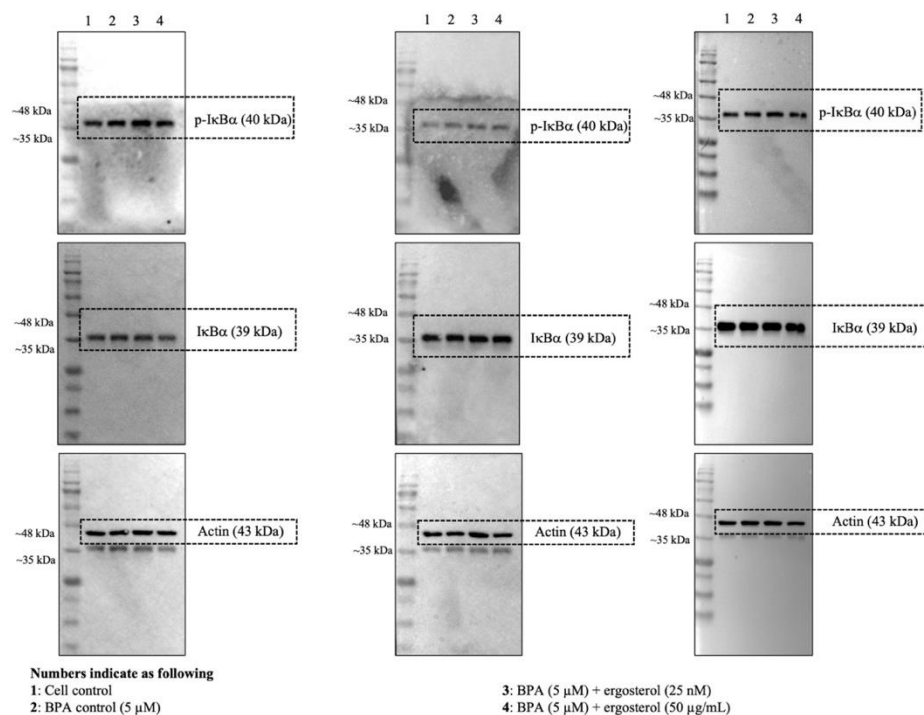


**Figure A 13** The original immunoblots of p-IκBα, IκBα, and actin in BPA-induced BV2 cells treated with ergosterol for 6 h.

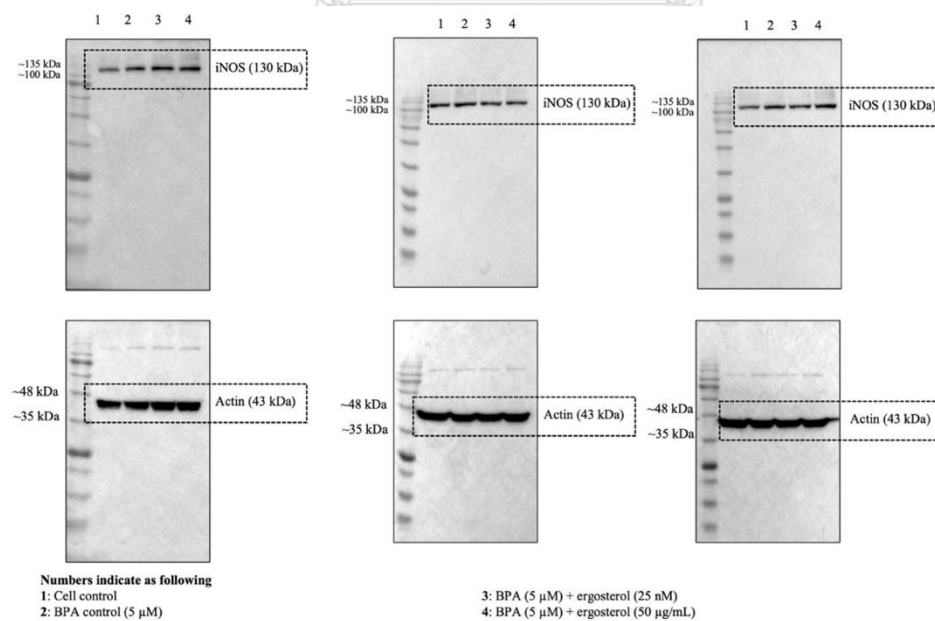


**Figure A 14** The original immunoblots of iNOS and actin in BPA-induced BV2 cells treated with ergosterol for 24 h.

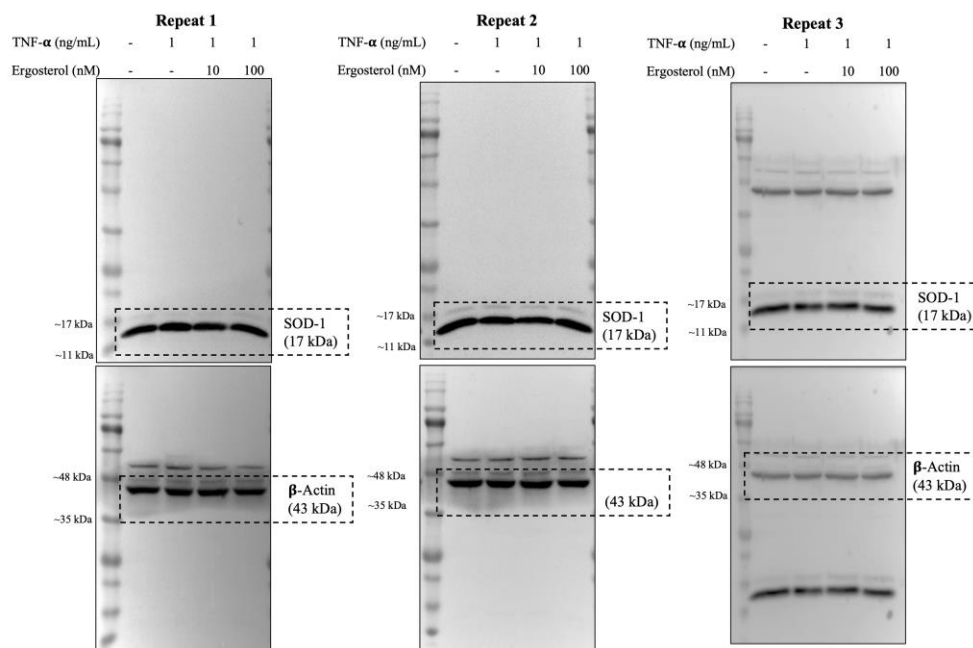


**Figure A 15** The original immunoblots of SOD-1 and  $\beta$ -actin in TNF- $\alpha$ -induced HT-22 cells treated with ergosterol for 18 h.

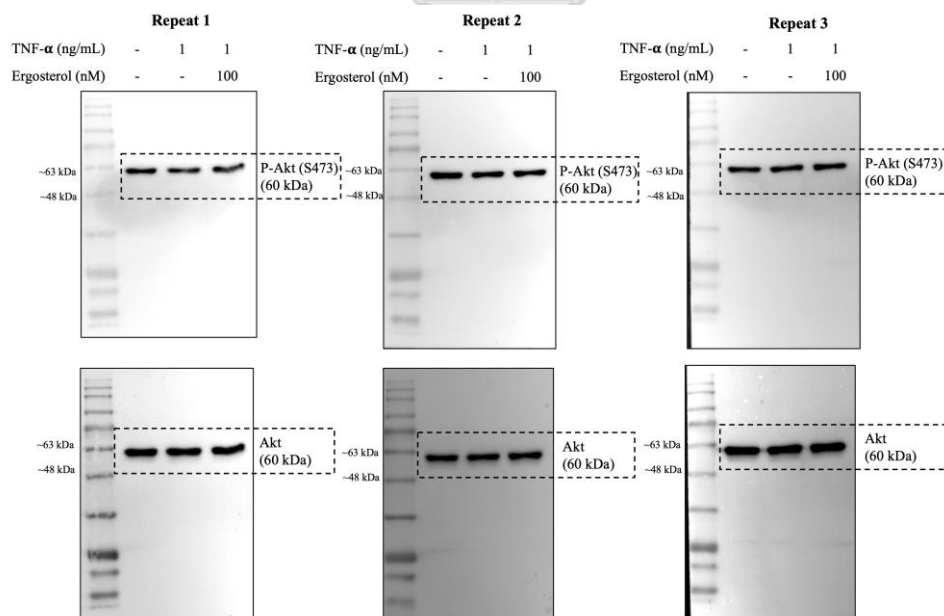


**Figure A 16** The original immunoblots of pAkt (S473) and Akt in TNF- $\alpha$ -induced HT-22 cells treated with ergosterol for 24 h.



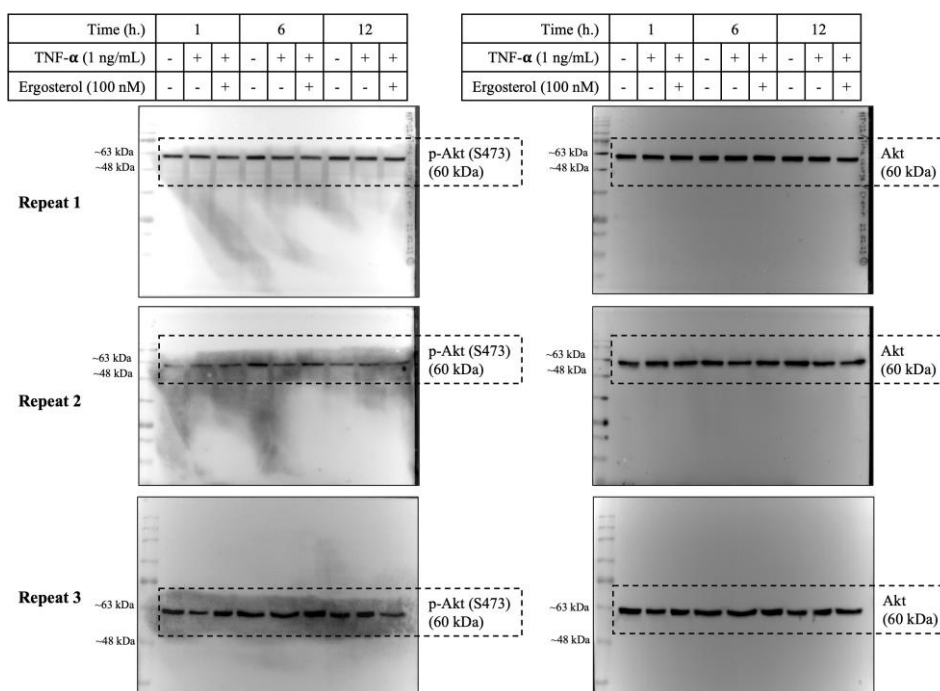


**Figure A 17** The original immunoblots of pAkt (S473) and Akt in TNF- $\alpha$ -induced HT-22 cells treated with ergosterol for 1, 6, and 12 h.

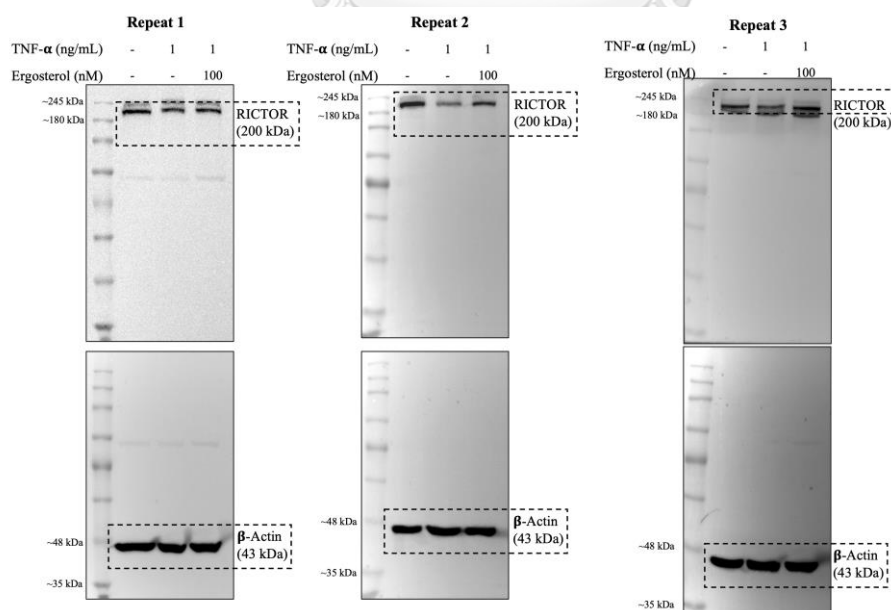


**Figure A 18** The original immunoblots of RICTOR and  $\beta$ -actin in TNF- $\alpha$ -induced HT-22 cells treated with ergosterol for 24 h.

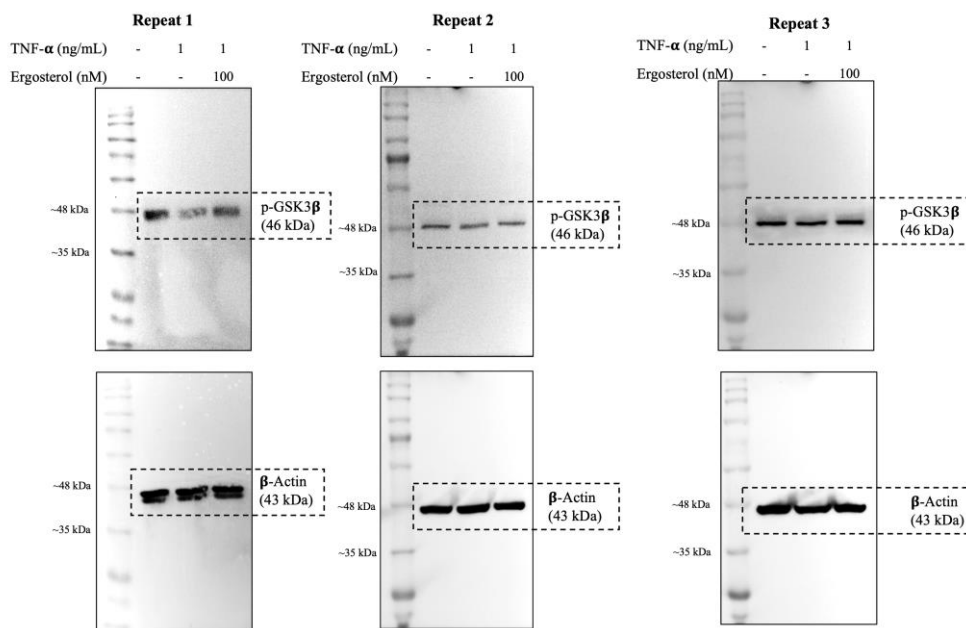


**Figure A 19** The original immunoblots of pGSK3 $\beta$  (S9) and  $\beta$ -actin in TNF- $\alpha$ -induced HT-22 cells treated with ergosterol for 24 h.

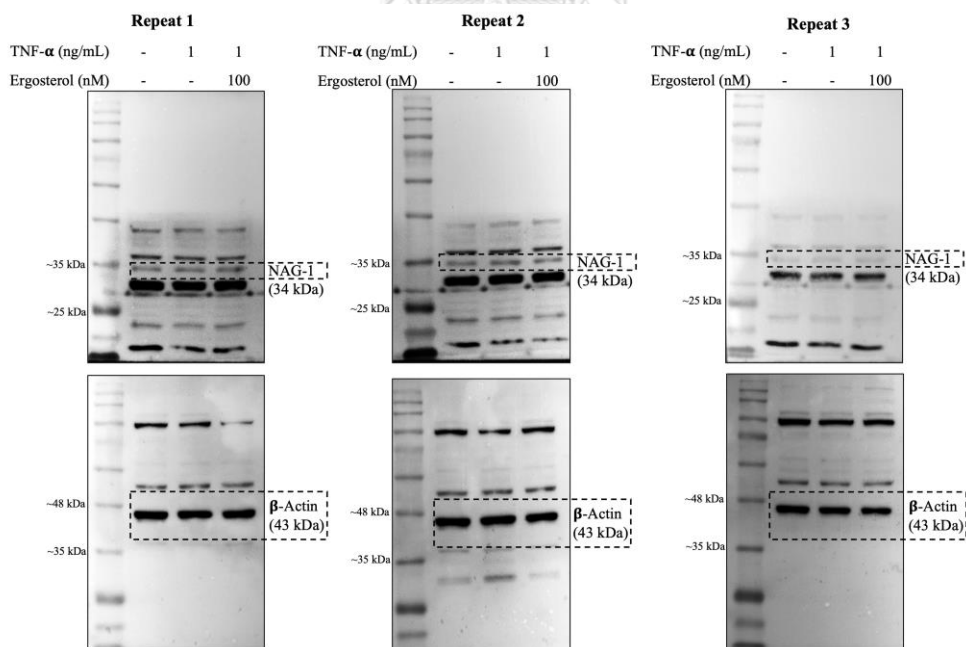


**Figure A 20** The original immunoblots of NAG-1 and  $\beta$ -actin in TNF- $\alpha$ -induced HT-22 cells treated with ergosterol for 24 h.

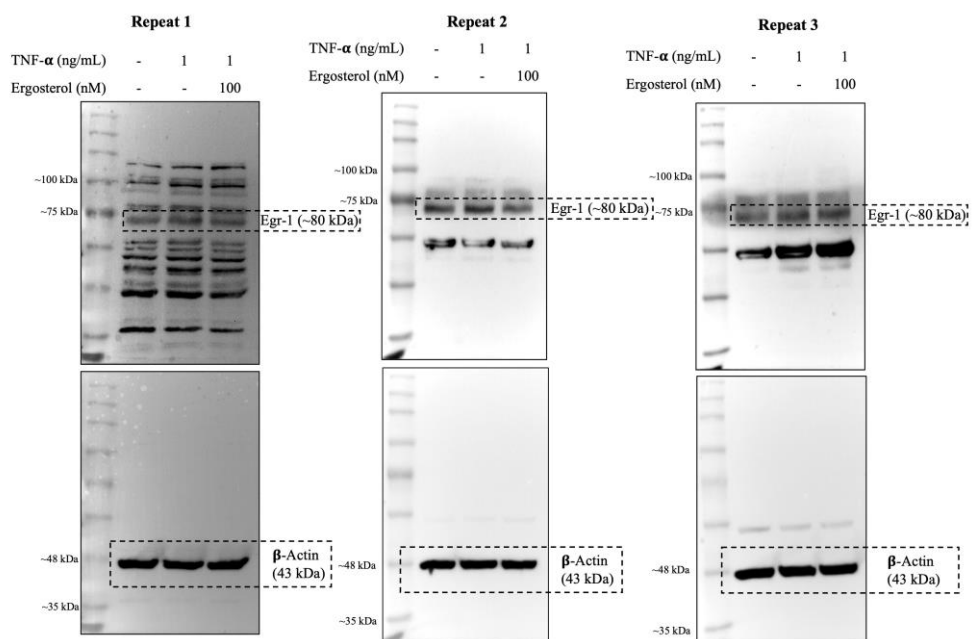


**Figure A 21** The original immunoblots of EGR-1 and  $\beta$ -actin in TNF- $\alpha$ -induced HT-22 cells treated with ergosterol for 24 h.

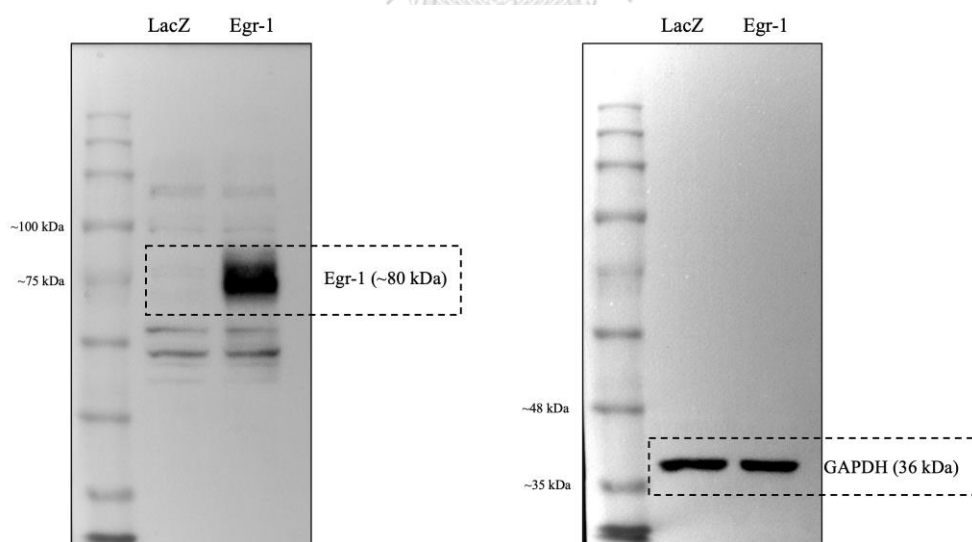


**Figure A 22** The original immunoblots of EGR-1 and GAPDH in EGR-1-overexpressed HT-22 cells.

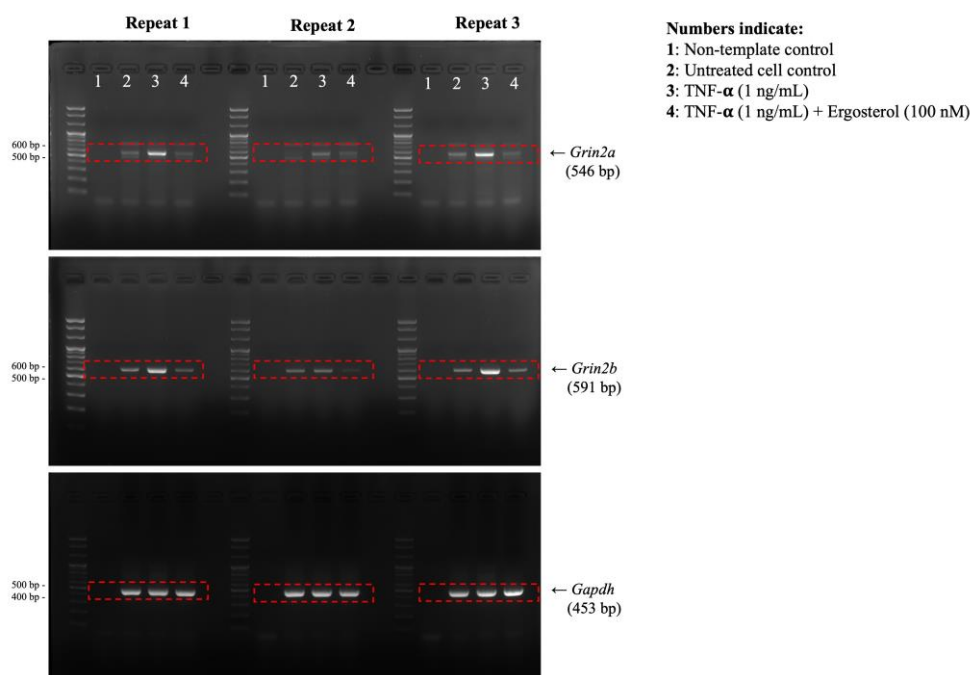


**Figure A 23** The original gel electrophoresis of *Grin2a*, *Grin2b*, and *Gapdh* mRNA expressions in TNF- $\alpha$ -induced HT-22 cells treated with ergosterol for 24 h.

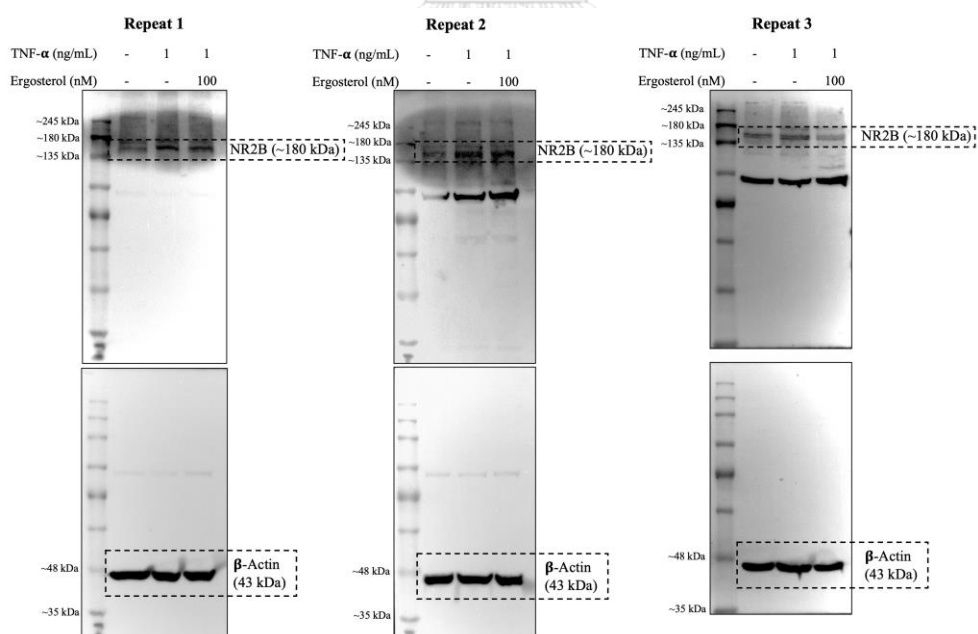


**Figure A 24** The original immunoblots of NR2B and  $\beta$ -actin in TNF- $\alpha$ -induced HT-22 cells treated with ergosterol for 24 h.

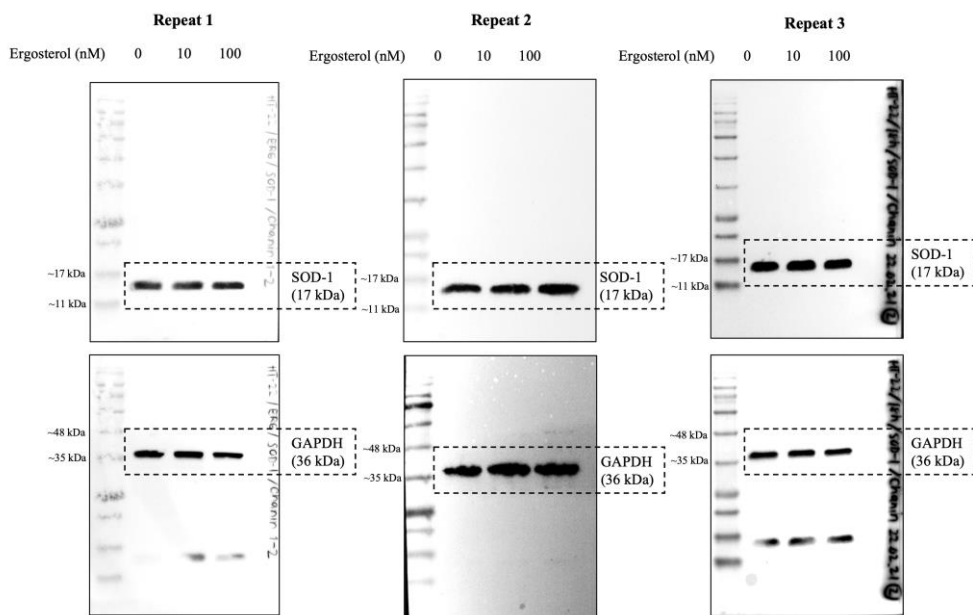


**Figure A 25** The original immunoblots of SOD-1 and GAPDH in HT-22 cells treated with ergosterol for 18 h.

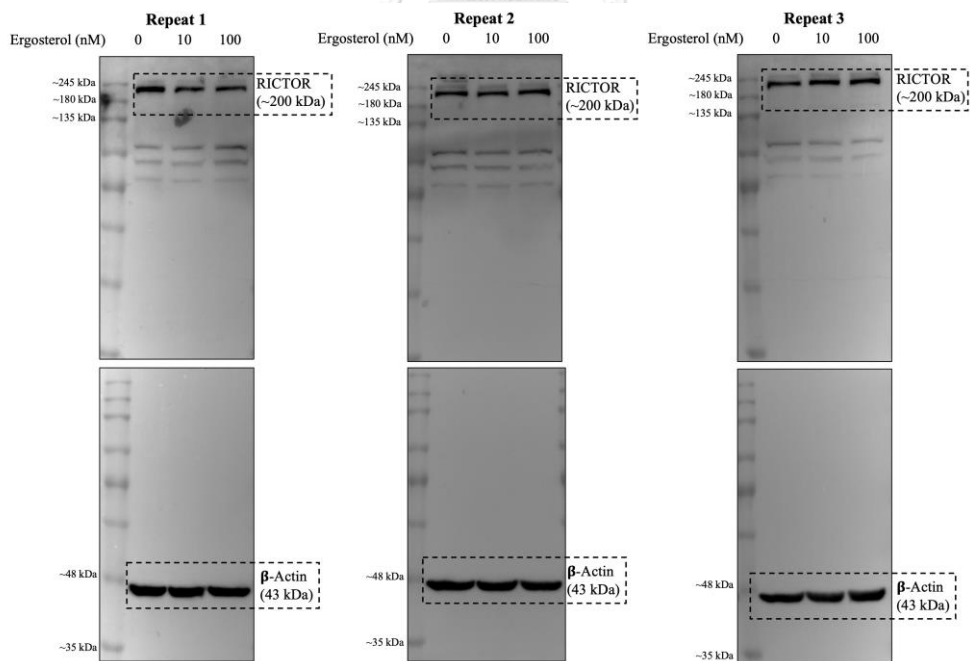


**Figure A 26** The original immunoblots of RICTOR and  $\beta$ -actin in HT-22 cells treated with ergosterol for 24 h.

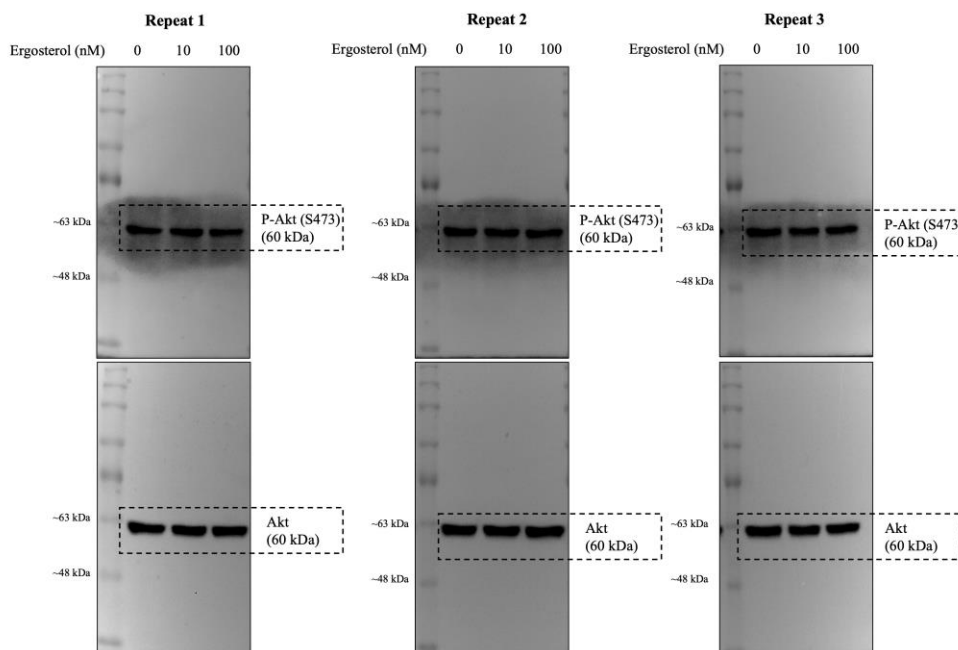


**Figure A 27** The original immunoblots of pAkt (S473) and Akt in HT-22 cells treated with ergosterol for 24 h.

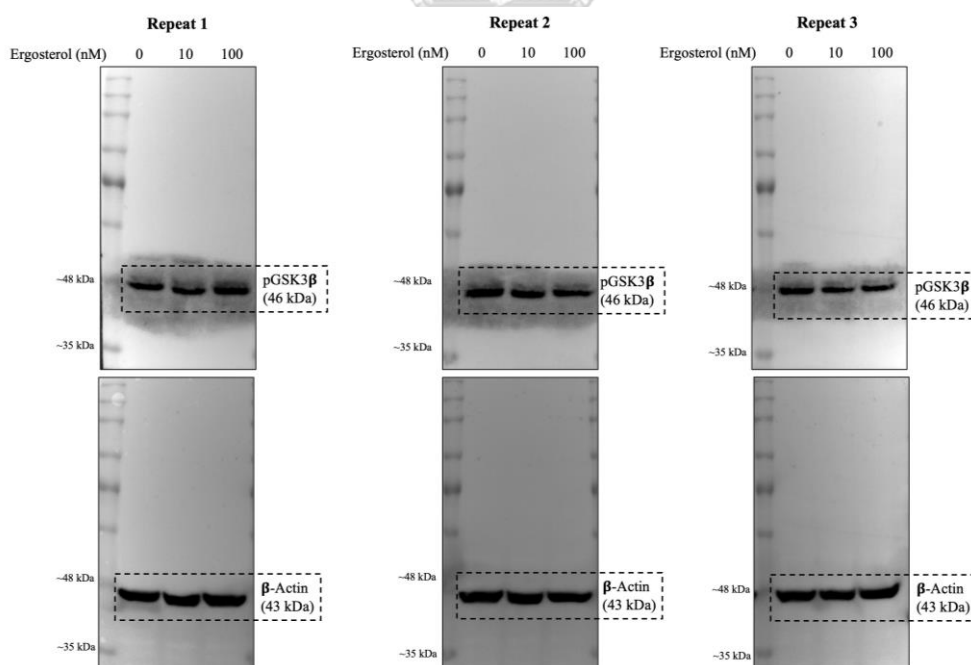


**Figure A 28** The original immunoblots of pGSK3 $\beta$  (S9) and  $\beta$ -actin in HT-22 cells treated with ergosterol for 24 h.

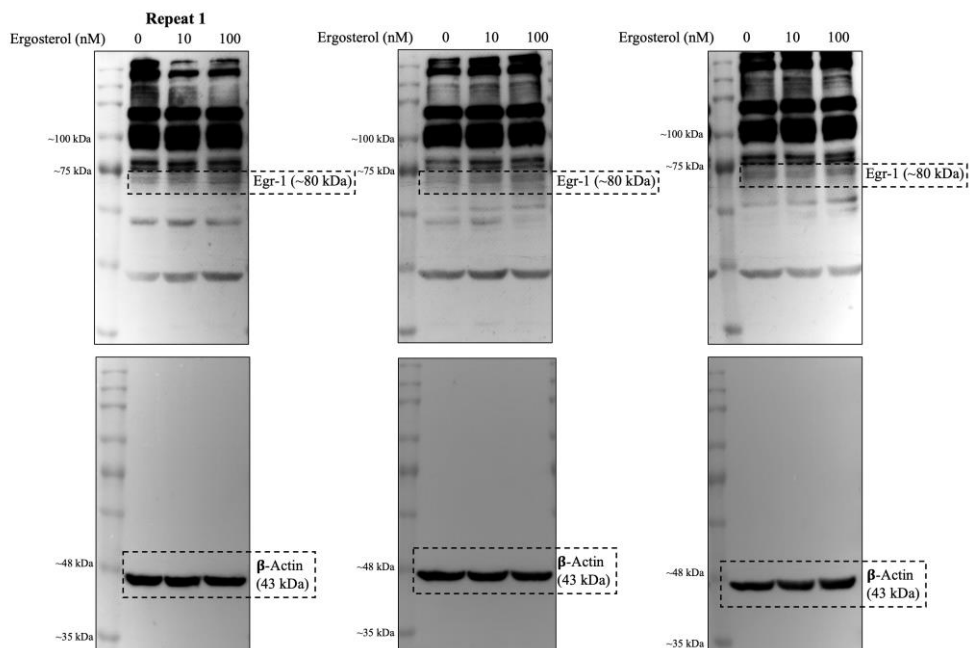


**Figure A 29** The original immunoblots of EGR-1 and  $\beta$ -actin in HT-22 cells treated with ergosterol for 24 h.

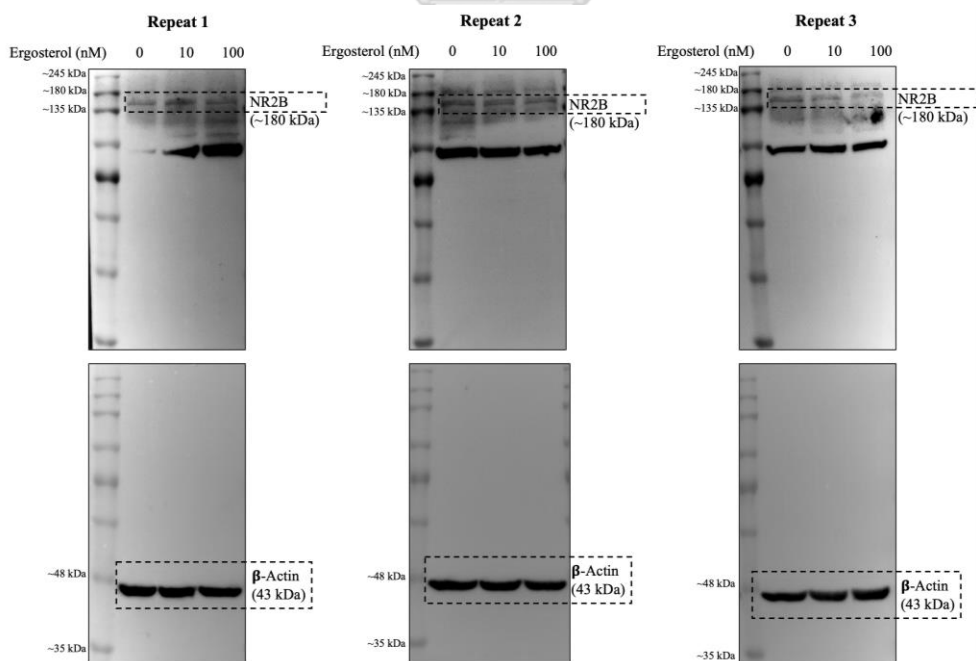


**Figure A 30** The original immunoblots of NR2B and  $\beta$ -actin in HT-22 cells treated with ergosterol for 24 h.

## VITA

**NAME** Chanin Sillapachaiyaporn

**DATE OF BIRTH** 11 October 1992

**PLACE OF BIRTH** Chonburi, Thailand

**INSTITUTIONS ATTENDED** Master of Science (Clinical Biochemistry and Molecular Medicine)  
Faculty of Allied Health Sciences, Chulalongkorn University, Bangkok, Thailand (2015-2018)

Bachelor of Business Administration (Management)  
Sukhothai Thammathirat Open University, Nontaburi, Thailand (2012-2016)

Bachelor of Science (Medical Technology), second class honors  
Faculty of Allied Health Sciences, Chulalongkorn University, Bangkok, Thailand (2011-2014)

**HOME ADDRESS** 24 M.2, Samed, Muang Chonburi, Chonburi, Thailand

**PUBLICATION**

1. Sillapachaiyaporn C, Mongkolpobsin K, Chuchawankul S, Tencomnao T, Baek SJ. Neuroprotective effects of ergosterol against TNF- $\alpha$ -induced HT-22 hippocampal cell injury. *Biomedicine & Pharmacotherapy*. 2022 Oct 1;154:113596.
2. Sillapachaiyaporn C, Chuchawankul S, Nilkhet S, Mounkote N, Sarachana T, Ung AT, Baek SJ, Tencomnao T. Ergosterol isolated from cloud ear mushroom (*Auricularia polytricha*) attenuates bisphenol A-induced BV2 microglial cell inflammation. *Food Research International*. 2022 May 28;111433.
3. Pattarachotanant N, Sornkaew N, Warayanon W, Rangsinth P, Sillapachaiyaporn C, Vongthip W, Chuchawankul S, Prasansuklab A, Tencomnao T. *Aquilaria crassna* Leaf Extract Ameliorates Glucose-Induced Neurotoxicity In Vitro and Improves Lifespan in *Caenorhabditis elegans*. *Nutrients*. 2022 Sep 5;14(17):3668.
4. Janpaijit S, Lertpatipanpong P, Sillapachaiyaporn C, Baek SJ, Charoenkiatkul S, Tencomnao T, Sukprasansap M. Anti-neuroinflammatory effects of *Cleistocalyx*



nervosum var. paniala berry-seed extract in BV-2 microglial cells via inhibition of MAPKs/NF- $\kappa$ B signaling pathway. *Heliyon*. 2022 Nov 28:e11869.

5. Rakkhitawatthana V, Sillapachaiyaporn C, Nilkhet S, Brimson J, Tencomnao T. (2022). Effect of Thai medicinal plants *Acanthus ebracteatus* Vahl. *Carthamus tinctorius* L. and *Streblus asper* Lour. on neurite outgrowth activity in Neuro-2A cells. *Journal of Associated Medical Sciences*, 56(1), 71–84.

6. Vongthip W, Sillapachaiyaporn C, Kim KW, Sukprasansap M, Tencomnao T. *Thunbergia laurifolia* Leaf Extract Inhibits Glutamate-Induced Neurotoxicity and Cell Death through Mitophagy Signaling. *Antioxidants*. 2021 Nov;10(11):1678.

7. Sangphech N, Sillapachaiyaporn C, Nilkhet S, Chuchawankul S. *Auricularia polytricha* ethanol crude extract from sequential maceration induces lipid accumulation and inflammatory suppression in RAW264.7 macrophages. *Food & Function*. 2021;12(21):10563-70.

8. Sillapachaiyaporn C, Rangsinth P, Nilkhet S, Mounkote N, Chuchawankul S. HIV-1 Protease and Reverse Transcriptase Inhibitory Activities of *Curcuma aeruginosa* Roxb. Rhizome Extracts and the Phytochemical Profile Analysis: In Vitro and In Silico Screening. *Pharmaceuticals*. 2021 Nov;14(11):1115.

9. Sillapachaiyaporn C, Rangsinth P, Nilkhet S, Ung AT, Chuchawankul S, Tencomnao T. Neuroprotective effects against Glutamate-Induced HT-22 hippocampal cell damage and *Caenorhabditis elegans* lifespan/healthspan enhancing activity of *Auricularia polytricha* mushroom extracts. *Pharmaceuticals*. 2021 Oct;14(10):1001.

10. Rangsinth P, Duangjan C, Sillapachaiyaporn C, Isidoro C, Prasansuklab A, Tencomnao T. *Caesalpinia mimosoides* Leaf Extract Promotes Neurite Outgrowth and Inhibits BACE1 Activity in Mutant APP-Overexpressing Neuronal Neuro2a Cells. *Pharmaceuticals*. 2021 Sep;14(9):901.

11. Prasansuklab A, Theerasri A, Rangsinth P, Sillapachaiyaporn C, Chuchawankul S, Tencomnao T. Anti-COVID-19 drug candidates: A review on potential

biological activities of natural products in the management of new coronavirus infection. *Journal of traditional and complementary medicine*. 2021 Mar 1;11(2):144-57.

12. Rangsinth P, Sillapachaiyaporn C, Nilkhet S, Tencomnao T, Ung AT, Chuchawankul S. Mushroom-derived bioactive compounds potentially serve as the inhibitors of SARS-CoV-2 main protease: An in silico approach. *Journal of traditional and complementary medicine*. 2021 Mar 1;11(2):158-72.

13. Sillapachaiyaporn C, Chuchawankul S. HIV-1 protease and reverse transcriptase inhibition by tiger milk mushroom (*Lignosus rhinocerus*) sclerotium extracts: In vitro and in silico studies. *Journal of traditional and complementary medicine*. 2020 Jul 1;10(4):396-404.

14. Sillapachaiyaporn C, Nilkhet S, Ung AT, Chuchawankul S. Anti-HIV-1 protease activity of the crude extracts and isolated compounds from *Auricularia polytricha*. *BMC complementary and alternative medicine*. 2019 Dec;19(1):1-10.

15. Sillapachaiyaporn C, Chuchawankul S. In vitro and in silico studies on HIV-1 protease and reverse transcriptase inhibitions of edible mushroom (*Astraeus hygrometricus*) extracts. The 1st RMUTT food innovation and smart farm international conference. 2019 July; 39-44. (Proceeding)

16. Ahmad R, Sahidin I, Taher M, Low C, Noor NM, Sillapachaiyaporn C, Chuchawankul S, Sarachana T, Tencomnao T, Iskandar F, Rajab NF. Polygonumins A, a newly isolated compound from the stem of *Polygonum minus* Huds with potential medicinal activities. *Scientific reports*. 2018 Mar 9;8(1):1-5.

#### **AWARD RECEIVED**

1. The 90th Anniversary of Chulalongkorn University Scholarship (2021) from Graduate School, Chulalongkorn University

- A scholarship for research financial supporting

2. Chulalongkorn University Second Century Fund (C2F) (2019-2021) from Chulalongkorn University

- A full-expense scholarship for Ph.D. students who have outstanding academic and research profiles

3. The Royal Golden Jubilee (RGJ) Ph.D. Program Scholarship (2019-2021) from The National Research

Council of Thailand (NRCT)

- A full-expense scholarship for Ph.D. students who have outstanding academic and research profiles
- A scholarship for conducting research at College of Veterinary Medicine, Seoul National University (SNU), Republic of Korea
- A scholarship for presentation at the 5th Global Conference on Neuroscience and Neurological Disorders, Berlin, Germany

4. Overseas Academic Presentation Scholarship Option II for Graduate Student's and Postdoctoral Fellow's Publication (2019) from Graduate School, Chulalongkorn University

- A scholarship for presentation at the international conference on traditional medicine and ethnomedical research, Tokyo, Japan

5. Academic Presentation Scholarship for Graduate Students (2019) from Graduate School, Chulalongkorn University

- A scholarship for presentation at the 1st RMUTT Food Innovation and Smart Farm International Conference, Pathumthani, Thailand

6. Overseas Academic Presentation Scholarship for Graduate Students (2018) from Graduate School, Chulalongkorn University

- A scholarship for presentation at the 30th International Symposium on the Chemistry of Natural Products and the 10th International Congress on Biodiversity, Athens, Greece

7. Student Exchange Support Program (Scholarship for Short-term Study in Japan) (2018) from Japan Student Services Organization (JASSO), Japan

- A scholarship for short-term exchange student to Tokyo Medical and Dental University (TMDU), Japan

8. Overseas Research Experience Scholarship for Graduate Student (2017) from Graduate School, Chulalongkorn University

- A scholarship for conducting research at Faculty of Science, University of Technology Sydney (UTS), Australia

9. The 90th Anniversary of Chulalongkorn University

Scholarship (2017) from Graduate School, Chulalongkorn University

- A scholarship for research financial supporting

10. ASEAN Youth Exchange Scholarship (2016) from ASEAN studies center, Chulalongkorn University  
- A scholarship for visiting Institute of Systems Biology, Universiti Kebangsaan Malaysia (UKM) and Department of Biosciences and Health Sciences, Faculty of Biosciences and Medical Engineering, Universiti Teknologi Malaysia (UTM), Malaysia

11. The 72nd anniversary of his Majesty King Bhumibala Aduladeja Scholarship (2015-2017) from Graduate School, Chulalongkorn University

- A full-expense scholarship for M.S. and Ph.D. students who have outstanding academic and research profiles

12. Chulalongkorn University – Rural Scholarship (CU-RR) (2011-2014) from Chulalongkorn University

- A full-expense scholarship for undergraduate students from lower-income families who have outstanding academic profiles